NP DIVISION
Internal Report 68-11
1 May 1968

ORGANISATION EUROPÉENNE POUR LA RECHERCHE NUCLÉAIRE
CERN EUROPEAN ORGANIZATION FOR NUCLEAR RESEARCH

THE OMEGA PROJECT

Proposal for a large magnet and spark chamber system

by the

Omega Project Working Group

Revised Edition

Preface

This report is the result of the work of a number of CERN physicists and engineers, the so-called Omega Project Working Group which was set up in April 1967. This group now consists of the following members:

W.F. Baker, W. Beusch, G.Brautti, G. Cocconi, B. French, O. Gildemeister, A. Michelini, M. Morpurgo, B.Nellen, G. Petrucci, P. Preiswerk, E. Quercigh, C. Rubbia, K. Tittel, and P. Zanella.

This group is grateful for much help from and discussions with several other people, especially to M. Borghini for discussions on the possible use of polarized targets for the "Omega".

CONTENTS

1. INTRODUCTION

During the last few years, the field of counter experiments in high-energy physics has been marked by the extensive use of spectrometer magnets associated with spark chamber systems. In most cases, because of the relatively small aperture of the magnets, a limited number of particle secondaries (< 2) were detected at each interaction.

In order to perform -- with high statistics and good measurement accuracy -- experiments on more complicated types of interactions with detection of many secondaries, larger spectrometer magnets with better resolution and wide solid-angle acceptance are necessary. In view of this natural development of high-energy experiments, the Omega Project Working Group has worked out, in the present report, a proposal for a large spectrometer magnet and spark chamber system to be built as a part of the improvement programme of CERN. The proposed instrument is expected to be installed in the new PS West Experimental Hall (see Fig. 1.1). The global cost of the magnet and of an optical spark chamber system including construction staff is estimated to be 13.9 MSFr. (1967 prices, no provision is made for contingencies). It is expected that the project will be completed approximately 3.5 years after approval.

The basic idea of the project is a large-aperture spectrometer magnet and a system of spark chambers to be operated within this magnet, associated with an efficient data-handling system. This configuration of magnet and spark chambers makes it possible to perform a new class of counter experiments, especially on interactions where a large number (≥ 2) of secondary particles or unstable mesons and baryons such as K^0, Λ^0, etc., have to be completely detected and measured. An additional merit of the proposed system is its ability to perform experiments on relatively simple types of reactions but with very small cross-section (≤ 1 μb) as in the case of large momentum transfer scattering detected over a large solid angle of acceptance. As examples of the use of the system, we have considered various experiments such as: the study of resonances with a missing-mass trigger on the recoil proton, and complete detection and measurement of the resonance secondaries (Section 3.1); the study of baryon exchange processes requiring an ingoing meson and a forward outgoing proton of a relatively high momentum (Section 3.2); and the study

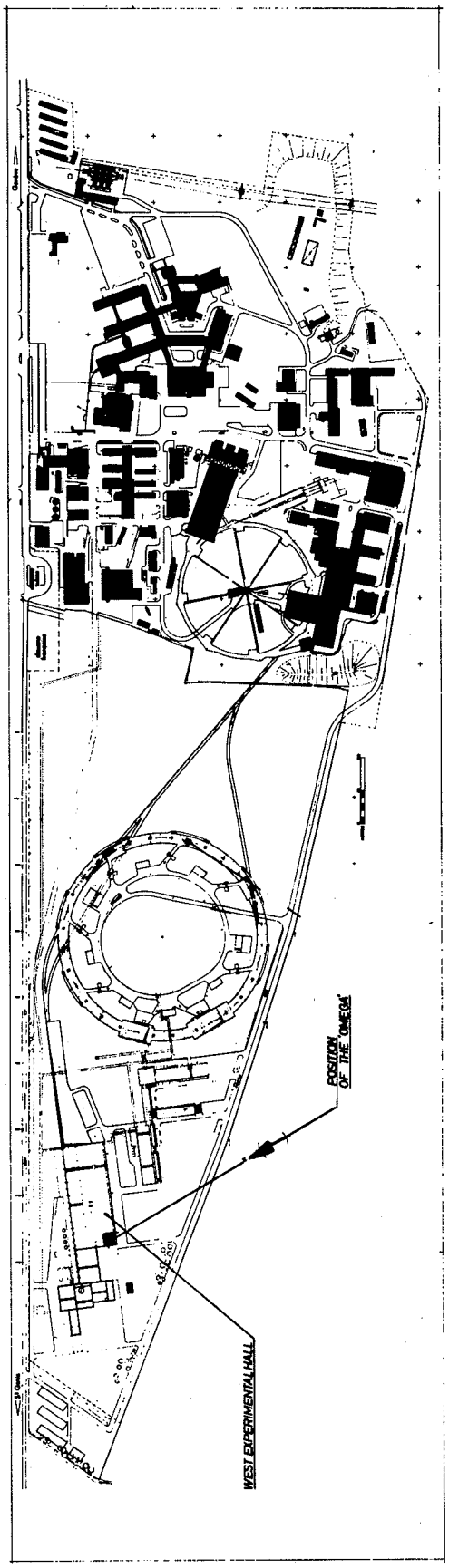

FIG.11. PROPOSED POSITION OF THE OMEGA MAGNET

of leptonic decays of hyperons (Section 3.3). These types of experiments will form a part of the experimental programme of the apparatus. However, it is impossible to foresee all the experiments that will be performed with the magnet, and the aim is therefore to build a flexible system which can be used in a large number of experiments over a period of many ($\gtrsim$ 10) years. The experience with the present CERN-ETH-Imperial College spectrometer magnet makes us confident that this can be done. In the following we state a few general properties and requirements of the various components of the proposed system, which are independent of the final design to be adopted.

Magnet

The design of the Omega magnet has to be flexible so that it can be easily adapted to the maximum number of experiments. This can be realized, in practice (see Fig.1.2), by restricting to a minimum its fixed mechanical parts: the coils, the horizontal yokes, and four vertical pillars which act as spacers. All other parts such as the vertical yoke and the poles are made removable. In particular, the vertical yoke is composed of modular elements to be mounted around the horizontal yoke in different geometrical configurations suggested by the explicit layout of each experiment. The choice of this design satisfies the following important requirements:

- maximum flexibility for mounting inside the field volume systems of spark chambers, counters, and targets in various configurations;
- possibility of photographing a system of optical spark chambers through the top pole;
- possibility of extracting from the field volume through side apertures those particles which originated at the target and must be detected outside the magnet.

The size of the magnet and the value of its field are chosen on the basis of the required large acceptance and good resolution up to the maximum beam energy available at the CERN PS.

The main characteristics of the Omega magnet are:

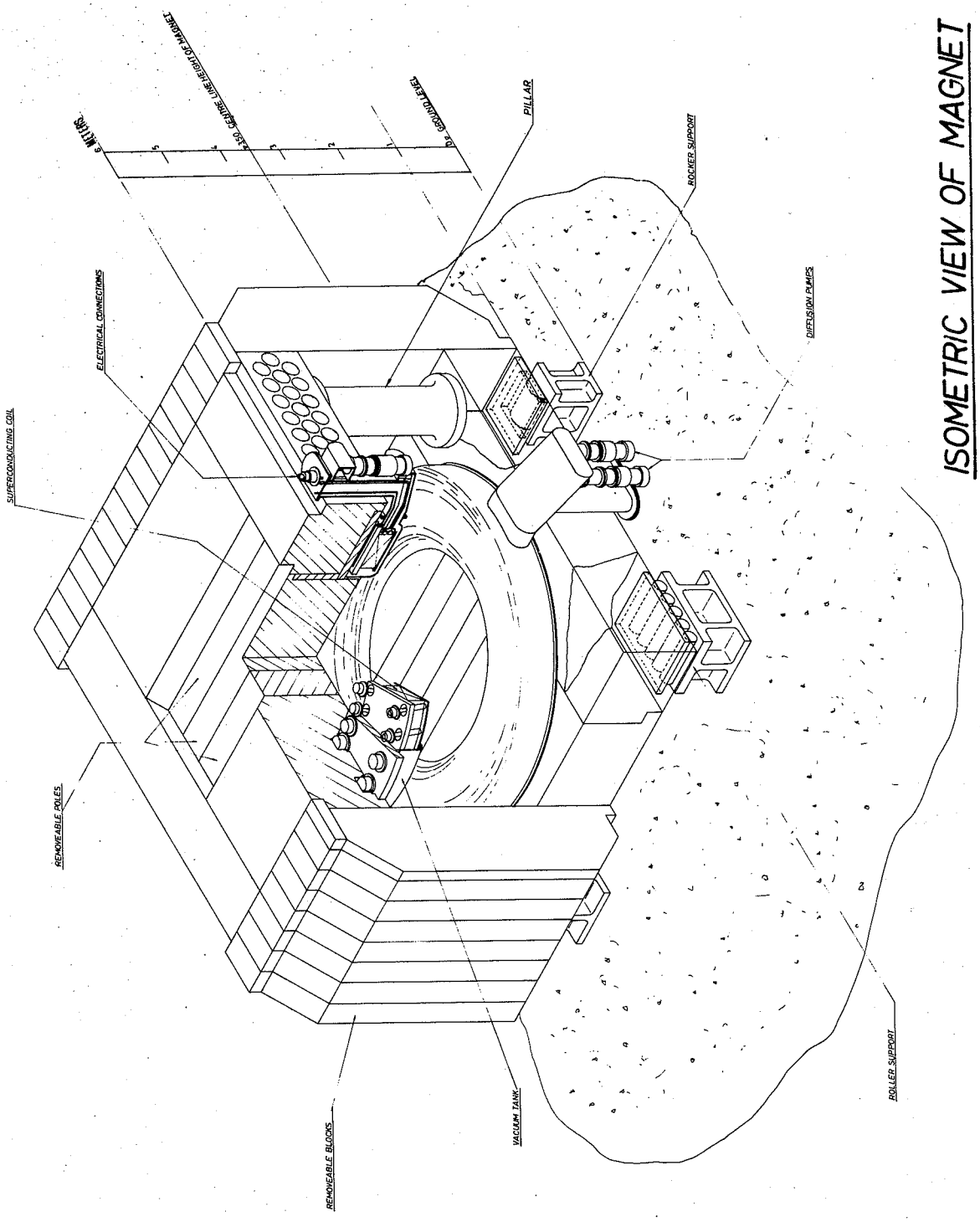

ISOMETRIC VIEW OF MAGNET

FIG. 1.2

Maximum field at the centre (with top pole removed)	18	kG
Inner diameter of circular coils	3.0	m
Free gap between coils	1.5	m
Free gap between poles	2.0	m
Weight	1300	tons .

In the present proposal we have considered two alternative solutions of conventional and superconductive coils for a magnetic field of 18 kG.

Because of its large size and weight, the magnet has to be considered as a fixed installation in the future West Experimental Area.

Targets

The operation inside the magnetic field of conventional targets of different nuclear composition (from liquid hydrogen to the highest Z) represents no problem. The operation of a polarized target in the gap of the Omega magnet can be considered as a possible and interesting future development. The interest lies in the possibility of using the Omega spectrometer to detect and measure all secondaries of an interaction -- an important feature for identifying the target nucleus.

Spark chambers

The operation of large-volume optical spark chambers in a magnetic field represents a well-established technique. However, it is very likely that other types of chambers, such as wire spark chambers with digitized read-out working in a magnetic field, will become available during the period of construction and operation of the Omega project. Some examples of digitized read-out, at present under test in a magnetic field, are the magnetostrictive and the sparkostrictive types; others, such as multiwire proportional counters*), can be considered as a possible future development. It is therefore reasonable to assume that the

*) See: The use of multiwire proportional counters to select and localize charged particles, by G. Charpak et al.(Submitted to Nucl. Instr. and Methods, 1968).

alternative read-out systems for both optical and digital spark chambers in a magnetic field, will be used for future experiments, each system having its well-defined field of application: the optical chamber for low trigger-rate and rather complicated types of events; digitized wire chamber for higher trigger-rate and relatively simpler events. It seems reasonable today to expect that after a first phase of operation of the Omega spectrometer with optical spark chambers, a second phase will follow during which both systems could be used alternatively.

Trigger system

The trigger system is defined by the experiment to be performed. Scintillation counters are used extensively as particle detectors for trigger systems because of their good time-resolution (a few nanoseconds). In the case of experiments with a spectrometer magnet, a part of the trigger system is very often required to operate inside the magnet. The photomulipliers which collect the light coming from the scintillators can only be operated in a region of low magnetic field ($\lesssim$ 1 kG). This problem can, however, be solved simply by the use of "long" (one-two metres) light-guides, provided the magnet has good access from the outside and a fringing field extending over short distances, as in the case of the proposed Omega spectrometer. No essential limitations are expected from the long light-guides on the performance of the scintillation counters. One exception could perhaps be the pulse-height analysis when used to distinguish between one or two particles traversing the counter.

Apart from the scintillation counters, new detectors could become available by the time the Omega spectrometer will be operating. One type now under study is the above-mentioned multiwire proportional counter. If it turns out to have adequate time-resolution, it would provide large-area low-mass counters. It would not only signal the presence of at least one particle, but the exact number of secondaries for each interaction and their position with a space accuracy down to a fraction of a millimetre.

Data-handling system

Under the hypothesis that the Omega runs at the PS with an effective data-taking time corresponding to 4×10^6 PS cycles/year, the maximum annual production can be estimated to be $\sim 12 \times 10^6$ pictures in an optical system, yielding about 4×10^6 events to be measured, or 50×10^6 wire chamber events on tape, yielding up to 20×10^6 good events to be analysed. The analysis of the data will be performed at CERN and in European laboratories and universities.

The data handling therefore represents a fundamental aspect of the whole project. A well-planned system should be sufficiently flexible to provide for the evaluation of film and wire chambers data; it should have the computer capacity required for experiment planning, data acquisition, sample event calculations, full analysis of the CERN share of the events, general computing, development work, etc. The size of the system has to be determined on the basis of reasonable estimates of the event rate, yet allowing for possible expansion, when necessary.

The system proposed in this report consists essentially of a computer connected on-line to both the experimental equipment and an HPD flying-spot digitizer, for the data acquisition and reduction stages of the analysis. For higher stages of the processing chain (geometry, kinematics, statistics) extensive use of CERN large central computers is foreseen.

Besides all general computing activities related to the running of the Omega project, the proposed system should be capable of handling approximately 25% of the films and 10-15% of the wire chamber events. This might be regarded as a reasonable CERN share of the experiment analysis.

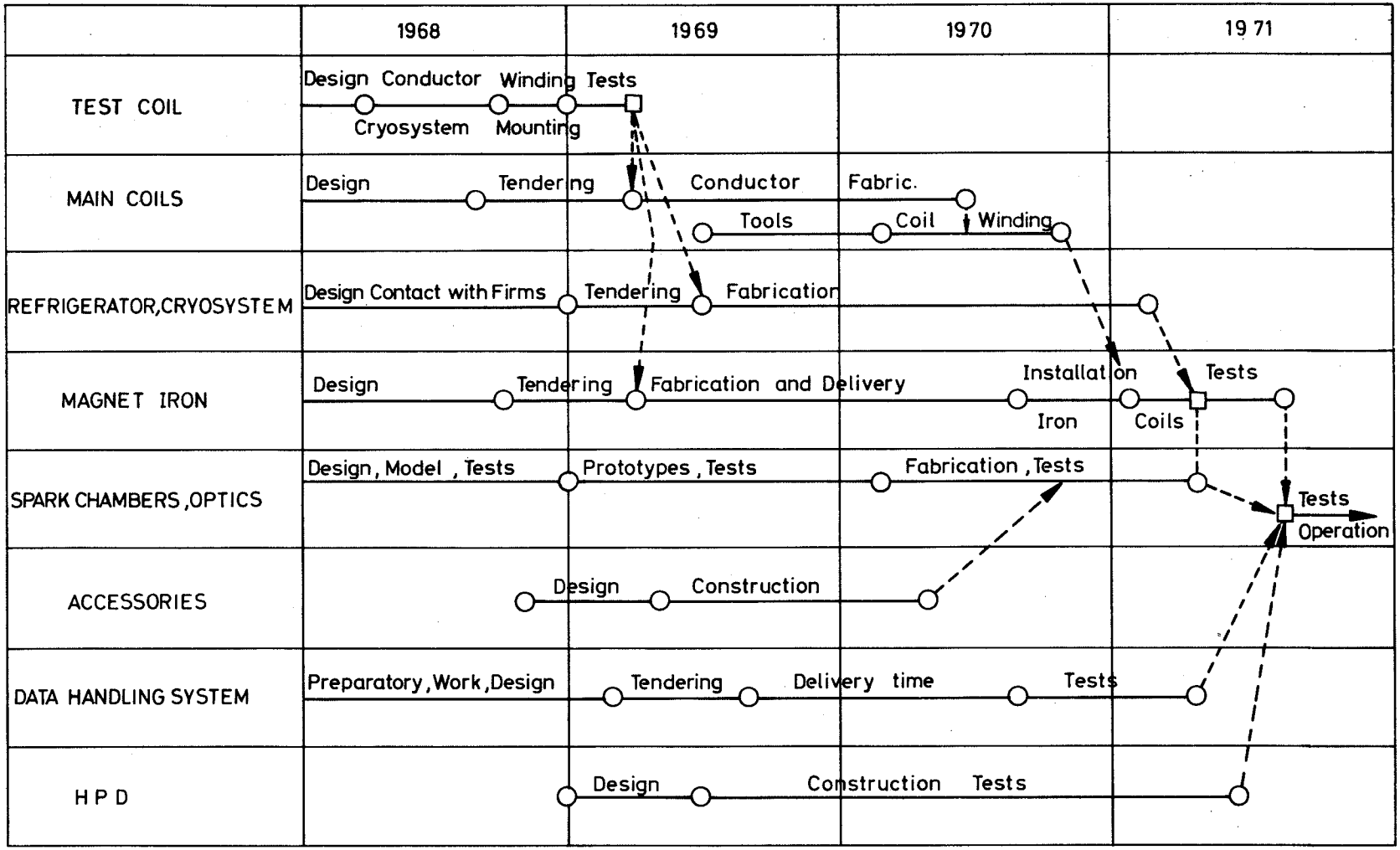

FIG. 1.1.1 PROJECT PLAN

1.1 Construction programme and costs

On the assumption that the detailed design work can start now and that the final decision on the project can be made at the middle of 1968, the project could probably be finished in 1971. Figure 1.1.1 shows a time-scale of the project.

The total costs are listed below. They are estimated on the basis of present prices. (The data-handling system is listed separately since it is not yet clear how the budgeting will be handled.)

Experimental part:

Magnet, refrigerator, etc. (superconducting coil)	MSFr.	9.6
Spark chambers, optics, etc.,		1.7
Staff during construction period		2.6
Total	MSFr.	13.9

Data-handling system:

Computers	MSFr.	5.8
HPD, interface, scanning tables, links		2.0
Buildings		0.6
Total	MSFr.	8.4

The running costs*) for staff, power, maintenance, film, and tape are estimated at 3.5 MSFr./year if superconducting coils are used.

The expected distribution of the costs over the years would be:

	1968	1969	1970	1971	Total
Experimental part	1.2	4.6	4.6	3.5	13.9
Data handling	-	4.0	4.0	0.4	8.4
Total	1.2	8.6	8.6	3.9	22.3

*) Including the analysis up to the event recognition.

1.2 Choice of the main parameters of the Omega magnet

The main parameters of the Omega magnet, i.e. coil diameter and magnetic field, are to be chosen on the basis of the required momentum resolution and mass resolution.

The momentum resolution for a magnet spark chamber system can be expressed as:

$$\frac{\Delta p}{p} = \frac{1}{H}\left\{\left(\frac{93.5\,\sigma_y\,p}{L^{5/2}\sqrt{N'}\cos^{3/2}\lambda}\right)^2 + \left(\frac{50}{\sqrt{L\,L_o}}\right)^2\right\}^{1/2} \qquad (1)$$

in units: [cm, kG, MeV/c], and where:

H = magnetic field;

σ_y = space resolution in the plane perpendicular to the magnetic field; [typically, $\sigma_y = (0.02 + 0.044\,|\delta|)$ cm, δ being the angle of the particle to the normal to the spark chamber plates];

p = particle momentum;

L = length of measurable track in space;

N' = number of measured sparks per cm of track (typically $N' = 0.33\ \text{cm}^{-1}$ for tracks perpendicular to the spark chamber plates);

λ = dip angle;

L_o = radiation length [$L_o = 3.5 \times 10^3$ cm (7×10^3 cm) for 25 μ (10 μ)Al plates and for particles perpendicular to the spark chamber plates].

The mass resolution in the case of a mass M decaying into two secondaries 1 and 2 can be expressed as:

$$\Delta M = \frac{1}{M}\left\{(E_2\beta_1 - p_2\cos\Theta)^2\Delta p_1^2 + (E_1\beta_2 - p_1\cos\Theta)^2\Delta p_2^2 + p_1^2 p_2^2 \sin^2\Theta\,\Delta\Theta^2\right\}^{1/2} = \left\{(\Delta M)^2_{\Delta p} + (\Delta M)^2_{\Delta\Theta}\right\}^{1/2} \qquad (2)$$

where p_1, E_1, p_2, E_2 are the momenta and the energies of the two secondaries and Θ is the angle between them.

As will be shown below, the diameter of the magnet coils and the value of the magnetic field can be chosen so that in each of the formulae (1) and (2) the various terms are matched.

1.2.1 Choice of the diameter of the magnet coils

Figure 1.2.1 shows how $\Delta p/p$ decreases with increasing L according to formula (1). In particular, $\Delta p/p$ varies much more rapidly in the region of relatively small L's ($\sim L^{-5/2}$), where the measurement error dominates, than in the region of large L's ($\sim L^{-1/2}$) where the error introduced by the multiple scattering dominates. It is therefore natural to choose as optimum track length L_{opt}, the value of L for which the two terms of (1) become equal. The resulting expression of L_{opt} is:

$$L_{opt} = \left\{ 1.8 \frac{\sigma_y}{\cos^{3/2} \lambda} \sqrt{\frac{L_0}{N'}}\, p \right\}^{1/2} , \qquad (3)$$

i.e. L_{opt} depends on the characteristics of the spark chamber used, namely, its radiation length L_0 and the relative space resolution σ_y.

In Table 1.2.1 are listed values of L_{opt} for different choices of L_0 and σ_y and for a fixed value of p = 20 GeV/c. For the particular case of $L_0 = 7 \times 10^3$ cm (10 μ Al plates) and $\sigma_y = 0.02$ cm (expected space resolution for an optical spark chamber system), we obtain $L_{opt} = 324$ cm.

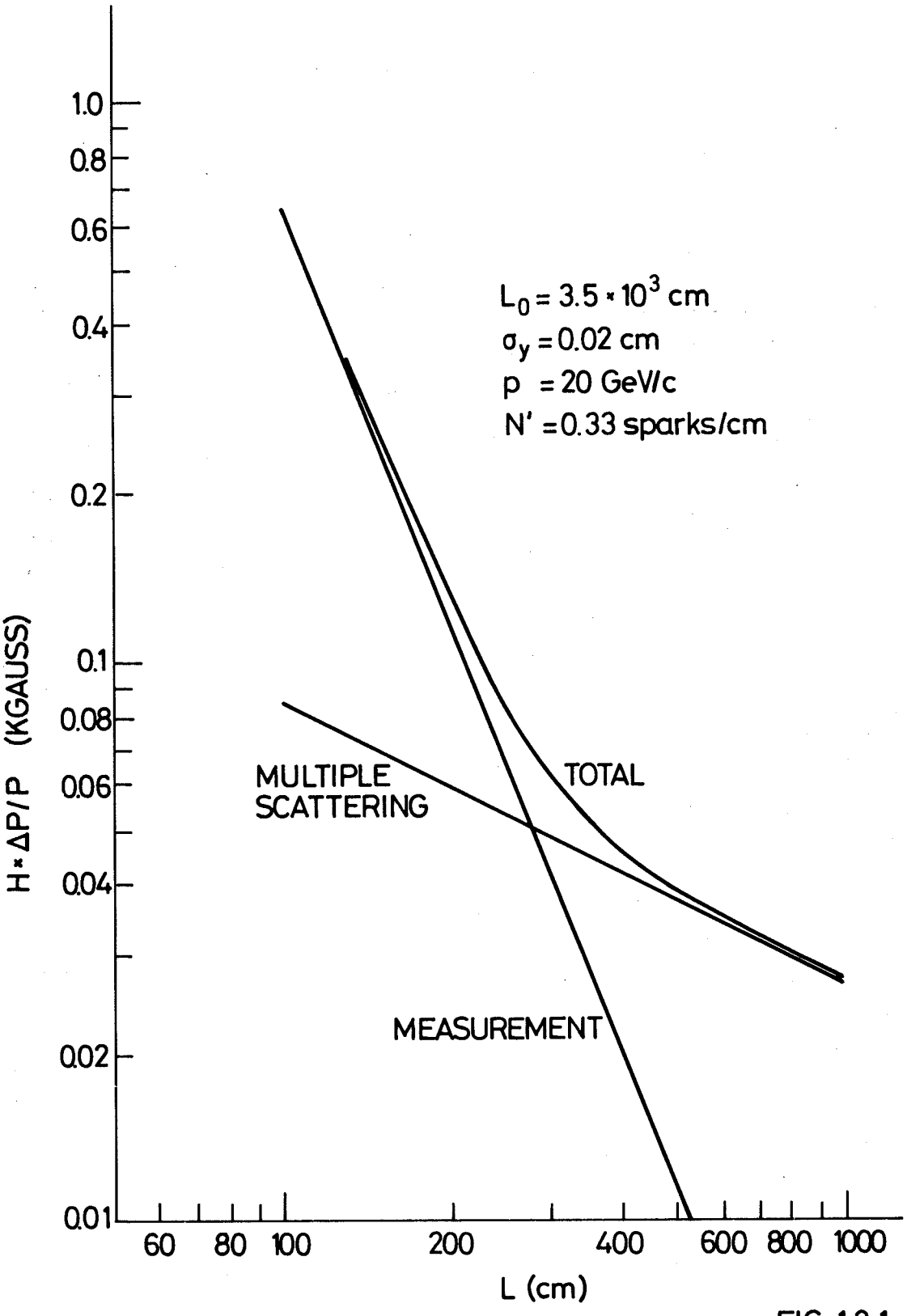
1.0
0.8
0.6
0.4
0.2
0.1
0.08
0.06
0.04
0.02
0.01
H * ΔP/P (KGAUSS)
$L_0 = 3.5 * 10^3$ cm
$\sigma_y = 0.02$ cm
p = 20 GeV/c
N' = 0.33 sparks/cm
MULTIPLE SCATTERING
TOTAL
MEASUREMENT
60
80
100
200
400
600
800
1000
L (cm)

FIG. 1.2.1

Table 1.2.1

Plate thickness μ Al	L_o [1] $\times 10^3$ cm	σ_y (cm)	L_{opt} (cm)
25	3.5	0.015	235
25	3.5	0.020	272
25	3.5	0.025	305
25	3.5	0.030	334
10	7	0.015	280
10	7	0.020	324
10	7	0.025	362
10	7	0.030	395
wire chambers: 60 μ Ø Be-Cu wire, 1 mm spacing	4.6	0.030	311

1.2.2 Choice of the magnetic field

Having fixed L_{opt}, $(\Delta M)^2_{\Delta\Theta}$ in formula (2) is also fixed. One can therefore choose as optimum magnetic field H_{opt}, the value of H which makes $(\Delta M)^2_{\Delta p}$ equal to $(\Delta M)^2_{\Delta\Theta}$. The results are illustrated in Fig. 1.2.2 for the case of a $K^*(1420)$ decaying into $K + \pi$ at 5, 10, 15, and 20 GeV/c. The plotted curves represent the variation with magnetic field of $(\Delta M)^2_{\Delta p}$ of formula (2):

$$M^2 \cdot (\Delta M)^2_{\Delta p} = (E_2 \beta_1 - p_2 \cos\Theta)^2 \Delta p_1^2 + (E_1 \beta_2 - p_1 \cos\Theta)^2 \Delta p_2^2 ,$$

and the *-points represent the corresponding values of $M^2 \cdot (\Delta M)^2_{\Delta\Theta}$, independent of H:

$$M^2 \cdot (\Delta M)^2_{\Delta\Theta} = p_1^2 p_2^2 \sin^2\Theta \, \Delta\Theta^2 .$$

H_{opt} is determined by the relation:

$$M^2 \cdot (\Delta M)^2_{\Delta p} = M^2 \cdot (\Delta M)^2_{\Delta\Theta}$$

---

1) 80 plates per metre, chamber gas and mylar foils included.

In the particular case of Fig. 1.2.2, H_{opt} ranges between 11 and 15 kG for $L_o = 7 \times 10^3$ cm, and $L_{opt} = 300$ cm. In the calculations we have assumed an average track length $L = (\frac{3}{4} L_{opt} - 25)$ cm in order to allow for some of the K* secondaries to leave the spark chamber sideways, and for a length of 25 cm occupied by the H_2 target. More values of H_{opt} corresponding to different combinations of L_{opt} and L_o are listed in Table 1.2.2.

Table 1.2.2

L_{opt} (cm)	L_o ($\times 10^3$ cm)	H_{opt} (kG)			
		$P_{K^*} = 5$ GeV/c	$P_{K^*} = 10$ GeV/c	$P_{K^*} = 15$ GeV/c	$P_{K^*} = 20$ GeV/c
250	3.5	16.9	15.2	14.0	13.6
300	3.5	14.7	13.1	12.4	12.1
350	3.5	12.3	11.6	10.9	10.6
250	7	15.8	15.8	13.9	13.2
300	7	15.0	12.4	11.5	11.1
350	7	12.1	11.0	10.3	9.8

Under all the possible conditions considered in Table 1.2.2 we can see that a value of $H \gtrsim 17$ kG would satisfy the requirement of matching the errors in formula (2).

According to what has been discussed so far, the criterion of matching the errors in (1) and (2) indicates as optimum values ~ 300 cm for the track length L_{opt}, and ~ 18 kG for the magnetic field H_{opt}. Whether this choice is reasonable can be decided by looking at the absolute value of the mass resolution and the momentum resolution that can be obtained. This is illustrated in the subsequent Figs. 1.2.3 to 1.2.6.

Figure 1.2.3 shows the effective mass resolution ΔM as a function of the magnetic field H in the case of the $K^*(1420)$ decay*) and for

*) The mass resolution becomes worse for increasing Q-values. The $K^*(1420)$ decay has one of the highest Q-values and is therefore a good example.

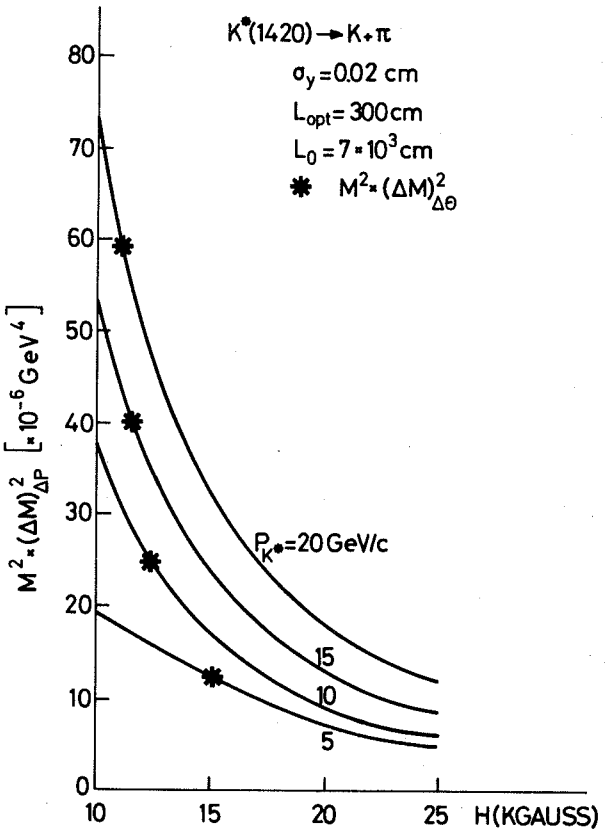

FIG. 1.2.2

EFFECTIVE MASS RESOLUTION

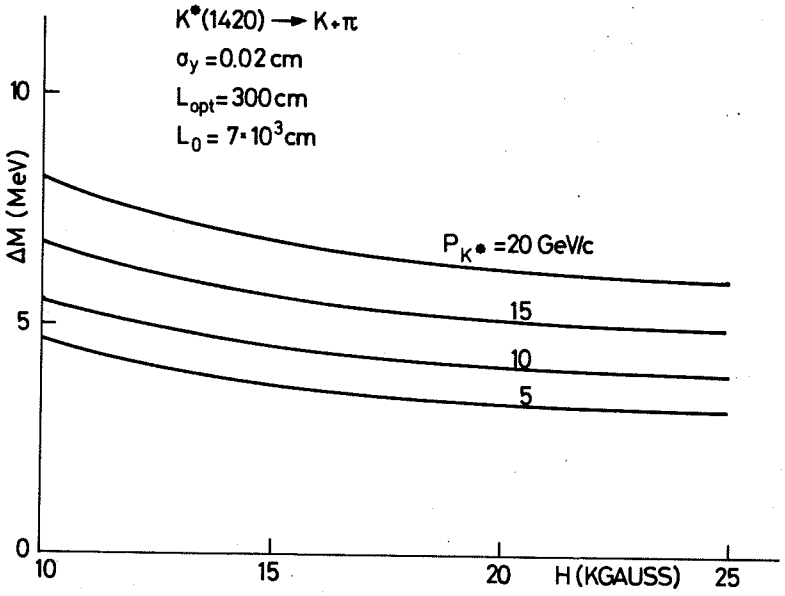

FIG. 1.2.3

L_{opt} = 300 cm and L_o = 7×10^3 cm. At H = 18 kG we expect mass resolutions between ΔM = 3.3 MeV (p_{K^*} = 5 GeV/c) and ΔM = 6.3 MeV (p_{K^*} = 20 GeV/c) *).

Figure 1.2.4 shows the mass resolution ΔM on the missing recoil-neutron when all other secondaries of an interaction are produced in forward direction and are measured (1C-fit type of event). The primary momentum is chosen to be 20 GeV/c. In this case ΔM can be expressed approximately as:

$$\Delta M \cong \left\{ \Delta p_i^2 + \Delta p_f^2 \right\}^{1/2} ,$$

where Δp_i and Δp_f are the momentum resolutions of the incident beam particle and of the outgoing final system, respectively.

The limited momentum resolution on the incident particle Δp_i = 40 MeV sets a lower limit to ΔM, independent of the magnetic field. We can expect to obtain a $\Delta M \sim \frac{1}{2} m_\pi$ at H = 18 kG and for the parameters of curve c in Fig. 1.2.4 (i.e. $L_o = 7 \times 10^3$ cm and L_{opt} = 300 cm).

Finally, in Fig. 1.2.6 are plotted the momentum resolution curves for particles emitted at zero angle with respect to the magnet axis for H = 18 kG. The geometrical configurations for different momenta assumed in the calculations of $\Delta p/p$ are illustrated in Fig. 1.2.5.

1.2.3 Conclusion

The choice of the parameters of the Omega magnet based on matching the different terms of the momentum resolution (1) and the effective mass resolution (2) lead to satisfactory small values, from the physics point of view, for the errors on effective mass and missing mass. We therefore choose for the magnet the following characteristics:

Magnetic field with open pole (optical spark chamber operation) = 18 kG;
Coil diameter = 300 cm **).

---

*) The expected K^0 mass resolution is about 3 MeV for a K^0 momentum of 10 GeV/c and an average track length of 2 metres.

**) In section 2.2, one of the proposed optical designs allows a maximum track length of ~ 350 cm to be obtained in the medium plane of the magnet.

MISSING MASS RESOLUTION FOR I-C FIT

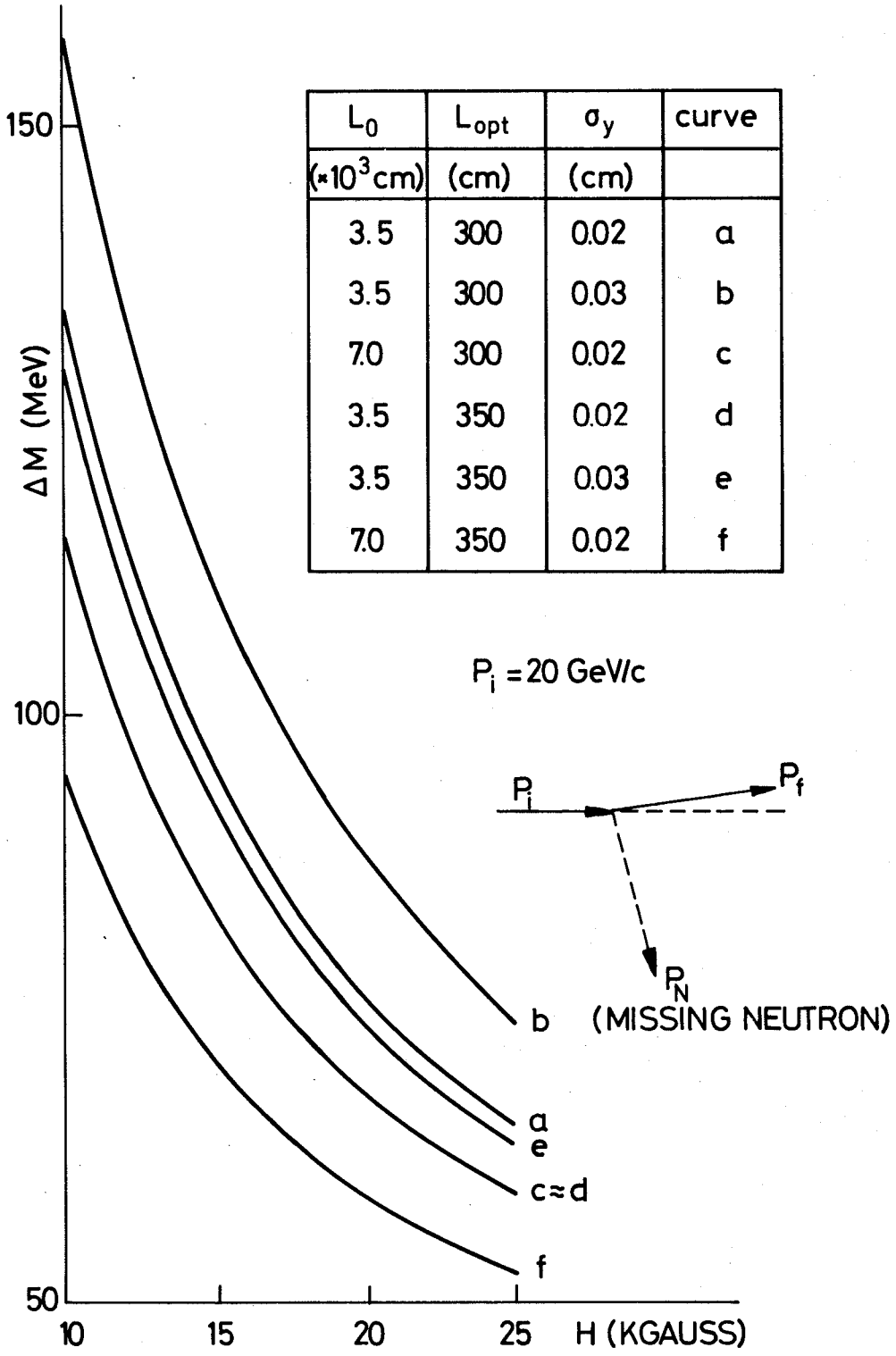

L_0 ($\times 10^3$cm)	L_{opt} (cm)	σ_y (cm)	curve
3.5	300	0.02	a
3.5	300	0.03	b
7.0	300	0.02	c
3.5	350	0.02	d
3.5	350	0.03	e
7.0	350	0.02	f

FIG. 1.2.4

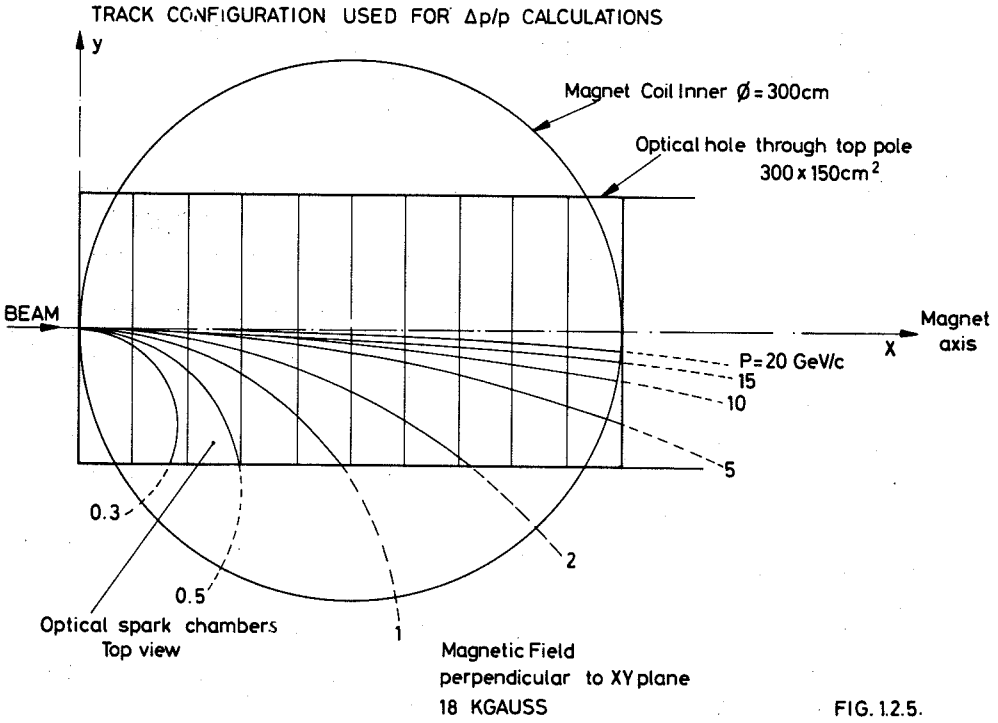

FIG. 1.2.5.

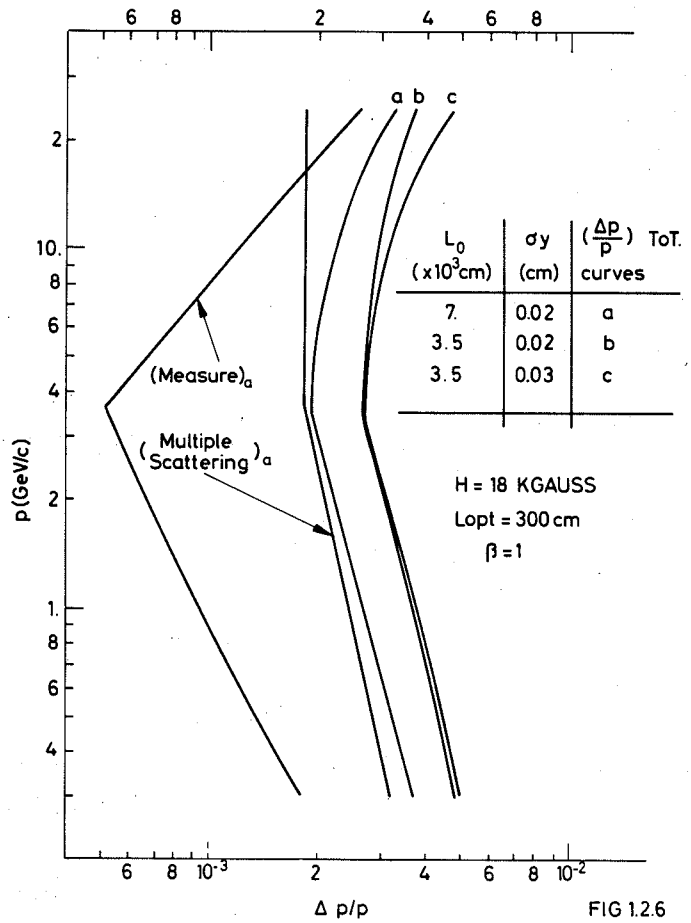

FIG 1.2.6

2. DETAILED DESCRIPTION OF THE PROJECT

2.1 Magnet

The general characteristics of the magnet are:

max. magnetic field at the centre	=	18 kG (without top pole)
inner diameter of circular coils	=	3.0 m
free gap between coils	=	1.5 m
free gap between poles	=	2.0 m

At a first approximation, taking the fringing field into account, the bending power of this magnet will be = 7.8 Wb/m.

A magnet having the above-mentioned characteristics can be designed either with superconducting or conventional copper coils. Both solutions are being studied in some detail; a decision as to which of the two alternatives will be used has not yet been taken. A cost estimate for both solutions is given below (Section 2.6). The magnet will have an iron yoke which has the purpose of increasing the magnetic field for a given number of ampere turns and to reduce the volume of the region occupied by the magnet stray field. A general layout of the magnet is shown in Fig. 1.2.

2.1.1. Iron Core

The iron yoke (see Fig. 2.1.1) will remain substantially the same, whatever type of coil is used. The two horizontal yokes [item (1)] of the magnet are spaced apart by means of four pillars (2) which are designed to withstand the weight of the iron and the attracting magnetic forces which are of the order of 4,000 tons. The top and bottom horizontal yokes are obtained by bolting together four iron slabs. The weight of each slab does not exceed 80 tons. In the horizontal yoke there is a rectangular window (3×1.5 m^2) to allow photographic operation of the spark chambers. The windows can be filled by removable pole pieces (4). The vertical yokes (3) are subdivided into a number of slabs (40 cm thick) which can be mounted in various positions along the perimeter of the horizontal yokes, so as to leave side apertures where required by the experimental needs. The total weight of the iron is approximately 1300 tons.

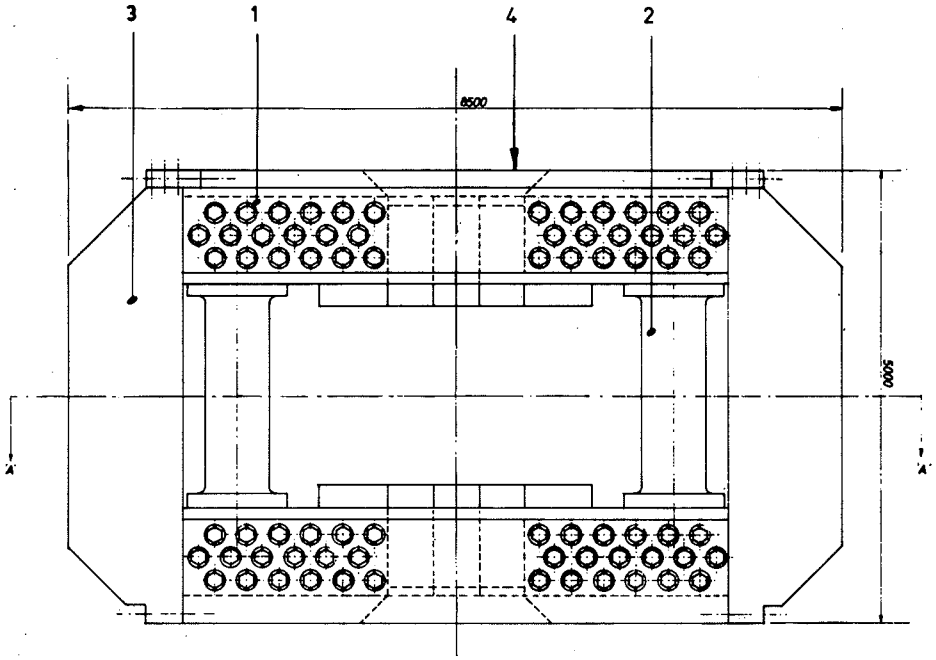

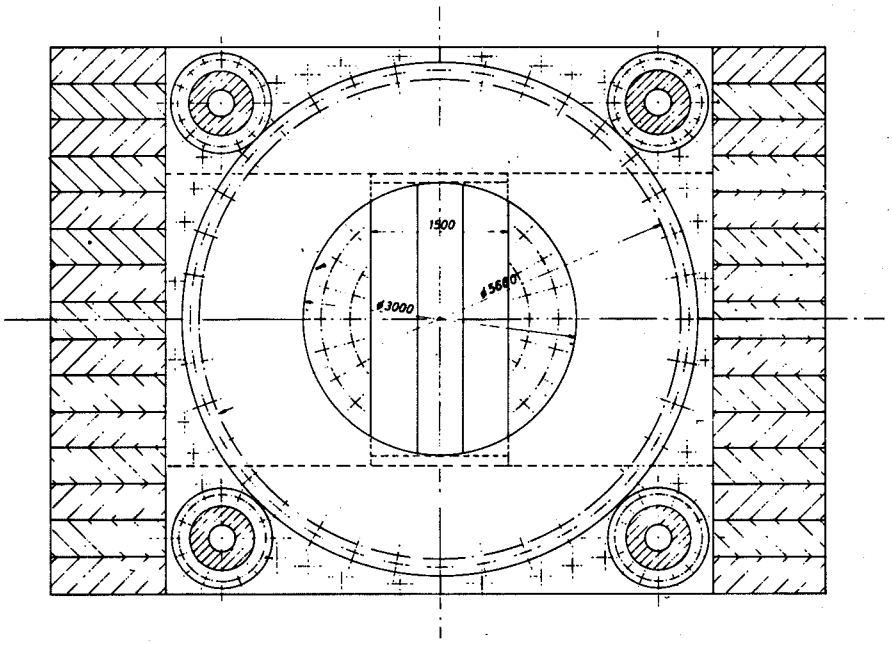

SECTION AA

IRON YOKE

FIG. 2.1.1

2.1.2 Superconducting coils

We are at present considering two possible designs of the superconducting coils. In both cases the coils will be fully stabilized by embedding the superconducting wires in a copper or aluminium substrate. Each coil will provide a maximum of 2×10^6 ampere turns. In the first solution the conductor (substrate + superconducting wire) will have the form of a ribbon, and the coils will be operated whilst completely immersed in a liquid helium bath.

In the second solution the conductor will be hollow and the cooling of the coils will be obtained by circulating supercritical helium (at a pressure of approximately 5 atm) through the hollow conductor. This second solution should allow a simpler and mechanically safer construction. However, a number of technical problems remain to be solved and an experimental investigation will be required.

A general layout of the magnet wound with hollow superconducting pipe is shown in Fig. 2.1.2.

In either case the coils will have to withstand very large vertical forces. In the present geometry, the direction of the vertical force (which will be approximately 2000 tons) will tend to push the coils against the iron yoke. Horizontal forces on the coils may be originated either by some asymmetry of the construction or by some other magnet or iron blocks installed in the neighbourhood of the Omega magnet.

The system by which the coils are clamped to the yoke is illustrated in Fig. 2.1.3. This clamping system will be capable of withstanding a vertical force of $\simeq$ 2000 tons and a horizontal force of 250 tons per coil.

The clamping system does not prevent the thermal contraction of the coils.

The heat losses through the clamping system will be approximately 100 W per coil.

The radiation losses will be $\simeq$ 25 W per coil. This value has been calculated assuming that the coils are insulated by a 3 cm thick layer of superinsulation and that there is no nitrogen shield. The current leads (there are two current leads per coil, each one carrying 5000 A)

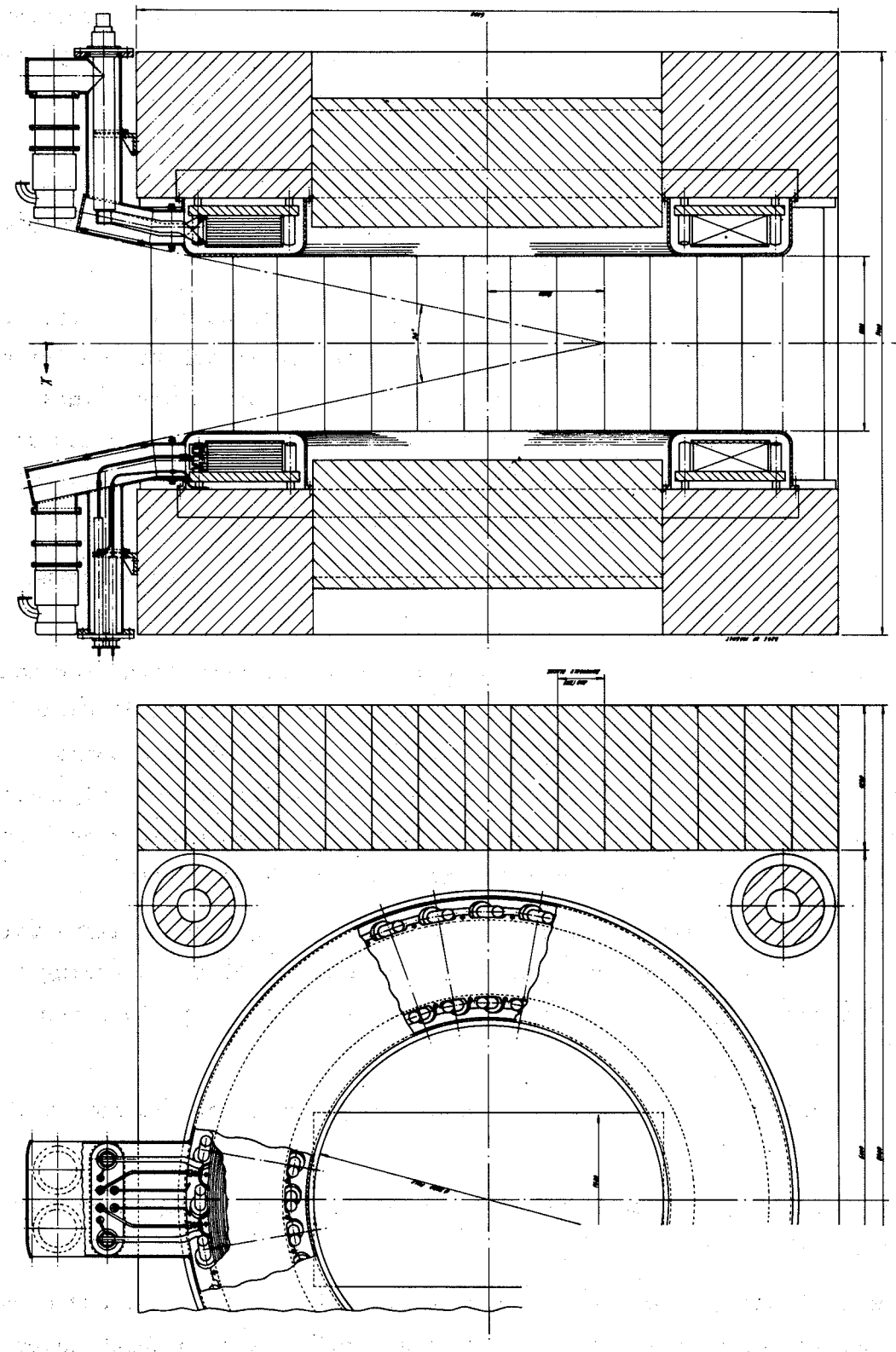

FIG. 2.1.2

GENERAL LAYOUT OF MAGNET - SUPERCONDUCTING COILS

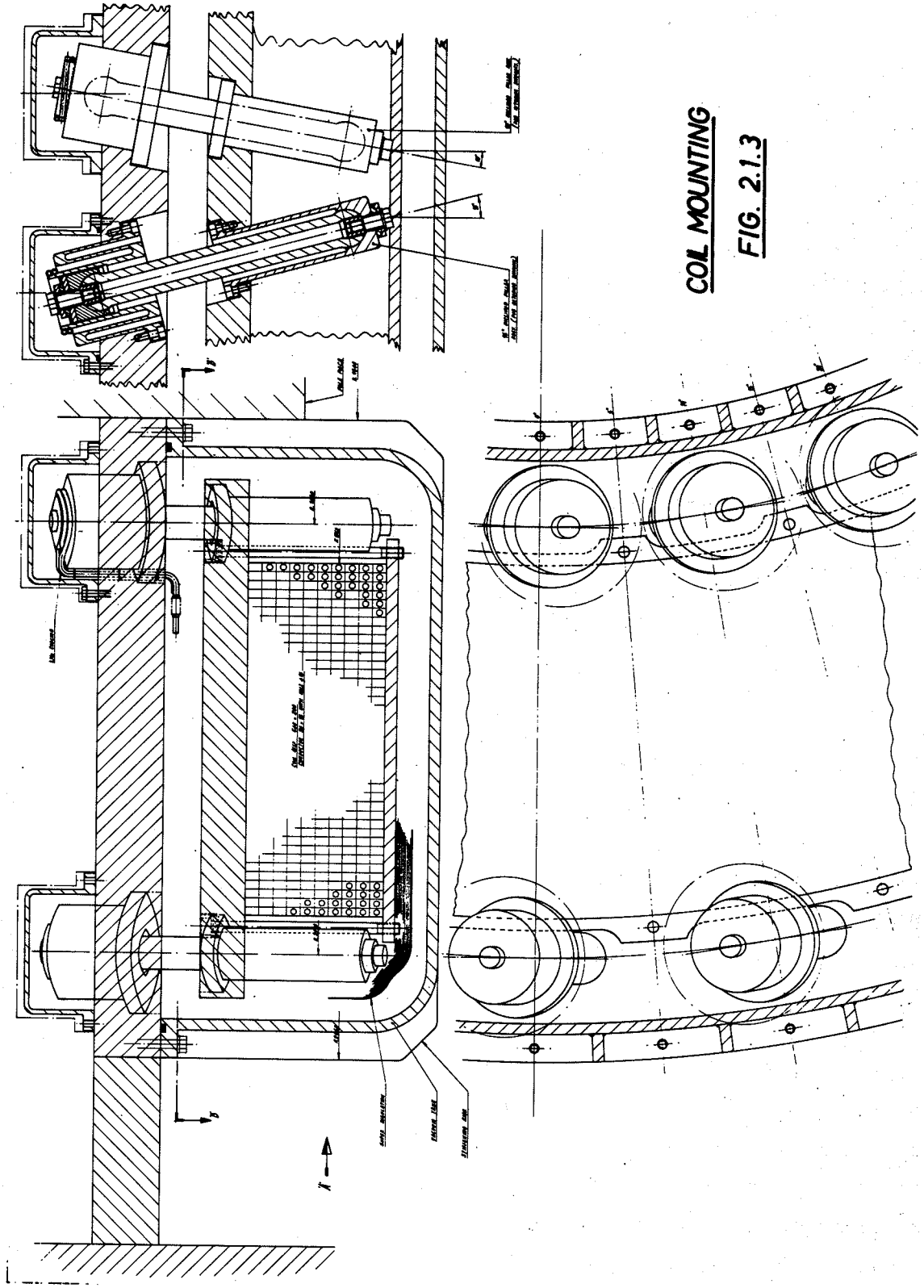

COIL MOUNTING

FIG. 2.1.3

will require a refrigeration capacity of $\simeq$ 75 W per coil. Taking into account a safety factor, we estimate that a refrigerator capable of supplying 750 W at 4.2°K would be sufficient (for both coils).

2.1.3 Conventional coils

The general layout of the magnet energized by conventional coils is given in Fig. 2.1.4.

Each coil consists of 10 simple pancakes wound with hollow copper conductor having a rectangular cross-section. Each of the pancakes, which are electrically connected in series, has two parallel water circuits. The total copper weight required for the two coils is approximately 85 tons.

The current is 10,000 A and the corresponding voltage (the two coils are connected in series) and power are 750 V and 7.5 MW. The magnet cooling will require a flow of 45 ℓ/sec of demineralized water at a pressure of 4 atm.

2.1.4 Field measurement for Omega magnet

The average accuracy for the field measurement should be better than 5×10^{-4}.

The Omega magnet yoke will be used in various configurations, according to the particular experimental requirements. The field is expected to vary correspondingly inside large limits. It is therefore important that the measuring equipment be capable of performing the complete field mapping in a reasonably short time. Apart from mechanical limitations, the rate of measurement is certainly limited by the minimum time required for conversion from analogue to digital, and particularly for the recording of the data (three field components and the space coordinates). Even using magnetic tapes to record the data, a reasonable rate seems to be not higher than 5-6 points/sec. The displacement speed of the field detectors will consequently depend on the density of points desired for the field mapping. This density may be determined as a function of the required accuracy and of the maximum estimated second derivative of the field. With 0.1% accuracy and estimating the highest (d^2B/dx^2) to approximately 2 gauss/cm^2, the minimum distance between two measured

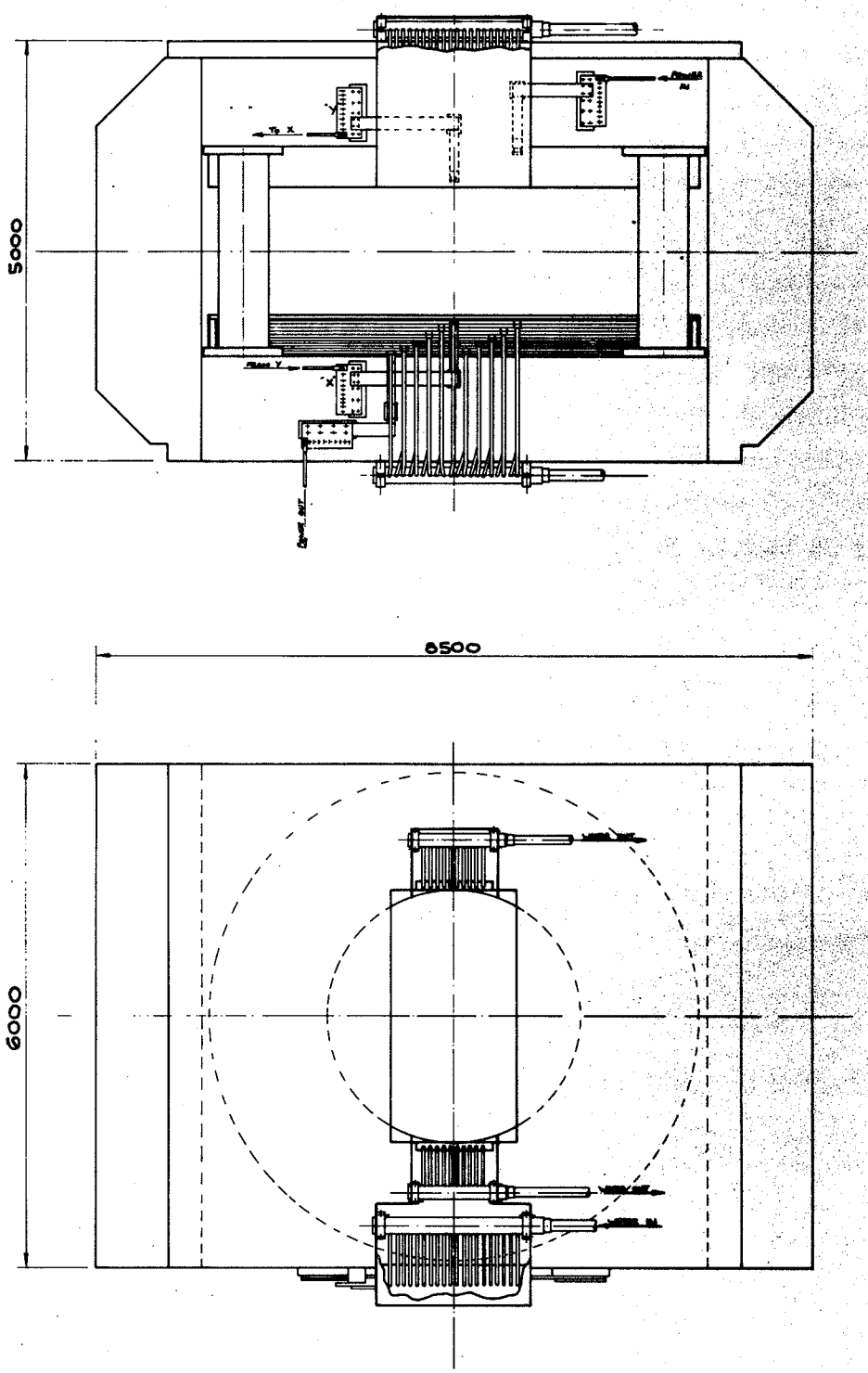

MAGNET WITH CONVENTIONAL COILS

FIG. 2.1.4

points will be about 5 cm. The whole system might be programmed to increase or decrease the density of measurement according to the gradient of the magnetic field. With this assumption it seems reasonable to take 1000 cm^3 as the average volume corresponding to one measure. Since the total volume to be mapped, inclusive of the useful and fringing field, totals 100 m^3, then for each yoke configuration and each excitation current one has to measure approximately 10^5 points. If we take into account that field mapping is normally needed at at least three different values of excitation current, this will result in 3×10^5 points to be measured for each yoke configuration. With a rate of 5 points/sec and a dead-time of 50% due to mounting, resetting, and checking operations between each set of measurements, a total mapping will require approximately 24 hours.

In order to have rough information on the field configuration and to allow a better magnet design, a reduced scale model (1:10) has been constructed. A general view of this model is shown in Fig. 2.1.5. The model magnet is energized by two conventional water-cooled copper coils and requires a power of about 0.7 MW.

In the model, as well as in the full-scale magnet, the top pole-piece is removable and the side yokes can be mounted in various positions.

Figures 2.1.6 and 2.1.7 give the results of preliminary magnetic measurements on the model.

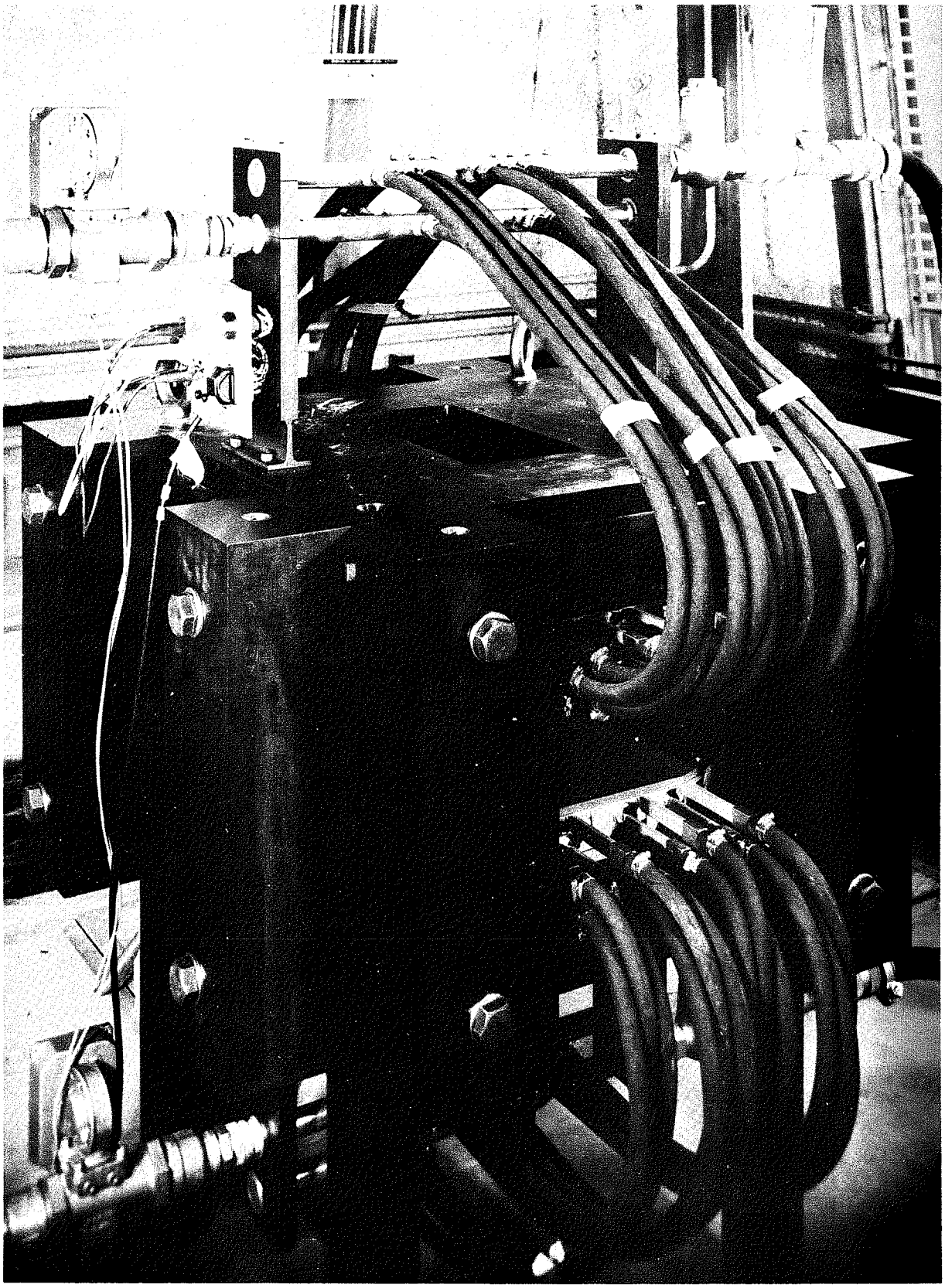

Fig. 2.1.5 Model magnet

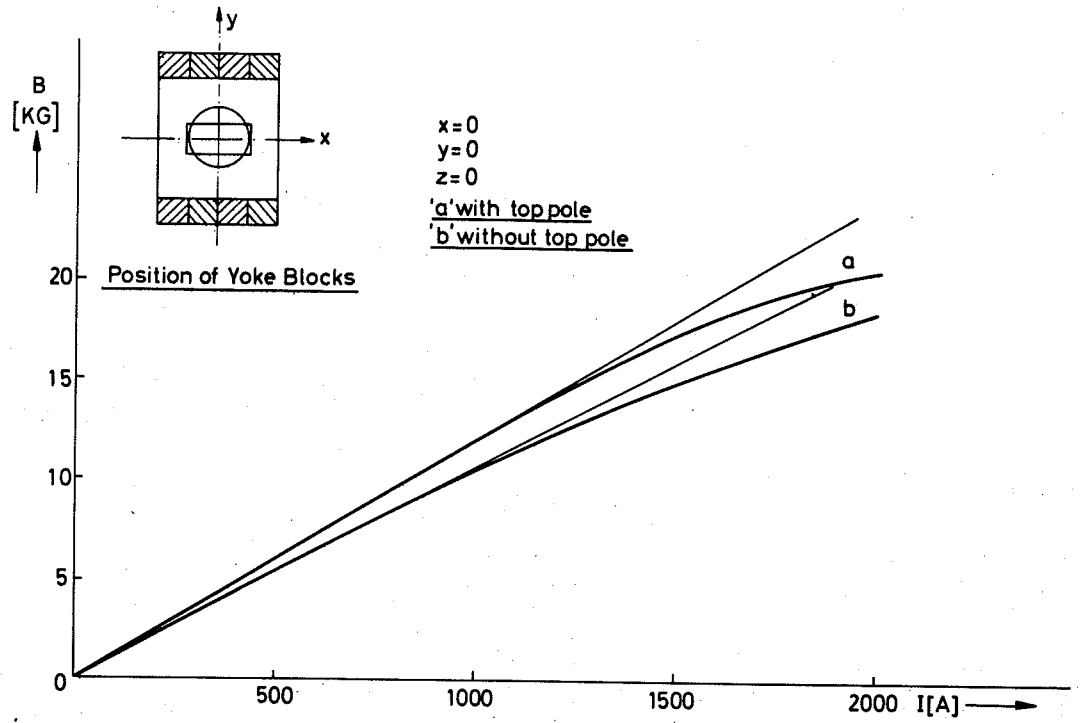

FIG. 2.1.6 MAGNETISATION CURVE FOR MODEL MAGNET

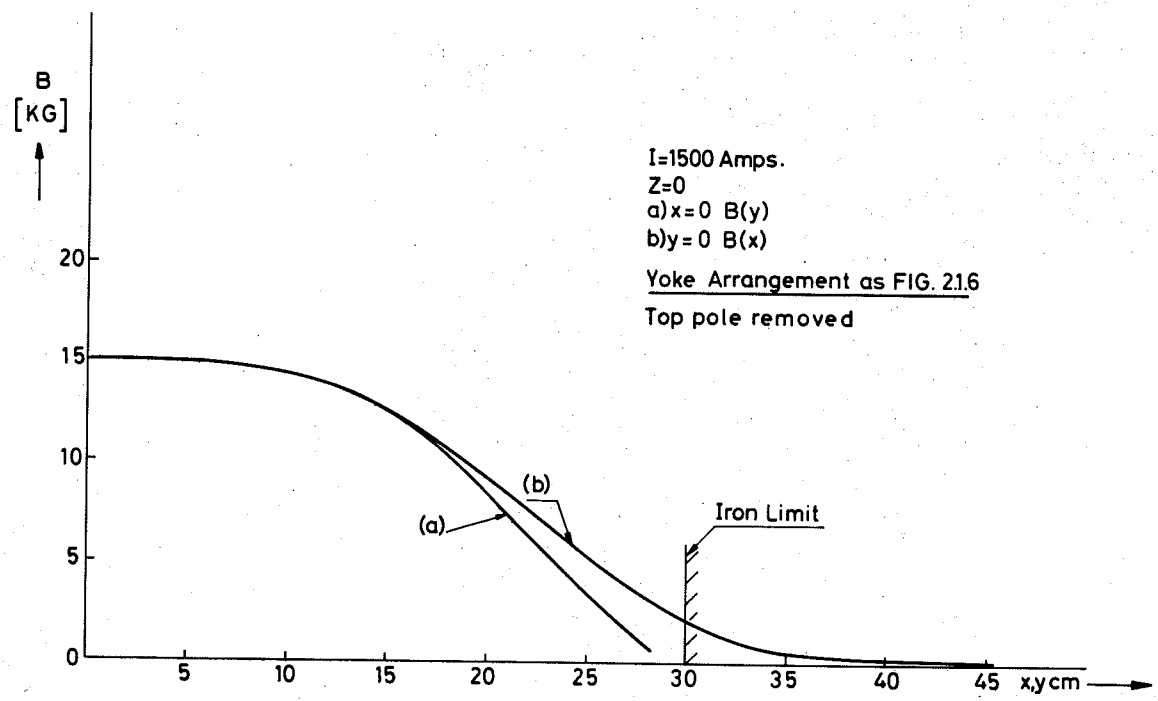

FIG. 2.1.7 FIELD SLOPE IN THE MEDIAN PLANE OF MODEL MAGNET

2.2 Spark chambers

2.2.1 Optical chambers and optics

2.2.1-1 Optical spark chambers. For optical spark chambers we have to consider the following types:

- sampling spark chambers; many gaps of $\approx$ 1 cm;
- wide-gap chambers, the spark follows the track up to a certain angle; gaps of 10 cm or more;
- isotropic streamer chambers, the track is displayed by localized streamers.

These chambers may be in plane, cylindrical, or other geometries, and contain opaque (foil) or transparent plates (wire mesh).

For the time being, we base the discussion on sampling spark chambers with opaque parallel plates. This very conservative approach results in an extrapolation of an existing magnet spark chamber (CERN-ETH-IC Group). We can therefore give reasonably safe predictions on the feasibility of chambers and optical system, accuracy in track parameter measurement, and scanning and measuring problems. Obviously, the system described here is not optimal for all experiments, and sufficient flexibility must be built into the camera and the HPD measuring technique in order to cope with other, more complicated, chamber arrangements.

2.2.1-2 Spark chamber arrangement. A possible arrangement is shown in Fig. 2.2.1. All gaps are perpendicular to the beam direction except for two gaps on one side of the system which are parallel to the beam. The gap width is 1 cm. The frames holding the foils may be chosen to be 1.5 cm thick. It is reasonable to arrange the spark chamber in the form of units of, say, 10 gaps each. Each unit has its own housing, consisting of a metal frame and mylar windows, and this housing is filled with the spark chamber gas. The width of each unit would amount to about 30 cm. Ten units could be mounted in the visible region of the magnet. This would result in a total number of 100 gaps or 200 foils on 3 m length. The spark chamber frames should be as thin as possible on one side in order to allow low-momentum particles to leave the spark chamber at the side to be used for triggering. A "typical event" is shown in Fig. 2.2.1.

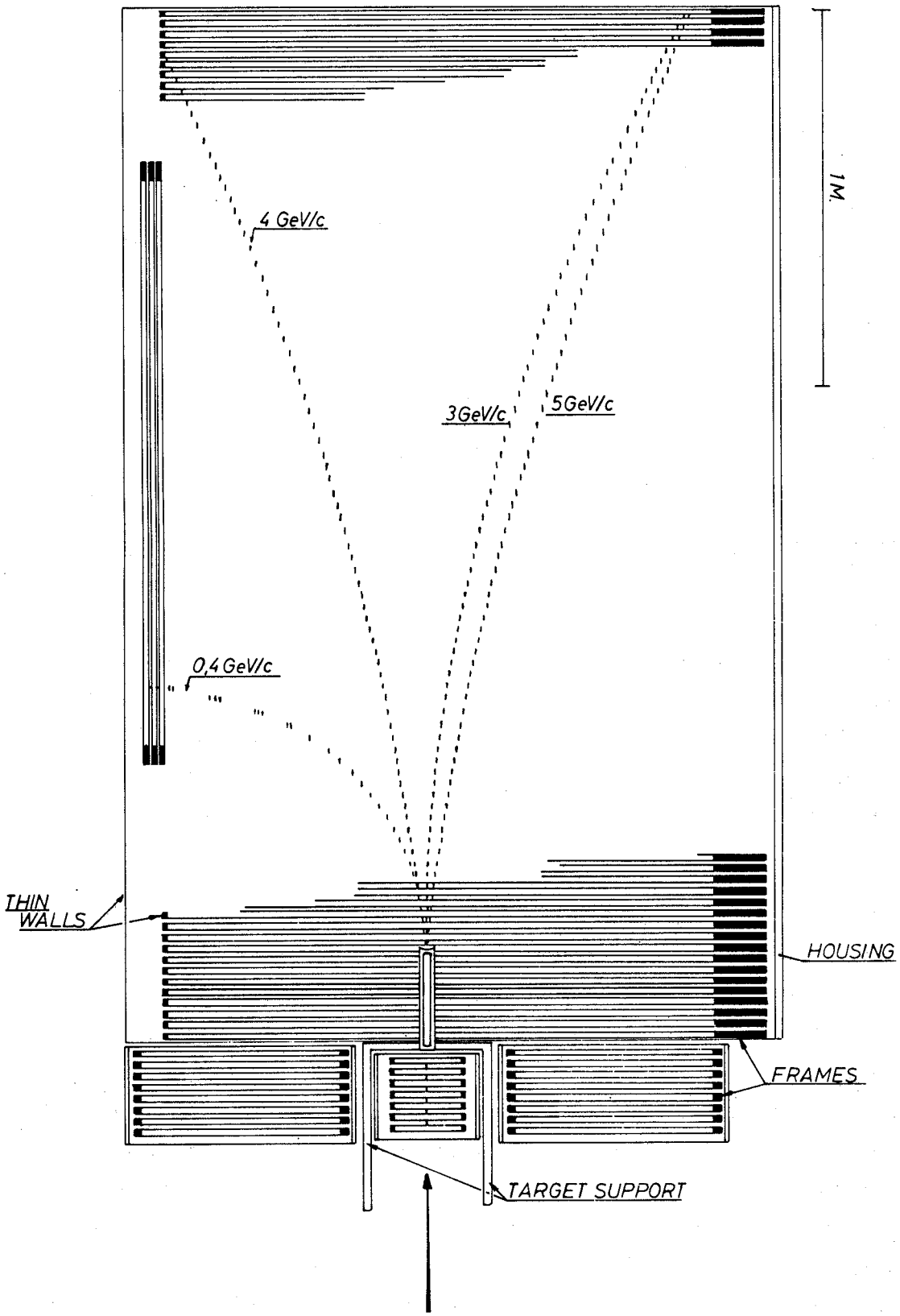

FIG. 2.2.1. TOP VIEW OF TARGET & SPARK CHAMBER

The material of the spark chambers should be kept to a minimum. Aluminium foils of 25 μ thickness are commonly used. Thinner foils, e.g. 10 μ, would be preferable and are being tested. Taking into account the contributions of the aluminium in the foils, the neon in the gaps, and the mylar foils, one finds for the radiation lengths L_o

$$25\ \mu\ \text{Al}: \quad L_o = 44\ \text{m}\ ,$$
$$10\ \mu\ \text{Al}: \quad L_o = 86\ \text{m}\ .$$

Any system of spark chambers (also wire) with planes oriented in more than one direction calls for some supporting structure inside the active volume. A very light one is proposed by G.L. Schnurmacher*). These Al/plastic-foam/Al sandwiches have a radiation length corresponding to 50μ Al. A system with a minimum of material near the target is obtained if the target is located inside a cylindrical hole in the spark chamber plates. It has been found that the foils stay flat if a hole is cut with appropriate care, for example by galvanic etching.

Particle trajectories turning parallel to the spark chamber planes are still quite well recorded in a sampling spark chamber, but the resolution is poorer. Since the particles in question generally have low momentum, a large relative momentum error results in a moderate error in the over-all momentum balance. Typical pictures taken with the existing spark chamber system are shown in Fig. 2.2.2 ($\pi^- p \to K^o \bar{K}^o n$) and Fig. 2.2.3 (six-prong event).

2.2.1-3 Optical system. This spark chamber system inside the magnet has to be photographed from the top with small-angle stereoscopy. In the case of parallel plates, a cylindrical lens of some kind is needed to bend the light from the sparks, emitted parallel to the plates, into the camera lenses. We believe that a system with a prism for each gap is simpler and more accurate than other solutions (mirrors, cylinder lens, etc.). Machining and polishing perspex prisms to the tolerances required seems to be just at the limit of the state of the art.

---

*) G.L. Schnurmacher et al., UCRL 17947.

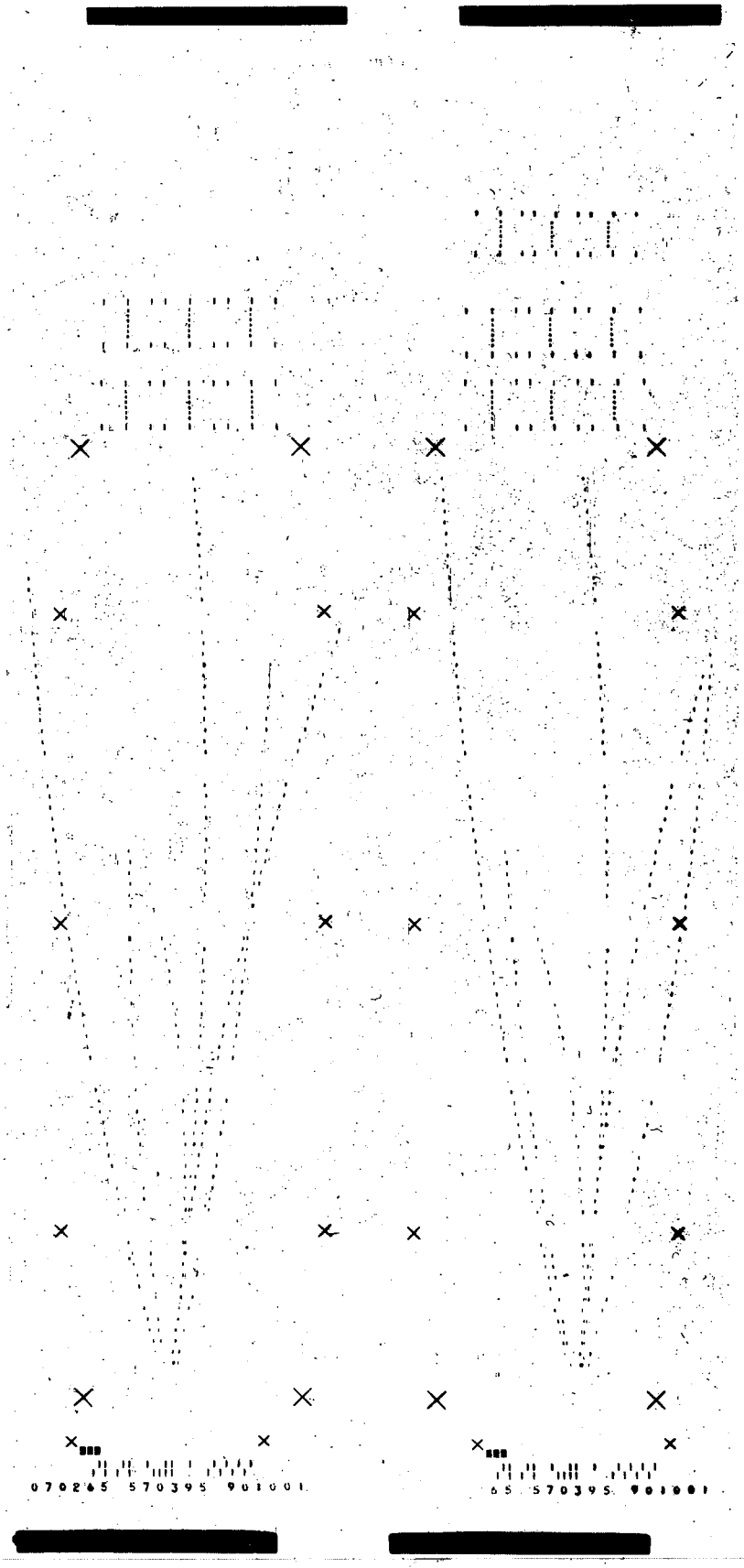

Fig. 2.2.3 Six-prong event taken with the existing magnet spark chamber

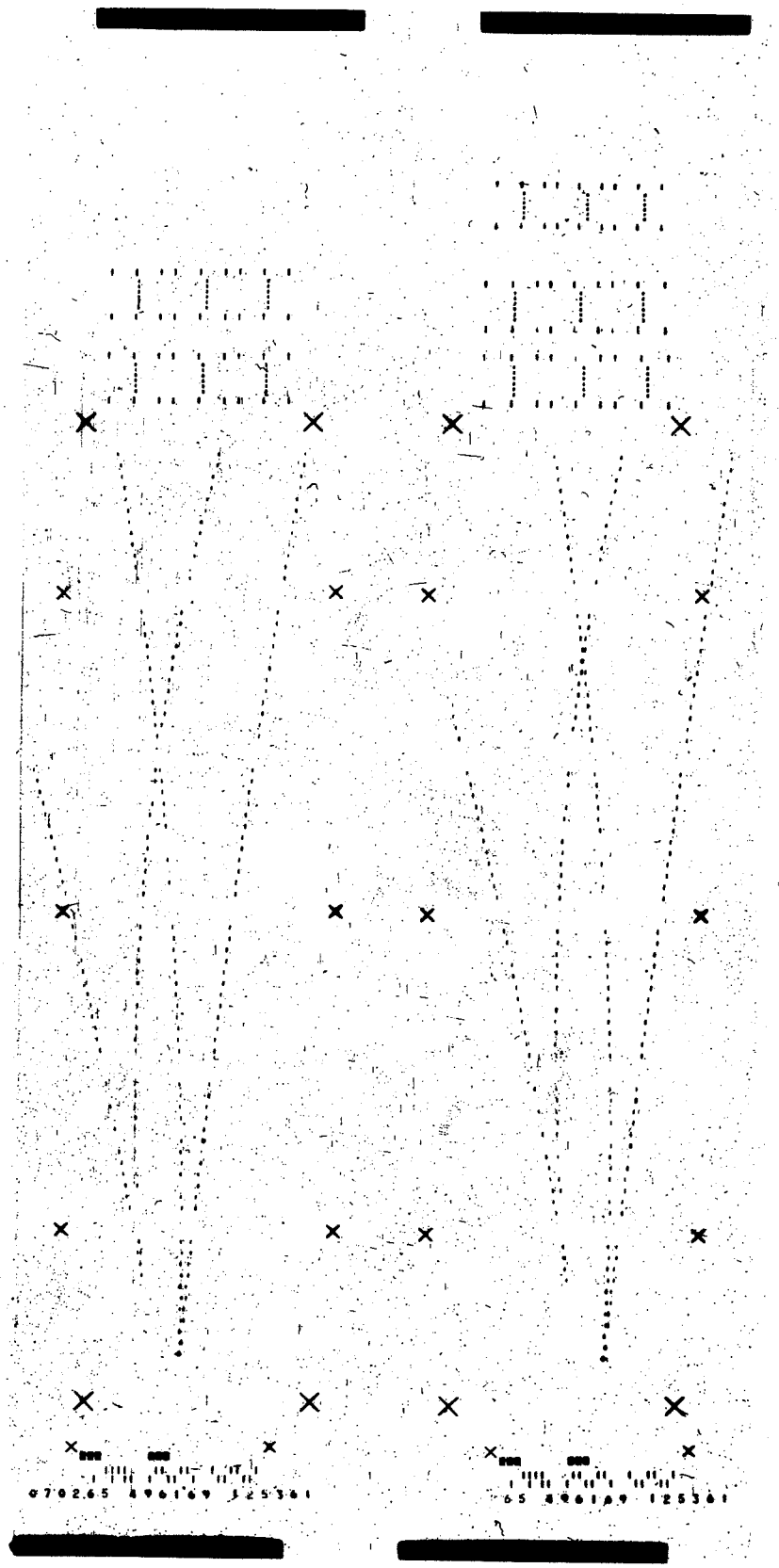

Fig. 2.2.2 $\pi^- p \rightarrow K^o \bar{K}^o n$

Picture taken with the existing magnet spark chamber (CERN-ETH-IC group)

The light paths are shown in Figs. 2.2.4 and 2.2.5. We propose to use 70 mm film (future standard perforation) and put the two stereo views side by side. This choice poses some problems for HPDs outside CERN that are designed for the 50 mm film of the 2 m CERN-HBC. However, 70 mm film is also foreseen for the 3.5 m CERN-HBC. Possible parameters of the optical system are:

- Optical distance to beam height	5 m
- Stereo angle	17°
- Proportionality constant for depth measurement	$dz/d(y_2 - y_1) = 3.5$
- Demagnification	m = 50
- Focal length of lenses	10 cm
- Width of spark image on film	0.04 mm
- Length of spark image on film	0.2 mm at centre 0.15 mm at far end
- Two images $30 \times 60\ mm^2$ side by side on film, frame length	$\approx$ 8 cm.

A larger stereo angle could be reached by reducing the optical distance. This would increase the variation of the spark-image length and the systematic errors of the prism system. In the proposed system these errors introduce a maximum apparent shift of spark position of 0.95 cm along the beam line. The corresponding sparks will be photographed after one reflection by a chamber plate surface; no appreciable error in position is introduced.

2.2.1-4 Spatial resolution. The r.m.s. spark position fluctuation in small-gap chambers is known to be somewhat less than 0.2 mm. Optical system and measurement should introduce only smaller errors. In the existing magnet spark chamber the combined random errors of optics and measurement are 0.09 mm in space*).

This may be looked at as a 5% error in centring on the width of a spark, and might be explained entirely by the non-uniformity of spark shapes. Under this assumption, about 0.1 mm of random error would also be expected in the proposed chamber, since the variation of spark shape

---

*) Astbury et al., Nucl.Instr.and Methods 46, 61 (1967).

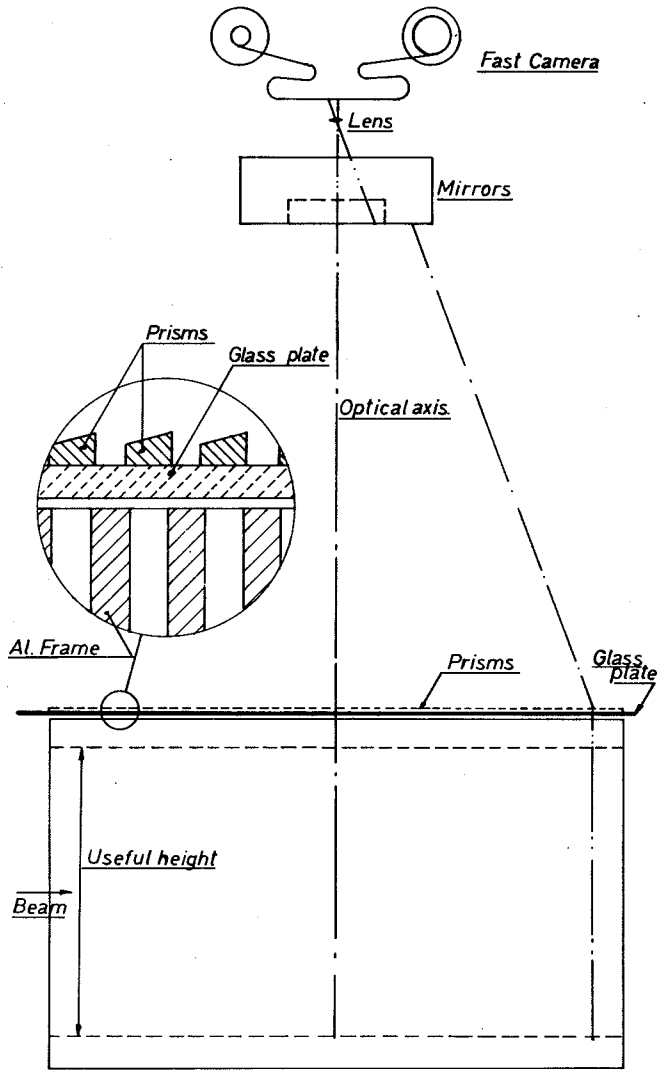

OPTICAL SYSTEM, SECTION ALONG BEAM. FIG. 2.2.4

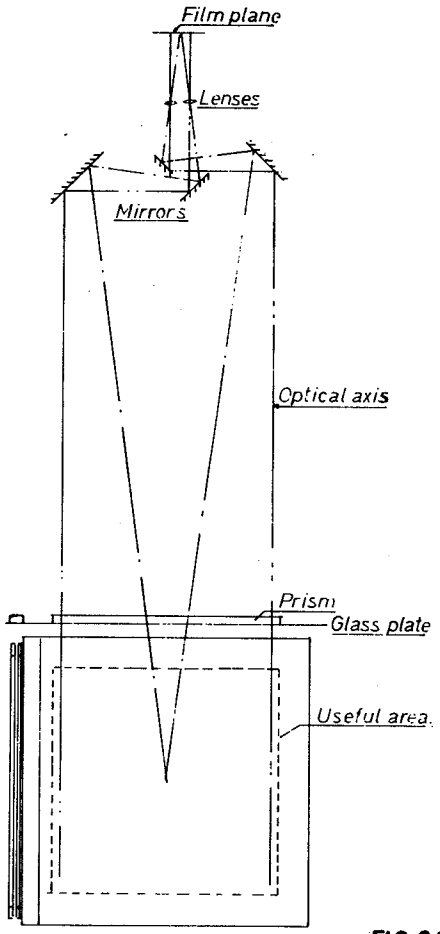

FIG. 2.2.5.

OPTICAL SYSTEM, SECTION ACROSS BEAM DIRECTION

is unlikely to change with the size of the chambers. This assumption gives a lower limit. An upper limit of 0.2 mm is obtained if this random error is thought to come from any combination of

- imperfections of optical surfaces (prisms);
- film resolution;
- HPD resolution

which would all increase with the linear dimensions, the picture size being kept constant. It seems unlikely that the error will be mainly due to film and HPD resolution (4μ on film). One can therefore hope to approach the 0.1 mm random error due to measurement and optics, provided the mirror and prism surfaces are sufficiently good.

The larger demagnification might create some problems of contrast due to the variation of spark brightness; however, the difficulties appear less severe than those met with in a large bubble chamber.

2.2.1-5 Alternative version of spark chamber arrangement.

Figure 2.2.6 shows an arrangement of spark chambers with the gaps being inclined out of the vertical position so as to see from the camera the whole volume of the gaps without the aid of optical prisms. Each spark chamber gap is still formed by two parallel plates (foils), but the frames between each two adjacent spark gaps are wedge-shaped.

Again, each ten gaps form one of a series of units, each one being equal to the other. The units are mounted at different angles of inclination to the vertical. Twelve units can be mounted in the visible region of the magnet. The maximum visible track length in beam direction in the medium plane is thus increased to 3.6 m. This fact, and the avoidance of the large number of precisely machined prisms, are the advantages of this version of spark chamber arrangement.

2.2.2 Wire spark chambers

As an alternative to optical spark chambers, digitized wire spark chambers can be used in the Omega magnet. The problems connected with the read-out of wire chambers within a strong magnetic field are discussed in Section 4.1. As shown there, one can hope that by using improved techniques it will be possible to achieve the same momentum resolution as with optical systems.

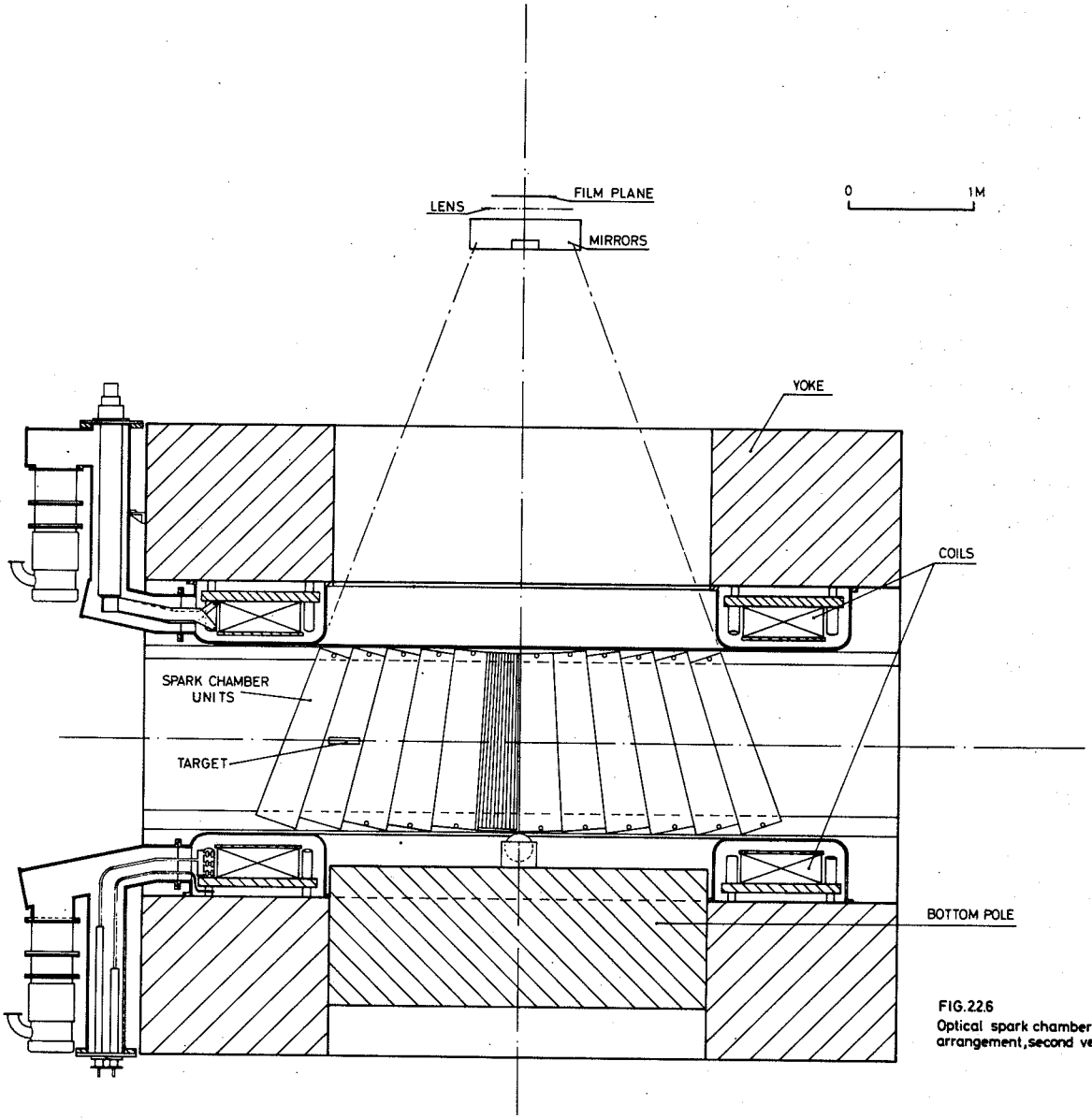

FIG.22.6
Optical spark chamber arrangement, second version

In general, a wire chamber arrangement offers the advantages of higher data-taking rate and of on-line control of the experiment. The data-taking rate is limited by the read-out time, which will be about 5 msec for 200 wire chamber planes of 1.5×1.5 m^2 (3×10^5 wires).

If one assumes that the average number of sparks per gap and event -- including beam tracks and spurious sparks -- is seven, then the on-line computer has to store 1400 coordinates per event. For a maximum of 50 events per burst this means the storage of 70K words per burst. Each word has to contain the coordinate value in one wire plane of one spark. Associated with a group of words containing the coordinate information of all sparks in one plane, the address of that plane has to be stored as an extra word. The minimum word-length depends on the kind of position quantization produced by the read-out technique. The position quantization is half the wire spacing if it is due to the wire structure of the chamber plane itself (core read-out or electronic read-out). In the case of magnetostrictive or "sparkostrictive" read-out (Section 4.1), the quantization is due to the clock giving the timing signals for the delay-time measurement. The timing resolution should not influence the total spark position resolution of the chamber, and must therefore be higher than the delay which corresponds to half the wire spacing. The number of timing signals for a chamber length of 1.5 m shall be assumed to be 7500, which corresponds to 13 bits. Thus a standard 16-bit word-length will in any case be sufficient. Therefore a 70K-word, 16-bit or 35K, 32 bit input buffer memory has to be used for the on-line computer.

Further computer requirements are discussed in Section 2.5.

2.3 Beam layout

To make the best use of the Omega apparatus, beams with high momentum resolution, good intensities, and large momentum range are needed. A possible design of two beams covering different energy ranges and satisfying these requirements is shown schematically in the optical diagrams of Fig. 2.3.1.

The features of these two beams are the following:

	High-energy beam	Medium-energy beam
Maximum momentum	24 GeV/c	8 GeV/c
Angular acceptance	10^{-4} sr	4×10^{-4} sr
Production angle	0 - 20 mrad	0 - 50 mrad
Momentum bite	± 2%	± 2%
Momentum resolution	± 0.05%	± 0.1%
Total length of the secondary beam	≃ 140 m	≃ 70 m
Bending magnet length required	≃ 14 m	≃ 7 m
Quadrupole magnet length required	≃ 18 m	≃ 14 m

The high-energy beam is a four-stage beam; the first two stages are intended to provide momentum selection and reduction of background; the third stage is used to perform momentum analysis; the fourth one compensates the momentum dispersion and matches the beam to the experiment target.

The medium-energy beam has only three stages. Actually, the first stage provides momentum selection and sufficient background reduction, so that in the second stage the momentum analysis can be performed.

In both beams the momentum analysis is done by means of a rather large bending (8° in the h.e. beam and 10° in the m.e. beam) and of three hodoscopes (A,B,C). Hodoscope B is placed in a position where in the analysis plane an optical image of A is formed. Hodoscope C, which should provide only a very rough resolution, is used to divide the angular acceptance of the beam and thus reduce the errors due to chromatic aberrations. To achieve the desired momentum resolution, hodoscopes A and B should provide

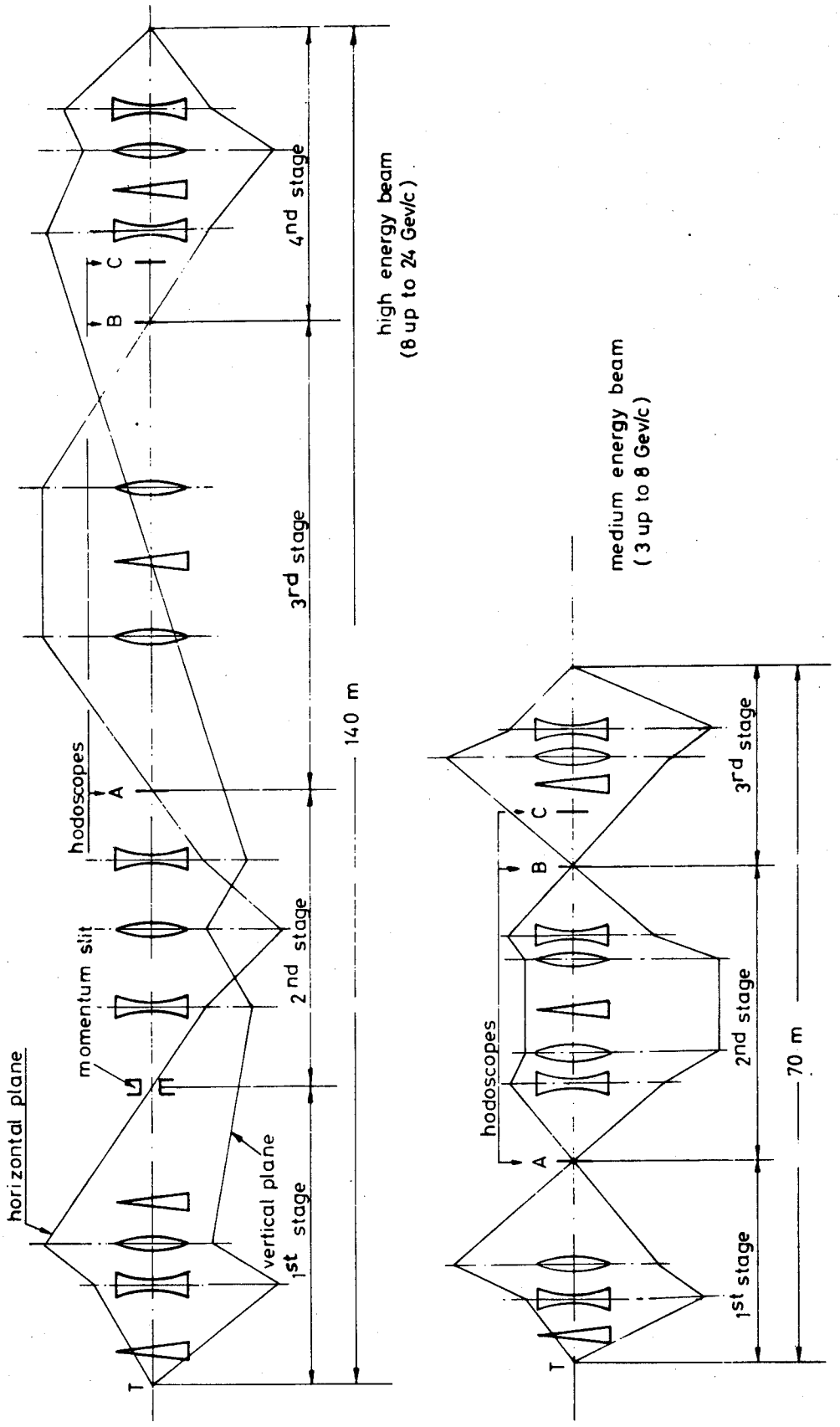

Fig. 231 Optical diagrams of high momentum resolution beams

a space resolution of about 1.5 mm for the first beam, and about 3 mm for the second one. Multiple scattering in the three hodoscopes does not, in practice, influence the precision of measurements.

The expected intensities at the end of the two beams can be deduced by the curves shown in Fig.2.4.15, taking into account the appropriate solid-angle acceptances and path length of the two beams.

Figure 2.3.2 shows a general layout of possible counter beams in the West Hall. The two high-resolution beams described above are shown to supply the Omega area as well as a possible lower energy separated beam (below 3 GeV/c). Because of the different beam lengths, different targets have to be located along the proton line. This line crosses the whole West Hall and starts at the far end of the switch yard, making an angle of 10° with the bubble chamber proton line, which runs along the building. It must be noticed that the beams for the Omega will be deflected also vertically to compensate for the difference in level between the Omega medium plane and the proton lines (0.5 - 1 m).

A possible improvement in the Omega exploitation of beams could be achieved by mounting long-pulse RF mass separators in the beam.

RF separators with a duty cycle matched to an electronics experiment could speed up considerably the experiments with particles that are a minority in the beam [see Section 4.3].

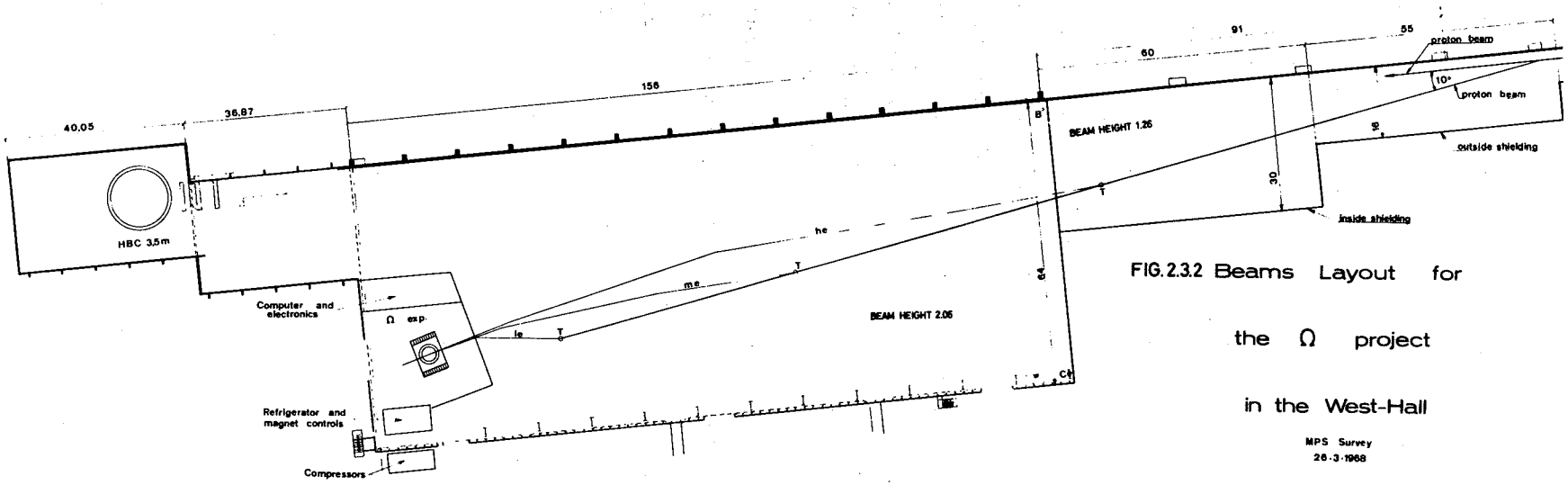

FIG. 2.3.2 Beams Layout for the Ω project in the West-Hall

MPS Survey
26.3.1968

2.4 Beam intensities and data-taking rate

The purpose of this Section is to estimate the rate of events to be analysed per year and the corresponding beam intensities required.

As it will be shown below, the results of this estimate depend on various assumptions about the operation of the PS, the beam, the spark chamber system and about the type of experiment performed. We will, therefore, present first a list of all the assumptions made (Section 2.4.1), we will then describe briefly the way the calculations have been carried out (Section 2.4.2), and finally we will discuss the results (Section 2.4.3).

2.4.1 The assumptions made can be listed as follows:

PS and beam operation

Some of the parameters assumed are:

i)	PS energy	19.2 GeV	19.2 GeV	25 GeV
ii)	Beam pulse	0.2 sec	0.5 sec	0.2 sec
iii)	PS cycle	1 sec	1.5 sec	2 sec

Further parameters are:

iv) A PS running efficiency of 50% due to machine maintenance

v) A beam halo of 0% to 100% *)

vi) A beam attenuation of 10% in the target and possibly in counters surrounding the target. This attenuation is responsible for the accidental interactions (see below).

---

*) A beam halo of 100% means that the beam which traverses the spark chamber has twice the intensity of the beam focused in the beam telescope.

2.4.2 By using the above assumptions the estimate is performed through the following calculations.

Firstly, the number of triggers recorded per PS cycle is calculated on the assumption of an exponential distribution of the time intervals between two subsequent triggers for a given dead-time [Section 2.4.1, point (ix)]. Secondly the efficiency for having a "useful trigger" is calculated [see Section 2.4.1, point (xiii)]. This efficiency is then used to obtain from the total number of triggers the number of useful triggers recorded per PS cycle.

Finally from these values we estimate the rate of events per year to be measured by making assumptions on various PS and data-taking efficiencies [Section 2.4.1, points (xiv) and (xv)].

2.4.3 The results are presented in Figs. 2.4.1 to 2.4.14. Figure 2.4.1 shows the number of triggers recorded per PS cycle as a function of the trigger level for different values of the spark chamber system dead-time. For a given value I of the beam intensity the trigger level scale has to be multiplied by the factor $I/1.6 \times 10^6$ to obtain the appropriate number of triggers. For the following calculations only the two cases of 0.01 and 0.05 sec dead-time have been considered.

Figure 2.4.2 shows the efficiency for "useful triggers" [as defined by Section 2.4.1, point (xiii)] as a function of the beam intensity. Various cases are considered according to the assumptions made on beam pulse, beam halo, unprotected and protected spark chamber plates [see Section 2.4.1, points (ii), (v), (x) and (xi)].

Figures 2.4.3 to 2.4.6 show the number of "useful triggers" recorded per PS cycle as a function of beam intensity.

Figures 2.4.7 to 2.4.10 show the maximum number of "useful triggers" recorded per PS cycle and the corresponding optimum beam intensities as a function of trigger level.

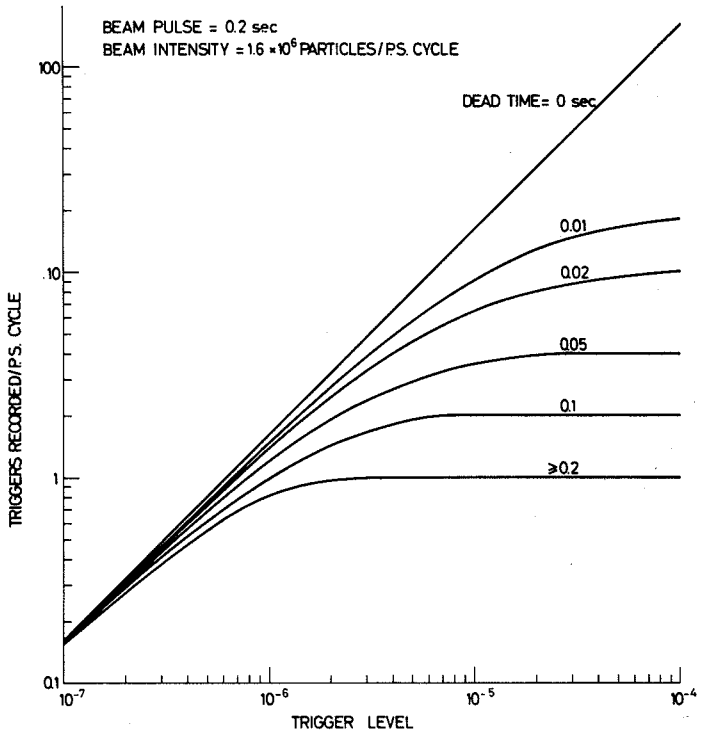

FIG. 2.4.1

LOSSES DUE TO ACCIDENTAL PARTICLES
INT. (B.) = ACCIDENTAL INTERACTIONS (BEAM PARTICLES)
INT.' (B.') REFERS TO 100% BEAM HALO
—— 0.2 sec BEAM PULSE
---- 0.5 sec BEAM PULSE

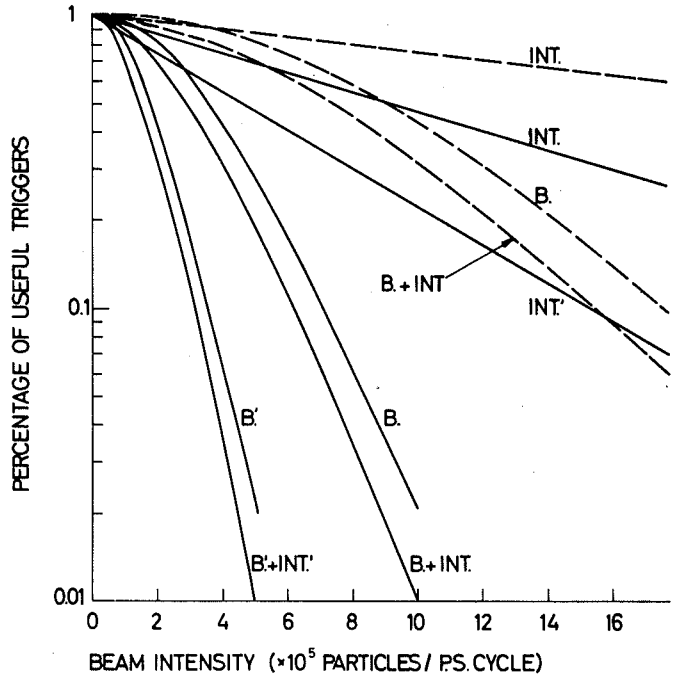

FIG. 2.4.2

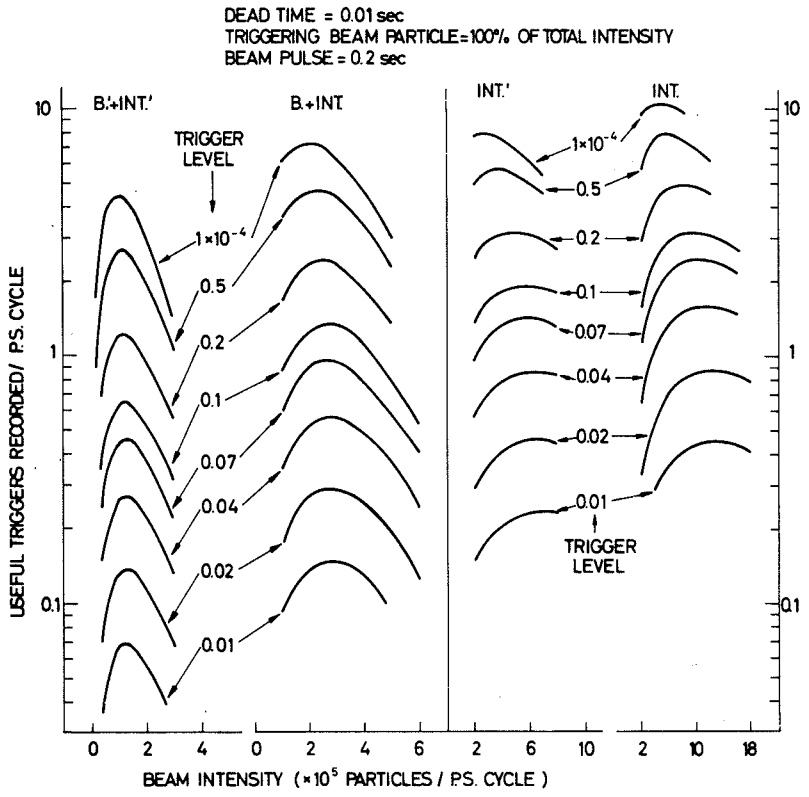

FIG. 2.4.3

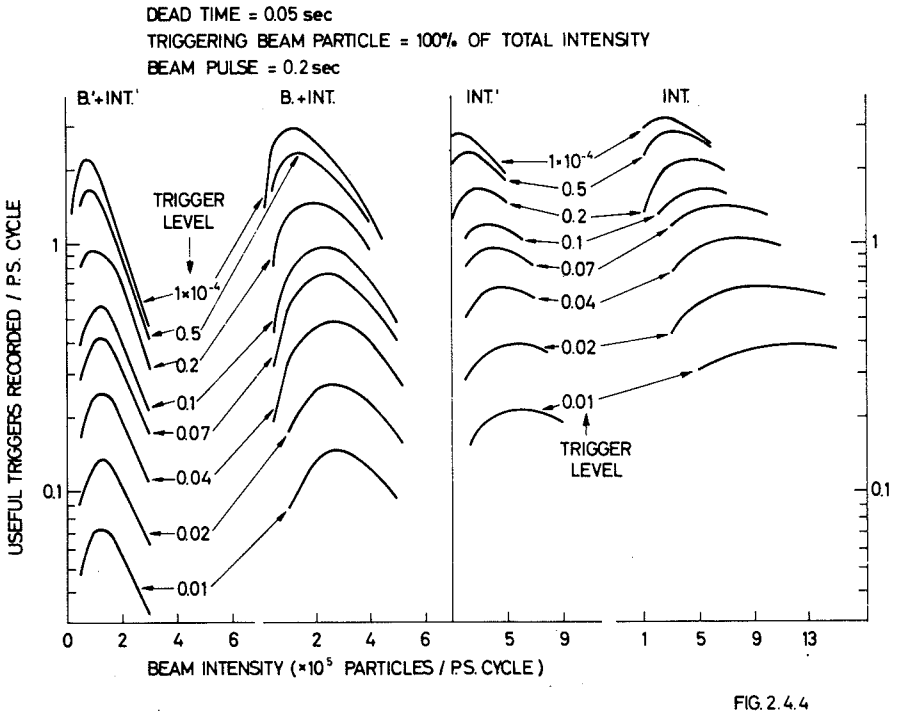

FIG. 2.4.4

DEAD TIME = 0.01sec —— AND 0.05sec – – –

TRIGGERING BEAM PARTICLE =1% OF TOTAL INTENSITY

BEAM PULSE = 0.2 sec

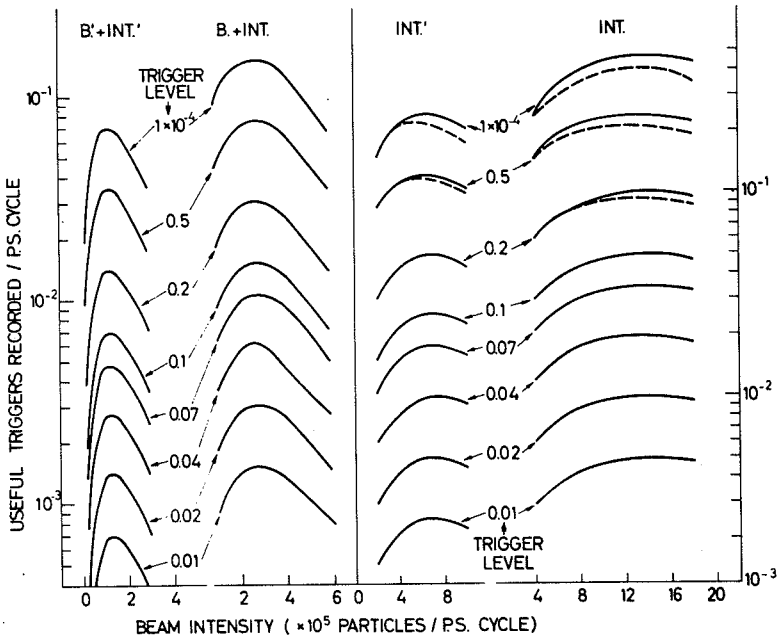

FIG.2.4.5

DEAD TIME = 0.05 sec

TRIGGERING BEAM PARTICLE = 100% OF TOTAL INTENSITY

BEAM PULSE = 0.5 sec

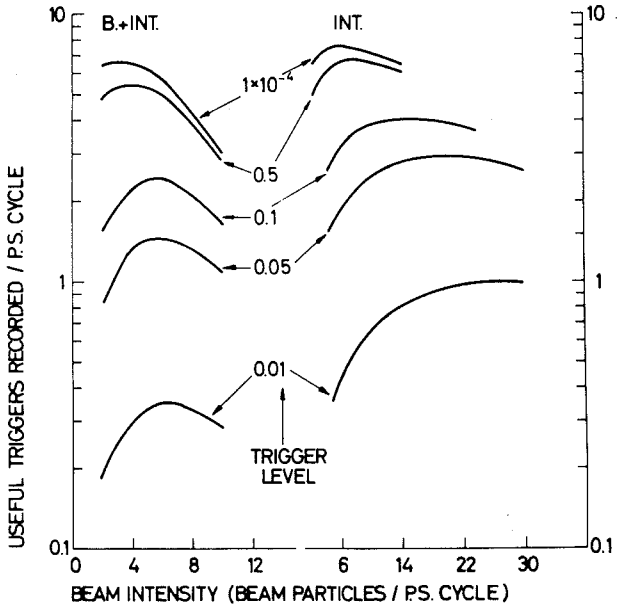

FIG. 2.4.6

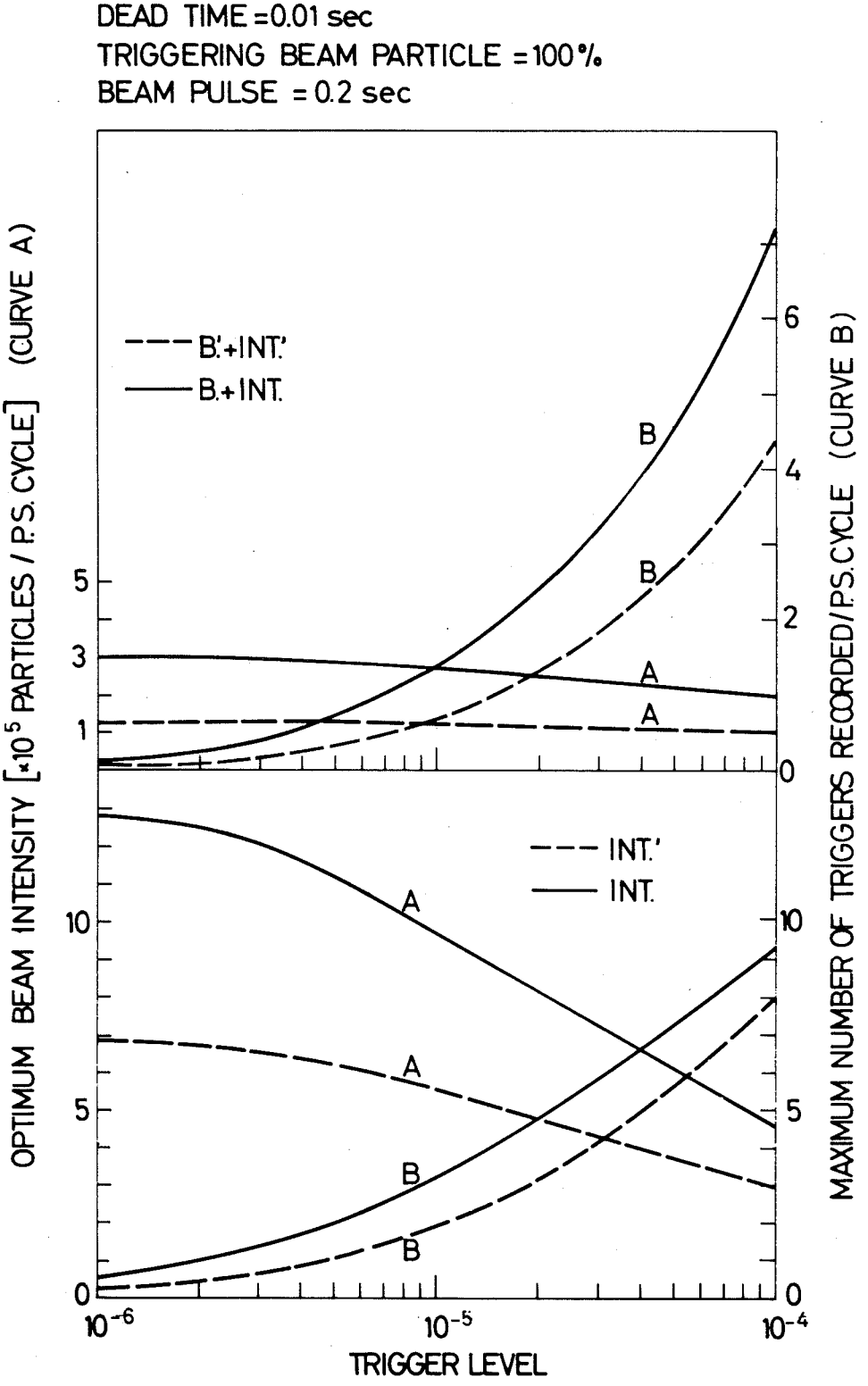
DEAD TIME = 0.01 sec
TRIGGERING BEAM PARTICLE = 100%
BEAM PULSE = 0.2 sec
B'.+INT.'
B.+INT.
INT.'
INT.
A
B
OPTIMUM BEAM INTENSITY [×10⁵ PARTICLES / P.S. CYCLE] (CURVE A)
MAXIMUM NUMBER OF TRIGGERS RECORDED/P.S.CYCLE (CURVE B)
TRIGGER LEVEL
10⁻⁶
10⁻⁵
10⁻⁴

FIG. 2.4.7

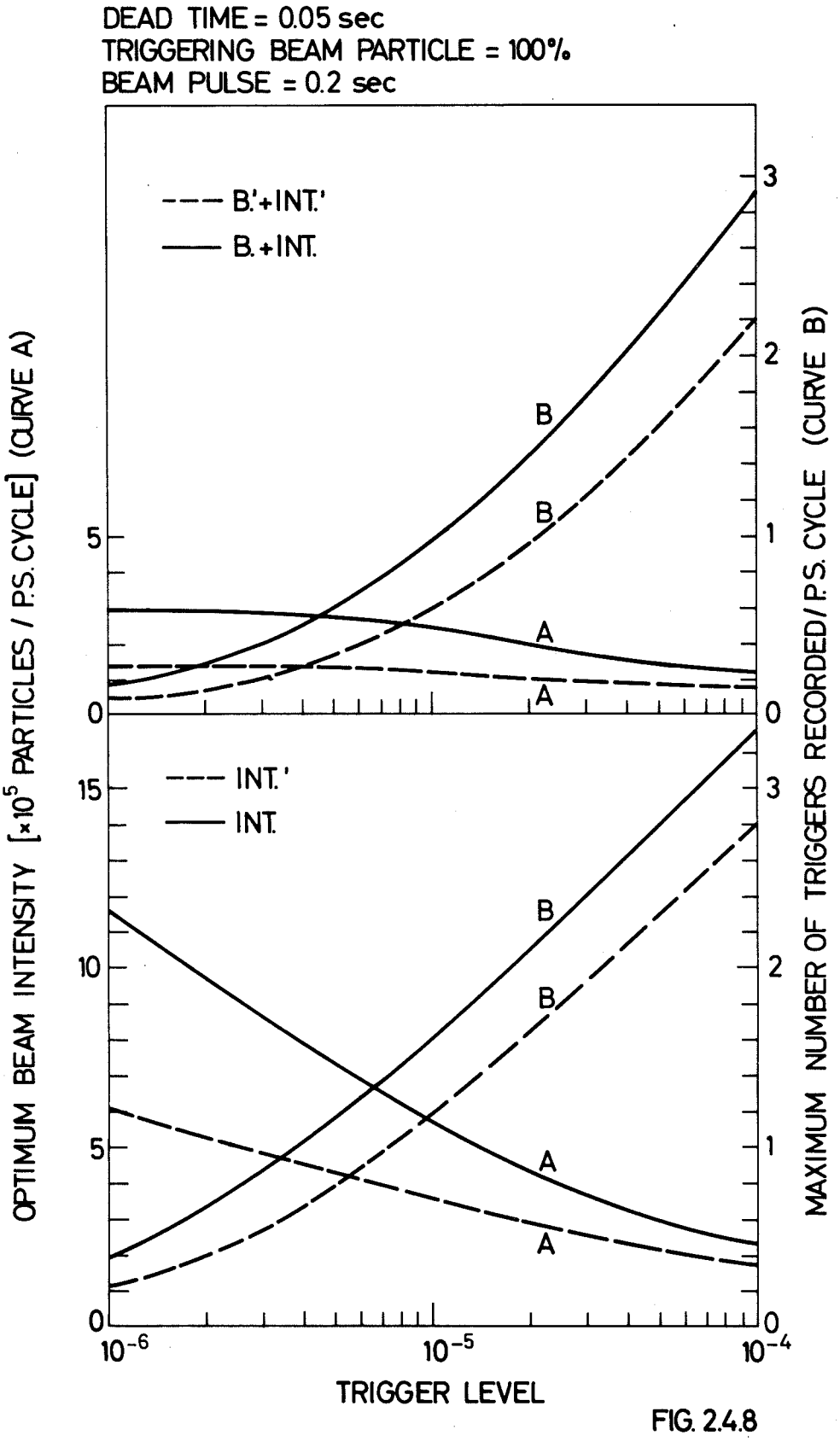
DEAD TIME = 0.05 sec
TRIGGERING BEAM PARTICLE = 100%
BEAM PULSE = 0.2 sec
B.'+INT.'
B.+INT.
INT.'
INT.
B
B
A
A
B
B
A
A
OPTIMUM BEAM INTENSITY [×10^5 PARTICLES / P.S. CYCLE] (CURVE A)
MAXIMUM NUMBER OF TRIGGERS RECORDED/P.S. CYCLE (CURVE B)
TRIGGER LEVEL
10^-6
10^-5
10^-4
0
5
15
10
1
2
3

FIG. 2.4.8

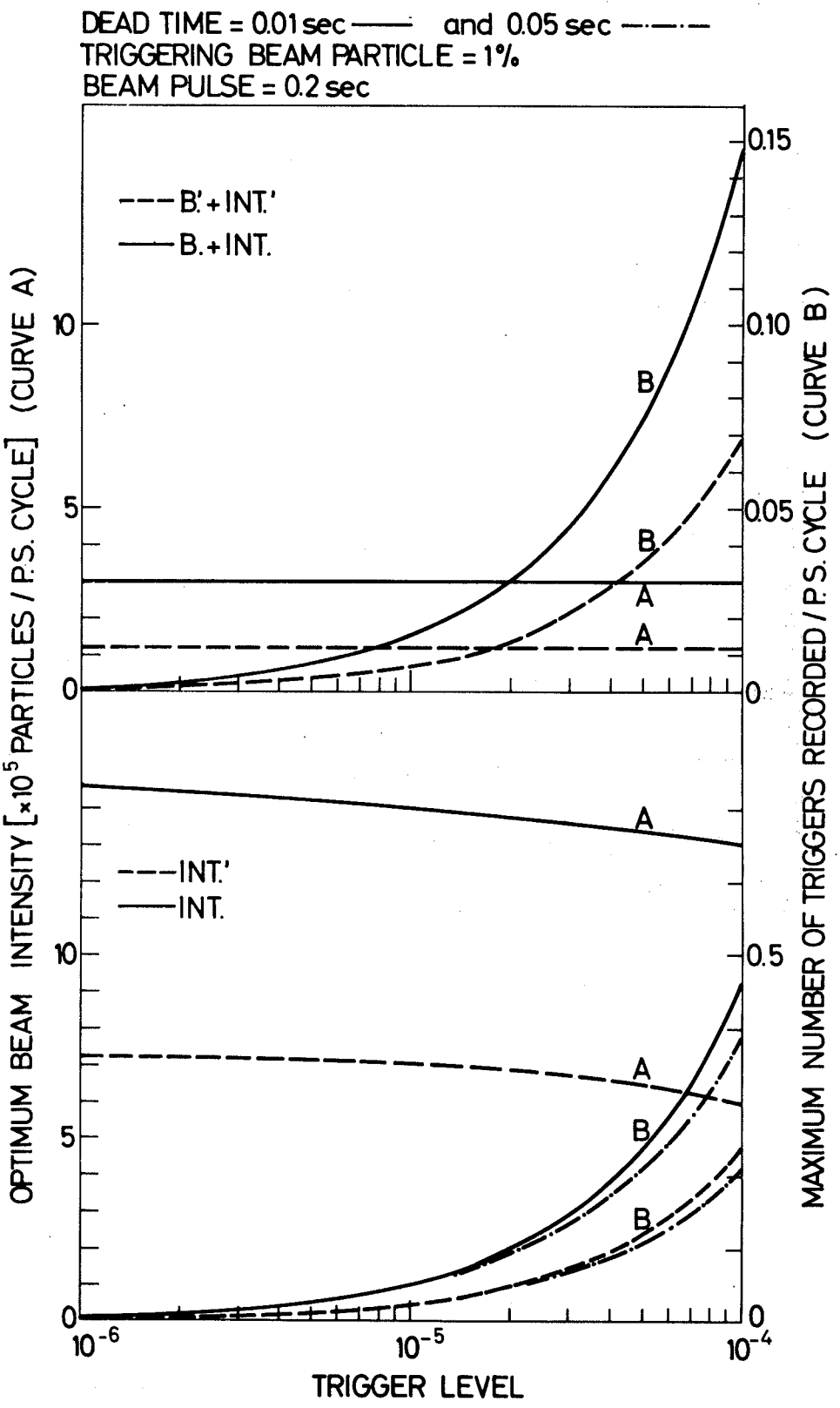
DEAD TIME = 0.01 sec —— and 0.05 sec —·—·—
TRIGGERING BEAM PARTICLE = 1%
BEAM PULSE = 0.2 sec
---B'.+INT.'
——B.+INT.
---INT.'
——INT.
OPTIMUM BEAM INTENSITY [×10^5 PARTICLES / P.S. CYCLE] (CURVE A)
MAXIMUM NUMBER OF TRIGGERS RECORDED / P.S. CYCLE (CURVE B)
TRIGGER LEVEL
10
5
0
10
5
0
0.15
0.10
0.05
0
0.5
0
10^-6
10^-5
10^-4
A
B

FIG. 2.4.9

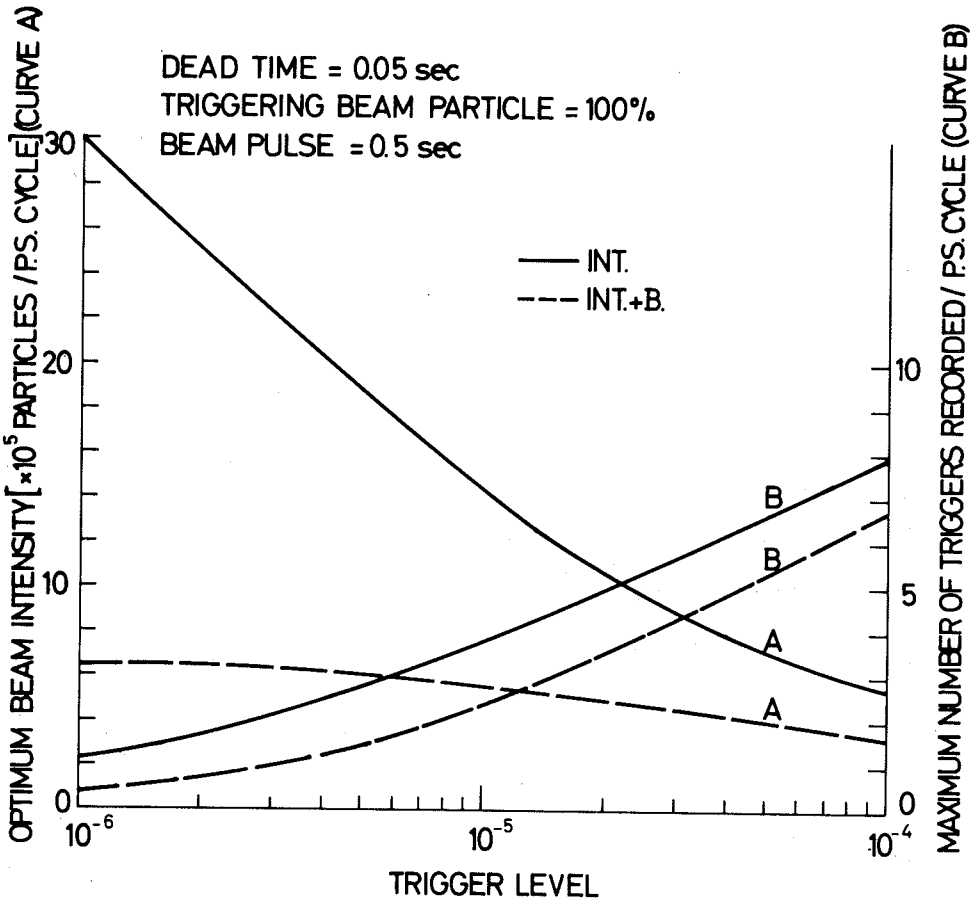
DEAD TIME = 0.05 sec
TRIGGERING BEAM PARTICLE = 100%
BEAM PULSE = 0.5 sec
INT.
INT.+B.
OPTIMUM BEAM INTENSITY [×10⁵ PARTICLES / P.S. CYCLE] (CURVE A)
MAXIMUM NUMBER OF TRIGGERS RECORDED / P.S. CYCLE (CURVE B)
TRIGGER LEVEL
30
20
10
0
10
5
0
10⁻⁶
10⁻⁵
10⁻⁴
A
A
B
B

FIG. 2.4.10

Finally Figs. 2.4.11 to 2.4.14 show the estimate of the number of events to be analysed per year as a function of the trigger level.

The parameters used in Figs. 2.4.3 to 2.4.14 are summarized in the following table:

Figure No.	Dead-time	Wanted beam particles	Beam pulse
2.4.3, 7, 11	0.01 sec	100%	0.2 sec
2.4.4, 8, 12	0.05 sec	100%	0.2 sec
2.4.5, 9, 13	{0.01 sec {0.05 sec	1%	0.2 sec
2.4.6, 10, 14	0.05 sec	100%	0.5 sec

The results displayed in Figs. 2.4.11 to 2.4.14 occasion the following remarks.

a) There are two main sources of large variations on the rate of recorded triggers to be measured: the trigger level and the percentage of wanted beam particles. As the trigger level goes from 10^{-4} to 10^{-6} or the percentages of wanted beam particles change from 10 to 100% the trigger rate changes by factors of 10 to 100. Consequently, the trigger rate depends on the type of experiment. Therefore it is difficult to make very definite predictions on the amount of triggers to be analysed per year.

As an example, in the case of the optical spark chamber operation one can estimate an average of 4×10^6 useful triggers to be analysed per year for a trigger level of 10^{-5} [i.e. 10 μbarn cross-section for 25 cm of liquid H_2 target and 100% detection efficiency or 1000 μbarns cross-section and 10^{-2} detection efficiency].

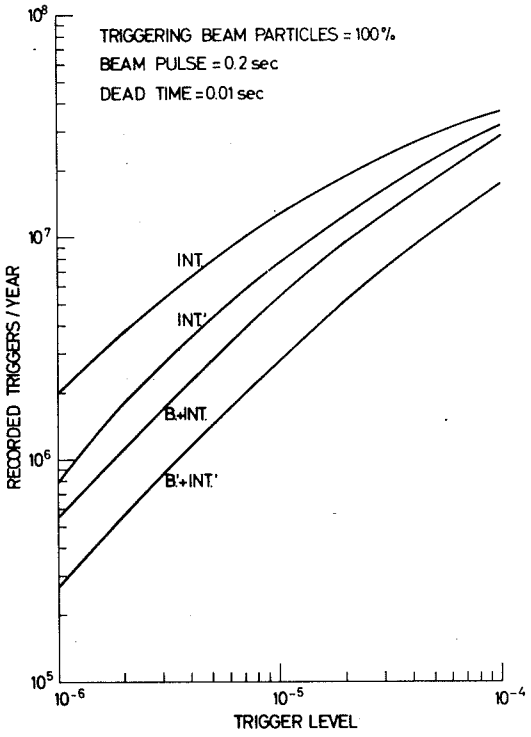

FIG. 2.4.11

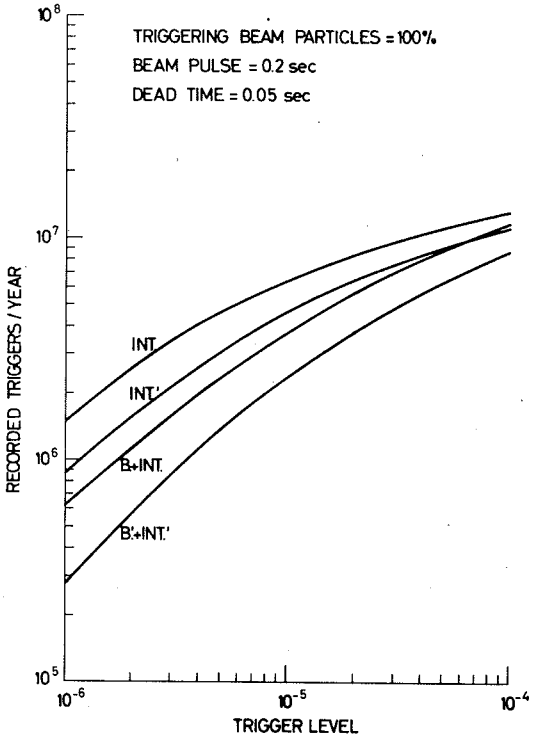

FIG. 2.4.12

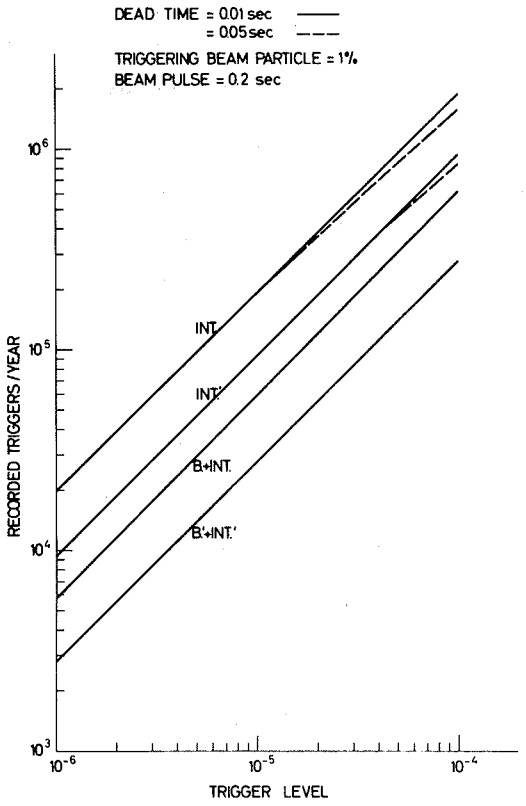

FIG. 2.4.13

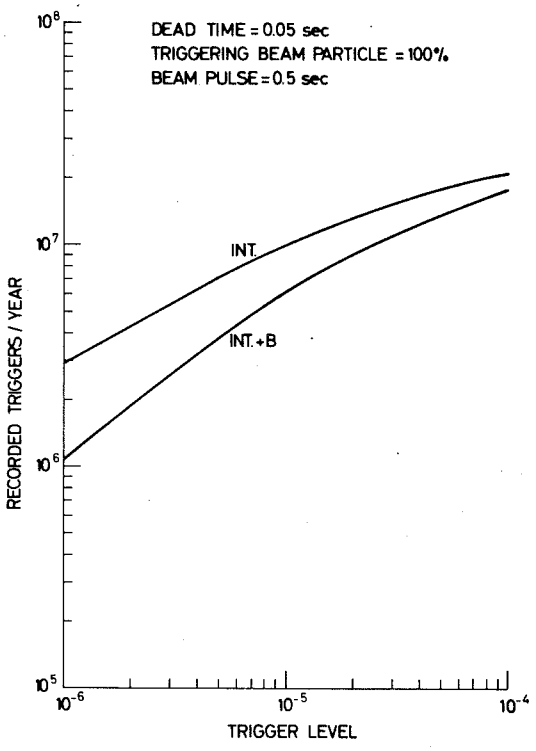

FIG. 2.4.14

b) There are still several possibilities of improving the triggering rate, namely:

Beam pulse: an improvement of a factor of ~ 2 can be obtained going from 0.2 to 0.5 sec.

Beam halo: an improvement of a factor of ~ 2 going from 100% to 0% beam halo.

Dead-time: an improvement of a factor of 1.5 to 3.5 can be obtained as the dead-time goes from 0.05 to 0.01 sec.

Protection of spark chamber plates (in the region traversed by the beam): again a factor of ~ 2 improvement can be obtained with respect to the case of unprotected plates.

c) The intensities which are required will be available for the designed beams as is shown in Fig. 2.4.15.

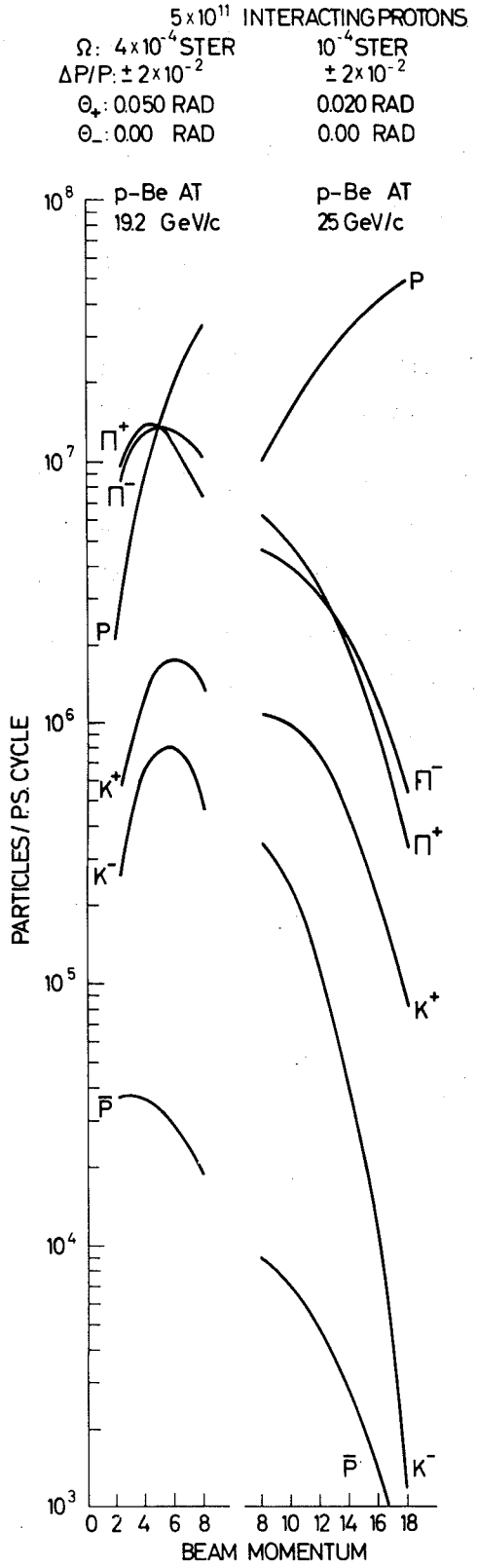
5 x 10^11 INTERACTING PROTONS
Ω: 4 x 10^-4 STER
ΔP/P: ± 2 x 10^-2
Θ+: 0.050 RAD
Θ−: 0.00 RAD
10^-4 STER
± 2 x 10^-2
0.020 RAD
0.00 RAD
p-Be AT 19.2 GeV/c
p-Be AT 25 GeV/c
PARTICLES / P.S. CYCLE
BEAM MOMENTUM
P
Π+
Π−
K+
K−
P̄

FIG. 2.4.15

2.5 Data-handling facilities

2.5.1 General specifications

During the foreseeable lifetime of the Omega project, two types of detector are going to be operated inside the magnet, i.e. optical and wire chambers. Hence the data-handling system should provide for the evaluation of both film and filmless data. It is difficult to predict the relative weights of the two techniques as a function of time; it is likely that both modes will coexist for a good fraction of the Omega lifetime.

However, it seems reasonable to assume that switching over from one mode to the other will not occur too frequently for reasons of efficiency (say, once a year). Of the total amount of data produced by the Omega in any one year, only a relatively small fraction ought to be fully analysed at CERN. The corresponding computing requirements have to be taken into account in designing the data-handling system, together with sufficient extra capacity for carrying out sample computations on the experimental data to be processed outside CERN. Also, some computer capacity should be foreseen for the development of any data-handling technique related to the Omega project. Finally, the system capacity should be determined by present knowledge and plausible estimates, whilst still ensuring that there are possibilities for expansion, if necessary.

2.5.2 Basic assumptions

In order to specify the data-handling requirements in some detail, it is necessary to make a set of hypotheses related to the data production of the Omega project.

i) Beam use - Data will be taken during 25% of the total time, i.e. $\approx$ 2000 hours/year.
Approximately 4×10^6 PS bursts per year will be exploited to record experimental data. The assumed beam characteristics are: 2 sec cycle and $\approx$ 300 msec flat top.

ii) Trigger rates

	Dead-time	Max. triggers/ burst	Average No. of triggers/ burst over one year
a) Optical chambers	50 msec	5 - 6	3
b) Wire chambers	5 msec	50 - 60	15

One also assumes that the ratio of triggers to good events to be analysed will be about 3, on the average.

In the film mode, events will generally be selected by manual scanning, while in the filmless mode the reduction will be performed automatically. Some 20% of the triggers should be rejected on-line, the rest off-line.

iii) Information format

a) Film : 70 mm film; two views recorded on a single 60 × 70 mm^2 frame.

b) Filmless : Half-inch tapes; one trigger will give a maximum of 2000 16-bit words, but an average of only 1200-1400 words.

iv) Maximum total annual production

a) Film $\simeq$ 12 million pictures, yielding 4 million events to be measured;

b) Filmless $\simeq$ 60 million triggers, yielding 50 million raw-events on tape, yielding

$\approx$ 20 million good events to be analysed.

Incidentally, film will be used at a rate of 10 frames/metre and tapes at a rate of 3000-4000 triggers/tape.

For 50 million wire chamber events, at least 15,000 magnetic tapes will be needed.

v) CERN quota

a) Film : Production measurement and full analysis of ≈ 1 million events (≈ 25% of the total). The measurement would be well within the capacity of one "HPD-2" flying-spot digitizer.

b) Filmless : Full analysis of 5 million triggers or 2 million events (≈ 10% of the total) and -- to control the experiments -- a sample evaluation of a few per cent of all events to be processed outside CERN, including test runs.

In both modes of operation an important allocation of the data-handling facilities should be made for development work.

2.5.3 Characteristics of the system

One can distinguish three stages in the data-processing chain:

STAGE I : data acquisition by a computer from an on-line HPD or an on-line experiment;

STAGE II : data reduction performed by automatic pattern recognition programs;

STAGE III: geometrical reconstruction and kinematic analysis of events; statistical analysis of experiments.

The essential features of the system are considered below for each of the three stages.

2.5.3-1 Stage I: Data acquisition. The size of the on-line computer is clearly determined by the filmless application. It is essential that the memory should be able to contain the data produced during one burst; that is, 50-60 triggers each yielding a maximum of 2000 16-bit words of information. The size of the input buffer must therefore be about 50K 32-bit words. The memory size should therefore be at least 64K 32-bit words. It should be expandable to 128K, if necessary. As one can see, memory size is closely related to trigger rates, flat top length, etc., and might be a limitation in some cases.

Access to memory should be at least 1 word per μsec, in order to limit the input time for one trigger to some 2 msec. However, such a rate would become a limiting factor if wire chamber systems with a one-millisecond dead-time had to be considered.

Tapes should be written at a speed of 120-150 kch/sec (kilocharacters/sec) in order to empty the buffer in the two seconds available between bursts. However, given a memory size of 64K, half of which is reserved for an input buffer, a tape speed of 90 kch/sec would be sufficient. This compromise could be acceptable in the beginning, but tape speed ought to be increased as soon as more memory becomes available. Incidentally, one half-inch tape mounted on a 90 kch/sec tape unit, would be filled in less than five minutes.

Unless tape capacity increases considerably in the 70's, or more suitable storage media become available, the bottleneck might well be the manipulation of tapes.

In order to perform some checks on the experimental data, thus giving real-time feedback to the physicists, the on-line computer should have a powerful CPU. However, since it is unthinkable to do anything more than very simple checks on the data (such as applying some selection criteria based on number of sparks in each gap, etc.), it is not necessary to have very fast floating-point arithmetic. The operations should be mainly of the "logical" and "fixed-point arithmetic" types.

As far as data acquisition from an HPD is concerned, the same computer could well be used when not working on the data-taking activity. Alternatively, the HPD could be attached on-line to a separate computer, which would have to be very similar to the Omega one. This could be part of a necessary expansion of data-handling facilities at a later stage. It is proposed that the initial configuration of the Omega data-handling system be based on an Omega computer attached both to the HPD and to the experimental equipment.

For reasons of economy and safety, it is suggested that a small "Control Computer" be inserted between the rather large Omega computer and the experimental equipment. This would serve several purposes:

i) control and data storage during film-mode data-taking leaving the Omega computer entirely to the HPD exploitation;

ii) as a setting-up aid, during experiment changes and switch over to or from wire chambers, minimizing the allocation of the Omega computer;

iii) emergency on-line data-taking in case of failures of the Omega computer;

iv) during on-line data acquisition, it would be by-passed by the flow of data and could be allocated to some useful control functions.

The Omega data-acquisition system is schematically shown in Fig. 2.5.1.

The characteristics of the computers and the HPD are:

a) Main computer configuration

1) Core memory size 64K words (expandable)
2) Word length 32 bits (should be a multiple of 16 bits)
3) Memory cycle time ≈ 1 μsec or less
4) Floating point hardware
5) Interrupt system
6) Card reader/punch
7) Line printer
8) 4 or 5 magnetic tape units (say ½", 7-9 tracks, density 800 bpi, 90 kch/sec).
9) Typewriter on-line
10) CRT + LP with controller
11) Backing store (disc driver for monitor, program overlays, and data)
12) Two buffered channels (32 bits) for the HPD and the on-line input
13) Memory protection
14) Auxiliary card-handling equipment
15) Software (FORTRAN compiler, ASSEMBLER, operating system)

The total cost of such a configuration is estimated to be about 5 million Swiss francs.

As this computer is to be located near experimental equipment, and as it will possibly be on-line to this equipment, it should be capable of operation under varying environmental conditions and should be highly reliable in its operation. Its processing speed should be particularly fast for logical and fixed-point arithmetic operations.

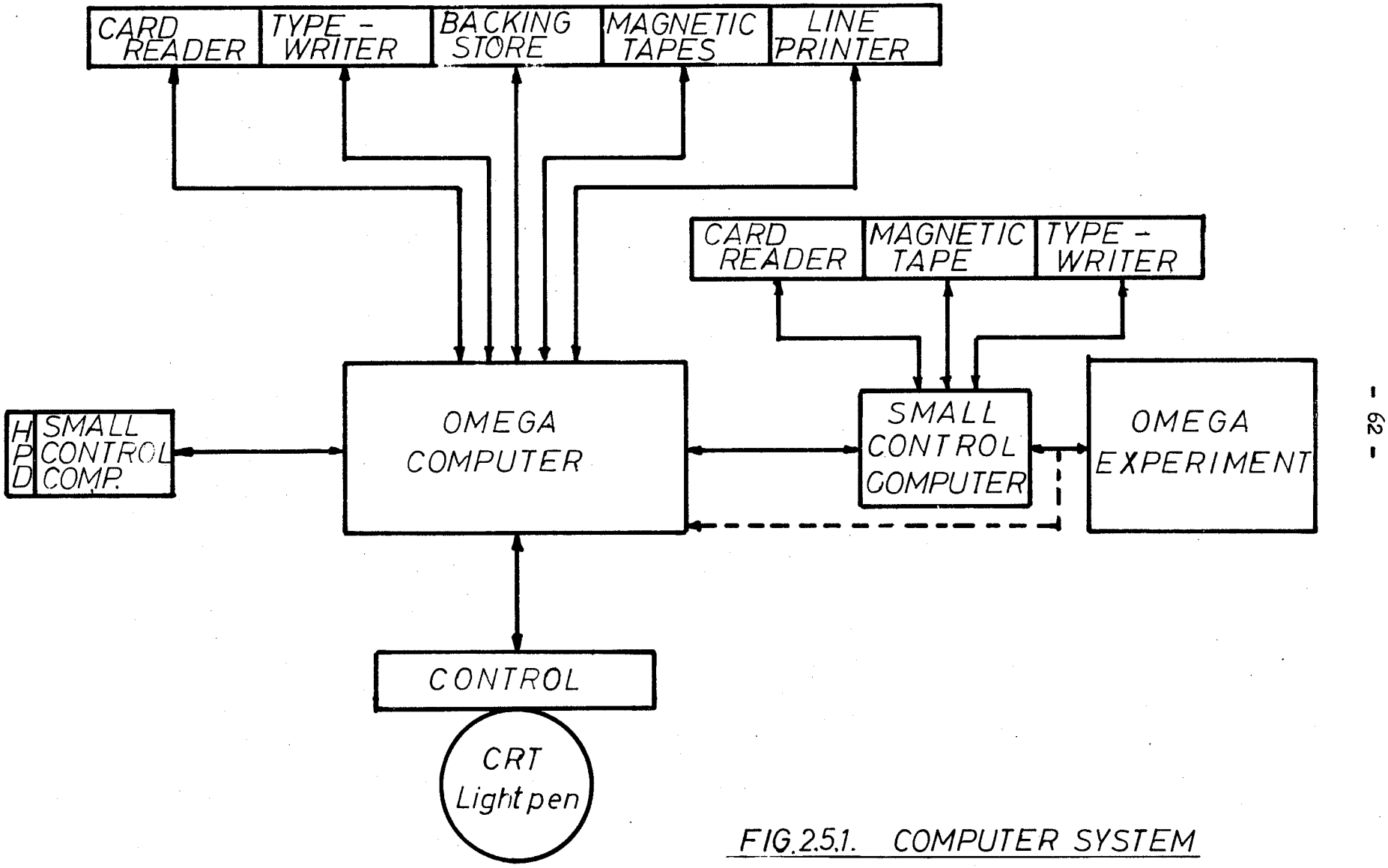

FIG.2.5.1. COMPUTER SYSTEM

b) Small control-computer configuration

1) Core memory size 16K (expandable)
2) Word length 16-32 bits
3) Memory cycle time ≈ 1 μsec
4) Priority interrupt system
5) Card reader/punch
6) 1-2 tape units
7) CRT display
8) Typewriter on-line
9) Software (FORTRAN compiler, ASSEMBLER, operating system).

The cost of such a configuration is estimated to be about 0.8 million Swiss francs.

Compatibility with the main Omega computer would be highly desirable.

c) HPD characteristics

The Omega picture format is assumed to be as follows:

- 70 mm film
- 70 × 60 mm^2 frame
- two views, side by side, each 30 × 60 mm^2
- spark dimensions on the film ≈ 40 × 200 μm^2

The basic features of the Omega HPD should be:

- 70 mm scan length
- 2 μm least count in both X and Y (16-bit coordinates)
- width measure optional
- HPD rotating disc designed for 6000 rpm.

The resolution of the device, defined as the ability to measure two distinct sparks lying very close together, should be 40 to 50 μm (distance between spark centres on the film).

The estimated time to measure one picture is in the region of 6 sec if one makes the following assumptions:

- all gaps parallel to a single direction of HPD scan
- 1200 scan lines raster to cover one frame
- scanning speed: 2.5 msec/scan-line
- overheads (film advance, stage setting etc) $\approx$ 3 sec/frame.

This leads to a peak measuring rate of 600 frames/hour. If one takes into account film changes, tests, operator interventions, breakdowns, and all other contribution to inefficiency, only about 60-70% of this maximum rate can be maintained over long production periods. Hence one would expect such an HPD to measure of the order of 2 million frames/year.

The HPD hardware is partly commercially available (mechanical and optical parts). A very small computer would be substituted for a substantial part of the electronics involved, and would constitute a flexible and reliable interface. The total cost of the HPD hardware is estimated at 0.9 million Swiss francs. Its construction will involve some 18 man-years and could be achieved in a period of about two years.

2.5.3-2 Stage II: Data reduction. The data acquisition activities and the development work will use the full capacity of the Omega computer for about 50% of the total time only. Since the computing requirements of pattern recognition are well adapted to the characteristics of the Omega computer, the rest of the time can be used effectively to run these programs. Stage III programs, on the other hand, are best run on the central computer facilities because they make greater use of floating-point arithmetic operations and, in any case, the sample event computations cannot be executed on the Omega computer because they are required during data-taking periods. One can imagine a possible schedule of the Omega computer relative to a two-year period near the central part of the project's lifetime, one year spent taking film and the other collecting wire chamber events. The available 15,000 hours could be subdivided as follows:

2500 for filmless stage I - (data acquisition during 25% of one year)
1500 for film stage I - (automatic measurement of 10^6 pictures)
6000 for filmless stage II - (pattern recognition of 5×10^6 triggers)
2000 for film stage II - (pattern recognition of 10^6 film events)
3000 for development work.

In order to achieve these processing rates, the computer would have to have a calculating speed of the order of one-fifth that of a CDC 6600. It is believed that only a small amount of time is lost for the main Omega computer during switching from film to filmless operation and vice versa. Most of the apparatus tests and measurements can be done with the help of the small computer.

Visual recovery application

A human operator will view on a CRT display the events that are not recognized by the computer programs. With the aid of a light-pen and a typewriter, the operator can supply some guidance to the programs in order to complete the pattern recognition. It is highly desirable that the operator has access to the pattern recognition programs sitting in the memory of the same computer which controls the CRT display.

This does not necessarily need to be the Omega computer. It is felt that this important application might grow to a non-negligible load of the computer if more than one or two displays were to be used continuously. Perhaps, one has to distinguish between an initial "development and limited production" phase where the CRT can be attached to the Omega computer and a second "large production" phase where an independent multi-display system would be required to satisfy the demand. Considering this possible future installation, one has to take into account the expected decrease of prices for CRT display units.

Experience is now being gained at CERN with these graphical input/output displays, and it is perhaps too early to foresee their future computer implications. Nevertheless, they have to be regarded as an important component of the Omega data-handling system, in view of the topological complexity of the events to be processed.

2.5.3-3 Load on the central computers. Although the particular data taking and data reduction requirements of the Omega project will be satisfied by its own computer, there will still be a large general computing load which would be processed more efficiently by central computing facilities. The main components of this load are:

i) stage III analysis of CERN's share of the events,
ii) sampling calculations during on-line data-taking,
iii) general computing (Monte Carlo calculations, development work, etc.).

On the basis of the assumptions made on the operation, one would have to analyse 0.5 million film events and 1 million wire chamber events per year. With an estimated analysis time of 3 "6600 CPU" sec/event, stage III processing would require the equivalent of 1250 hours per year of CDC 6600 CPU.

As far as sampling calculations are concerned, if one analyses a few per cent of all wire chamber triggers, another 300-600 hours of CDC 6600 CPU would be needed.

The remaining load which is made up of development, experiment preparation, etc., and which also includes reasonable provision for repeated calculations and possible overflow from the Omega computer, might account for 1000-1500 more hours. This makes a total of 2500-3500 hours/year, in other words a large fraction of the capacity of one CDC 6600.

This figure should be seen in proportion to the expected total CERN computer load in say 1973/74, which will be substantially higher than it is now and which will probably be handled by a computer system more powerful than the CDC 6000 series system used at present.

2.6 Cost estimate

The estimates are based on interpolations or extrapolations of the costs of existing systems, and are thus not extremely accurate. They are based on present (1967) prices. No provision is made for contingencies. (The data-handling system has been estimated separately.)

Experimental part:

Magnet incl. supplies	MSFr.	9.6
Instrumentation		1.7
Staff		2.6
Total	MSFr.	13.9

Data-handling system	MSFr.	8.4

a) Experimental part

Magnet with superconducting coils:

Iron yoke (1300 t at 2.5 SFr./kg)	MSFr.	3.25
Superconducting stabilized cable		1.0
Coil winding, insulation, tools		0.5
Helium container, vacuum tank, supports		0.6
Superinsulations		0.3
Vacuum pumps, valves, pipes		0.5
Power supply and controls		0.4
Refrigerator (750 W)		1.4
Liquid-helium container (2000 ℓ)		0.15
Gas-helium storage (2000 m^3)		0.15
Helium		0.1
Foundation		0.5
Measurement gear		0.25
Cryogenic tests		0.4
Compressor building (100 m^2, 1000 SFr./m^2)		0.1
Total	MSFr.	9.6

Magnet with conventional coils:

Iron yoke	MSFr.	3.25
Copper coil (75 t)		1.9
Power supply		1.3
Cooling towers		0.7
Cables, piping, etc.		0.5
Foundations		0.5
Measurement gear		0.25
	Total MSFr.	8.4

Instrumentation:*)

Spark chambers (100 frames)		
Material MSFr. 0.1 / Labour 0.3	MSFr.	0.4
Prisms, supporting glass plate		0.15
Camera, lenses, mirrors, supports		0.2
Electronics, pulse system		0.2
Film-developing machine		0.3
Accessories		0.15
SB-installations		0.3
	Total MSFr.	1.7

*) Only optical spark chamber system included.

Staff

A large part of the work will be done by existing staff of the NP and DD Divisions. The numbers of these staff members are given in brackets and are not taken into account in the total cost estimation. The numbers before the brackets represent the additional staff to be hired for the Omega Project. The numbers before and after the bars mean:
higher grades ($\geq$ 10)/lower grades (< 10)

	1968	1969	1970	1971	1969-1971 man-years
Magnet system	1/2[1/2]	1/4[1/2]	1/4 [1/1]	1/5 [1/0]	4/15[4/5]
Instrumentation	- [1/2]	1/2[1/2]	2/2 [1/2]	2/2 [1/2]	5/6 [4/8]
Data-handling system	- [1/0]	2/2[1/1]	3/4 [2/3]	3/7 [3/3]	8/13[7/7]
General	1/0[1/0]	1/1[1/0]	1/1 [1/0]	1/1 [1/0]	4/3 [4/0]
Total	2/2[4/4]	5/9[4/5]	7/11[5/6]	7/15[6/5]	21/37[19/20]

Total man-years of (additional) staff : 21/37
Average costs per man-year : 0.044 MSFr./year
Total staff costs during construction period : 2.6 MSFr.

b) Data-handling system

Main computer + CRT	MSFr.	5.0
Auxiliary computer		0.8
Electronic interfaces, links		0.1
HPD: components		0.9
construction staff		0.7
Scanning tables		0.25
Buildings:		
computer and HPD-room 250 m^2, about 2000 SFr./m^2		0.5
scanning room, offices, etc., 200 m^2, 750 SFr./m^2		0.15
	Total MSFr.	8.4

c) Running costs including analysis*)

Magnet, power, maintenance (supercond. coils)	MSFr./year	0.5
Film		0.5
Tapes (CERN quota only)		0.2
Staff (operators, programmes, etc.)		1.5
Computer maintenance		0.6
Prescanning		0.2
	Total MSFr./year	3.5

In the case of normal conducting magnet coils, the running costs would be higher by 1 MSFr./year.

*) The time of a central computer for the final analysis is not included.

3. EXPERIMENTAL PROPOSALS

3.1 Missing-mass experiment at low momentum transfer

3.1.1 Introduction

In the Omega project we can either treat the instrument as being similar to a bubble chamber (triggering whenever an interaction occurs in the target) or take advantage of the triggering possibility and bias ourselves to some specific interaction configuration. The former possibility may be interesting both from a rate and accuracy point of view, but with the latter we may in addition choose an interaction configuration so as to
(a) reduce the experimental errors (though not without some bias), or
(b) trigger on a specific mass region in which one is interested (e.g. to determine the spin-parity, decay branching ratios, and Δ^2 dependence of a resonance without having to consider the total mass spectrum).

There are two ways in which one might reduce the errors. Consider the reaction $\pi^- p \to pX^-$ and trigger on the recoil proton

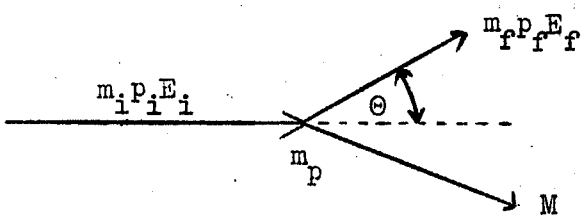

$$M^2 = m_i^2 + m_f^2 + m_p^2 + 2m_p(E_i - E_f) - 2(E_i E_f - p_i p_f \cos\Theta) \qquad (1)$$

$$\delta M_\Theta = \frac{\partial M}{\partial \Theta}\,\delta\Theta = -\frac{1}{M}\,p_i p_f \sin\Theta\,\delta\Theta \qquad (2)$$

$$\delta M_{p_i} = \frac{\partial M}{\partial p_i}\,\delta p_i = \frac{1}{M}\left[p_f \cos\Theta - \beta_i(E_f - m_p)\right]\delta p_i \qquad (3)$$

$$\delta M_{p_f} = \frac{\partial M}{\partial p_f}\,\delta p_f = \frac{1}{M}\left[p_i \cos\Theta - \beta_f(E_i + m_p)\right]\delta p_f\,. \qquad (4)$$

Now since $dM^2 = (\delta M_\Theta^2 + \delta M_{p_i}^2 + \delta M_{p_f}^2)$ we can choose, for a given $\delta p_i/p_i$ of the primary beam (which fixes δM_{p_i}), to operate in such a condition that either $\delta M_{p_f} = 0$ or $\delta M_\Theta = 0$.

Method a): $\delta M_{p_f} = 0$. From Eq. (4), $\delta M_{p_f} = 0$ when $p_i \cos \Theta - \beta_f(E_i + m_p) = 0$. This is the same condition for the maximum angle of the recoil proton in the lab. system as can be seen from Eq. (1) by solving for cos Θ and differentiating thus

$$\cos \Theta = \frac{M^2 - [(m_i^2 + m_f^2 + m_p^2 + 2mp(E_i - E_f) - 2E_iE_f)]}{2p_ip_f}$$

$$\frac{\partial(\cos \Theta)}{\partial p_f} = \frac{(m_p + E_i)\beta_f - p_i \cos \Theta}{p_ip_f} = 0 \text{ for minimum } \left[\frac{\partial E}{\partial p} = \beta\right].$$

In this condition we therefore operate with the recoil proton at its maximum angle in the lab. system, and in order to achieve maximum accuracy in the measurement of the missing mass we must measure Θ accurately. Clearly δM_{p_i} should, if possible, be reduced below δM_Θ. This is called the "Jacobian peak method".

Method b): $\delta M_\Theta = 0$. From Eq. (2), $\delta M_\Theta = 0$ if $\Theta = 0$. In this case the error on M depends only on δM_p. That is, p_f must be measured accurately. Clearly δM_{p_i} should be made smaller than δM_{p_f}, that is $\delta p_i/p_i$ must be made sufficiently small.

Δ^2 consideration. Since $\Delta^2 = -2 m_p T_f = -2 m_p(E_f - m_p)$ we have that, for a given M, Δ^2 is smallest when p_f is smallest. Now since

$$E_f = \gamma_c(E^* + \beta_c p^* \cos \Theta^*),$$

then

$$\Delta^2 = -2m_p\left[\gamma_c(E^* + \beta_c p^* \cos \Theta^*) - m_p\right]$$

and this will be the smallest for $\cos \Theta^* = -1$.

Thus method (b) selects events with the smallest possible Δ^2, which is of interest since most Δ^2 distributions fall off exponentially with Δ^2, and one therefore might expect to attain larger rates with method (b).

We have thus considered as a first study a missing-mass experiment using method (b) (cf. Kienzle et al., EEC proposal 10 April, 1967).

3.1.2 Experimental set-up for method (b)

The idea is to trigger the Omega on recoil protons leaving the target at $\Theta \simeq 0^\circ \pm 12^\circ$ and to select the protons by time-of-flight. For example, the locus of the protons with $\Theta = 0^\circ$ and p_f in the range from 0.35 GeV/c to 1.5 GeV/c with a flight time of 30 nsec is shown in Fig. 3.1.1. Protons with $\Theta = \pm 12^\circ$ arrive ±2 nsec before or after those with $\Theta = 0^\circ$. On the other hand, relativistic pions take ~ 20 nsec from the target to the counter. The time spread due to protons coming from different points in the target is ~ 1 nsec.

3.1.3 Errors on missing mass M

For the Omega the error in p_f in the region of 0.35 to 1.5 GeV/c is limited by multiple scattering (X_o = 30 m), and is ~ 0.5%. Table 1 gives the error contributions from Θ, p_i, p_f at various incident momenta for a ±4 mrad (¼°) error in Θ, 0.2% error in p_i, and 0.5% error in p_f.

Table 1

		$\Theta = 0^\circ$			$\Theta = 8.5$			$\Theta = 15^\circ$		
p_i	Range of M	δM_Θ	δM_{p_i}	δM_{p_f}	δM_Θ	δM_{p_i}	δM_{p_f}	δM_Θ	δM_{p_i}	δM_{p_f}
20	3.35 → 4.96	0	±4.6	±6.5	±2.0	±4.6	±6.5	±4.0	±4.6	±6.5
11	2.49 → 3.63	0	±3.6	±5.5	±1.7	±3.6	±5.5	±3.0	±3.6	±5.0
8	2.12 → 3.33	0	±3.0	±5.0	±1.5	±3.0	±5.0	±2.5	±3.0	±5.0
4	1.48 → 1.95	0	±2.2	±4.5	±1.0	±2.2	±4.5	±2.0	±2.2	±4.5
GeV	GeV	MeV			MeV			MeV		

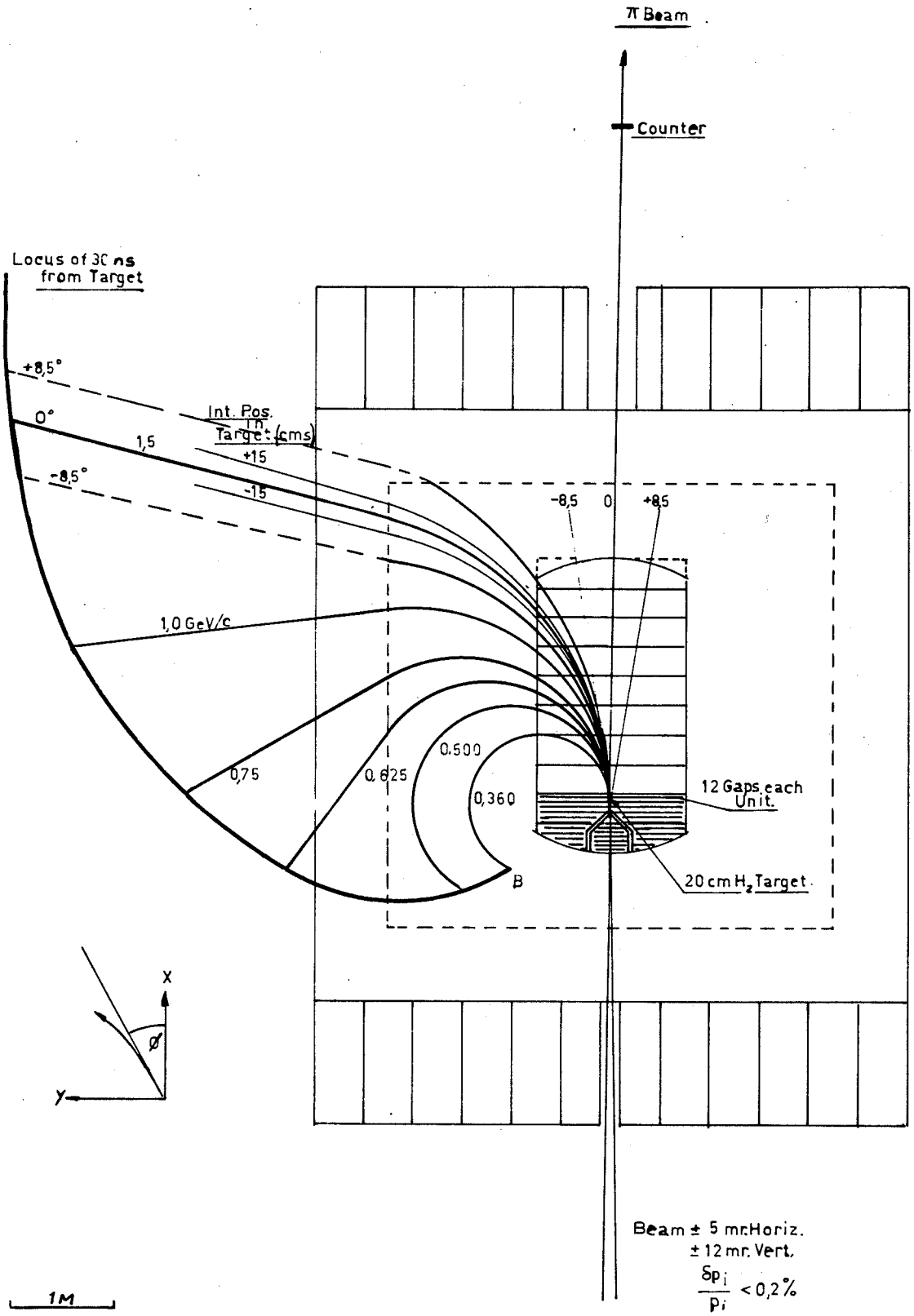

FIG 3.1.1. MISSING MASS TRIGGER

From this table it can be seen that:

a) $\delta p_i/p_i$ should be a little less than 0.2%, say 0.1% if δM_{p_i} is to be negligible compared to δM_{p_f};

b) Θ should not be increased much beyond 15° to keep δM_Θ negligible;

c) increasing X_o by a factor 2, i.e. reducing δM_{p_f} by a factor $\sqrt{2}$ could be interesting -- that is, thinner plates or wider spacing;

d) one might expect to reduce these errors by a small amount for 4-constraint and 1-constraint kinematic fits.

These results may be compared to those expected by Kienzle et al. For example, for p_i = 11 GeV/c and M of about 3 GeV/c they predict $\delta M = \pm$ 9 MeV, whereas with a $\delta p_i/p_i$ of 0.1% the Omega gives $\delta M = \pm$ 5.5 MeV (unfitted events). [Note: Kienzle et al. get same δM if they have same $\delta p_i/p_i$.]

Thus the main features of this experimental arrangement are large solid-angle, high data rate (limited by 20 to 50 msec dead-time of camera in the case of optical spark chambers or $\lesssim$ 10 msec dead-time for wire spark chambers), missing mass to $\pm$ 6 MeV, complete kinematic fitting of the event as in the bubble chamber, observation of the various decay modes of resonances.

3.1.4 Other errors and systematic effects

1) Error in δp_f due to $\pm$ 0.4 cm uncertainty in interaction point in H_2 target. For non-relativistic protons

$$E = \frac{p^2}{2m}$$

$$\Delta p = \frac{m}{p} \Delta E \ .$$

In liquid H_2,

$$\frac{dE}{dX} = \frac{0.24 \text{ MeV/cm}}{\beta^2} \ .$$

Ex. For $p_f = 0.4$ GeV/c, $\beta = 0.4$

$$\frac{dE}{dX} = 1.5 \text{ MeV/cm, giving } \delta p_f = \pm 1.5 \text{ MeV/c for } \Delta x = \pm 0.4 \text{ cm.}$$

Such an error on δp_f leads to a $\delta p_f/p_f$ of $\pm 0.37\%$ which should be compared to the $\pm 0.5\%$ coming from multiple scattering.

2) Energy loss in H_2 target and 1 mm mylar window. If target is 20 cm long we have a momentum loss of $\sim$ 75 MeV/c in 20 cm, and in 1 mm mylar $\sim$ 2 MeV/c (systematic and correctable).

3) Error on Θ of recoil proton at target due to ± 0.4 cm uncertainty of point of interaction. For $p_f = 0.4$ GeV/c, $\rho = 80$ cm.

$$\Delta\Theta = \frac{\Delta X}{\rho} = \frac{0.4}{80} \rightarrow \pm 5 \text{ mrad giving } \delta M_\Theta \sim \tfrac{1}{2}\, \delta M_{p_f}, \text{ therefore all right.}$$

4) Error on Θ at production due to multiple scattering in the H_2 target and mylar window.

$$\Theta = \frac{15(\text{MeV})}{pv(\text{MeV})} \sqrt{\frac{L}{X_o}} \ .$$

$$X_o(H_2) = 10 \text{ m} \quad X_o(\text{mylar}) = 40 \text{ cm.}$$

For 10 cm H_2 $\Theta = \pm 3.2$ mrad
0.1 mm mylar $\Theta = \pm 1.6$ mrad
} leading to $\delta M_\Theta \leq \frac{1}{3}\, \delta M_{p_f}$.

3.1.5 Monte Carlo computer study

In order to understand, in more detail, the problems associated with a given experimental arrangement, we have used the data summary tapes of the 8 GeV/c $\pi^+ p$ bubble chamber experiment which contain all the relevant information on the 4, 1, and 0 constraint events.

3.1.5-1 Experimental arrangement for method b): $\delta M_{\Theta} \sim 0$. In this case the apparatus is triggered on recoil protons in the momentum range ~ 0.35 to ~ 1.5 GeV/c and emitted at small laboratory angles ($\Theta \sim 0^{\circ}$) to the incident particle. The locus of the positions of protons emitted at $\Theta = 0^{\circ}$ and with momenta in the above-mentioned range was determined after they had travelled for a flight time of 30 nsec from the target (see Fig. 3.1.1). A hypothetical scintillator was placed at this locus, and the properties of trigger studied as a function of the time gate ($30 \pm \Delta t$ nsec) and the shape of the scintillator in the z direction ($\perp$ to plane of Fig. 3.1.1). It is clear that Δt determines the angles Φ in the xy plane of the accepted protons. We found that a $\Delta t = \pm 2$ nsec accepts a $\Delta\varphi = \pm 12^{\circ}$ about $\Phi = 0^{\circ}$ (see Fig. 3.1.2).

a) Accidental triggers on π^+

Figure 3.1.3 shows the arrival times of protons and π^+ at the scintillator having dimensions in the z direction of $\pm$ 50 cm. We see that the number of π^+ arriving within 30 ± 2 nsec is $\sim 1.5\%$ of the protons. These π^+ will give spurious triggers. However, on measuring the events, these π^+ can essentially be identified since it is found that the probability of the π^+ having a $|\Phi| < 12^{\circ}$ is $\sim 3\%$. The Δt can be increased to ± 4 nsec without too much π^+ contamination, but then the Φ accepted becomes rather too large if one wishes to keep δM_{Θ} smaller than δM_{p_f}.

b) Shape of the scintillator and the mass spectrum

If one wishes to maintain the angle of proton emission in the xz plane (λ or dip) also $< 12^{\circ}$, then the counter dimension in z must decrease as one goes from the high momentum side to the low momentum side (region A to B of Fig. 3.1.1). However, this gives rise to a missing-mass spectrum which is peaked at high masses. The reason for this is that high masses are associated to small c.m.s. momenta (p*) of the proton, and a larger fraction of these, than for events with higher p* (lower missing mass), are transformed into the laboratory system with angles $< 12^{\circ}$. We thus attempted to compensate for this effect by having a counter with z dimensions constant at ± 50 cm. In this case the dip angle λ reaches 25° at $p_f = 0.35$ GeV/c and decreases to 12° at $p_f = 1.5$ GeV/c. A mass spectrum for two intervals of the final

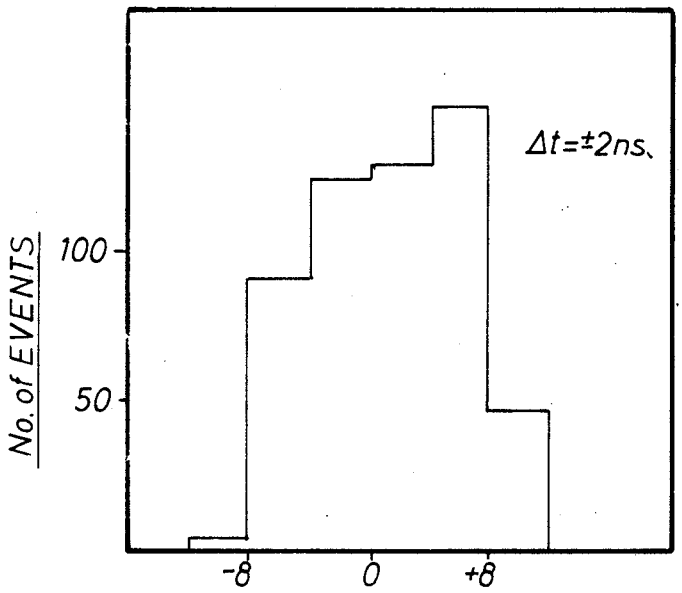

PROTON EMISSION ANGLE TO INCIDENT PARTICLE IN xy PLANE

FIG 3.1.2 SELECTION OF PROTON ANGLES BY TIME OF FLIGHT TRIGGERS

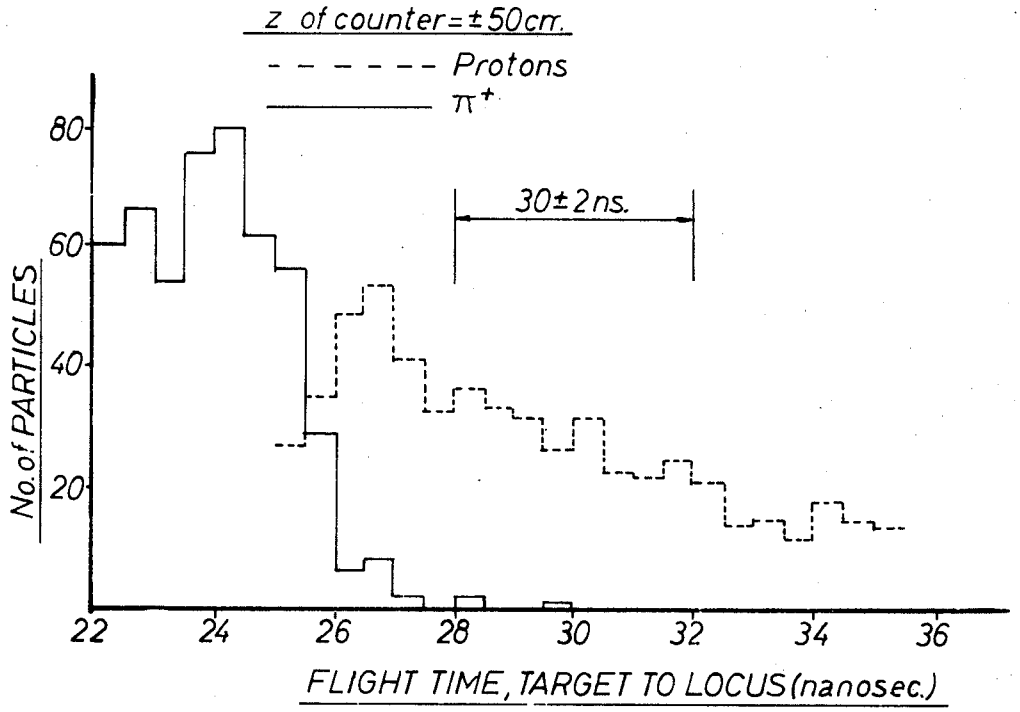

FIG. 3.1.3. TT-TRIGGER BACKGROUND VERSUS TIME OF FLIGHT

recoil proton momentum 0.6 to 1.5 GeV/c and 0.6 to 1.3 GeV/c is shown in Fig. 3.1.4. The peak in the region of 1.3 to 1.5 GeV/c comes from the rapid increase in solid angle accepted in the c.m.s. for small p*.

c) Confusion between proton and π^+ arriving earlier

For the events selected by the trigger, there is a finite probability for a π^+ of the same event to follow a trajectory which could have triggered the apparatus if it had been a proton. For these events one does not know which of the two particles actually caused the trigger, although in fact the π^+ arrived too early. The number of events where this possible confusion occurs is 4%, and can be reduced by dividing the scintillator into sections along the path of the locus.

d) Accidentals due to K^+

A study in which all the π^+ were assigned the mass of the K meson showed that the problems arising from accidental triggers due to K^+ mesons, and confusion between K^+ and proton from the same event, were similar in magnitude to those for the π^+. Since the K^+ production is an order of magnitude lower than the π^+, the problem is one in the 0.2% region.

e) $N^*_{3,3}$ production

The study showed that the percentage of events having a $p\pi^+$ mass combination lying in the $N^*_{3,3}(1238)$ region did not appreciably change, in the events selected by the trigger, from the 25% of all $p\pi^+$ mass combinations for the unselected events.

f) Conclusion on method (b)

It seems to be possible to trigger the apparatus by time-of-flight and obtain a reasonable mass spectrum with a rather small contamination and little bias coming from the need to reject ambiguous events. The trigger rate changes according to the pion multiplicity of the channel but is of the order 2% for recoil momenta between 0.6 and 1.5 GeV/c. Assuming a cross-section of 1 mb and trigger efficiency of one, we would obtain ~ 7 events/burst of 10^6 π's from a 10 cm H_2 target.

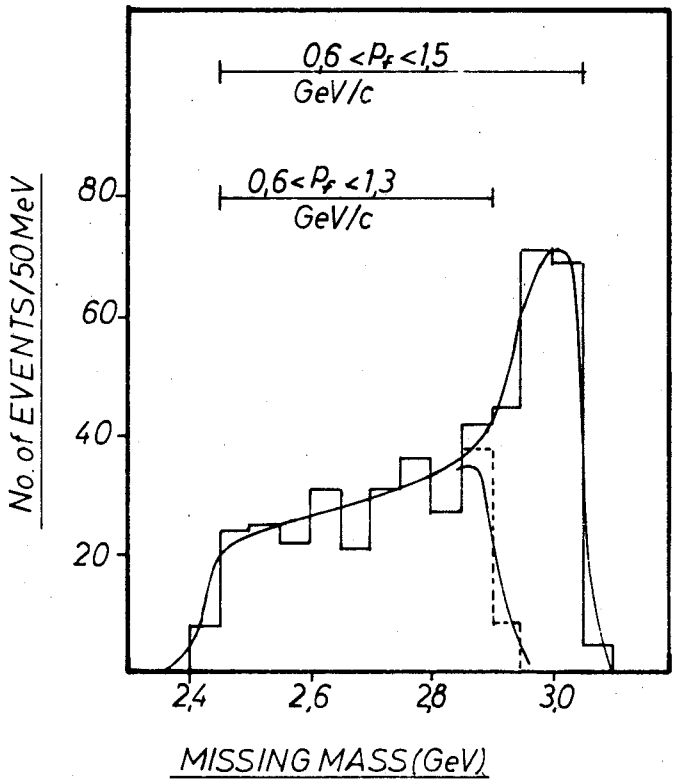

FIG. 3.1.4. MISSING MASS SPECTRA FOR TWO TRIGGER CONDITIONS

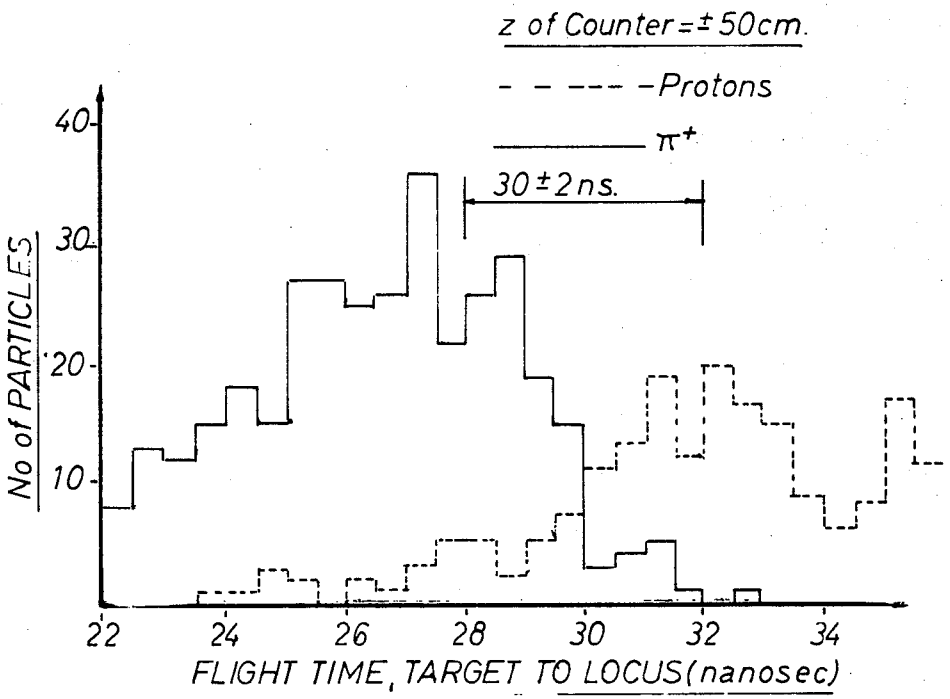

FIG. 3.1.5. TT- BACKGROUND IN A TRIGGER ON A GIVEN MISSING MASS

3.1.5-2 Experimental arrangement to select on a given mass interval for all Δ^2. Once it is known that a certain region of the missing mass spectrum is interesting, it would be useful to be able to trigger on events lying in this region in order to study it in more detail, e.g. a specific resonance. The locus of the protons after a flight path of 30 nsec coming from events with a missing mass of 2.6 GeV was determined, and the arrival times of the protons and π^+ crossing a scintillator placed at this locus (with z = ±50 cm) is shown in Fig. 3.1.5. In this case we see that ~ 60% of the triggers between 30 ± 2 nsec would be due to π^+. On the other hand, if we accept these triggers, nearly all could be rejected after measurement as the φ distribution of the π^+ and the protons do not overlap (see Fig. 3.1.6).

Figure 3.1.7 shows the mass region at about 2.6 GeV, which is chosen by selecting the protons which arrive at the target in the time interval 30 ± 2 nsec.

Thus it appears that such a trigger is possible if one accepts an equal number of unwanted events which can be rejected cleanly after measurement.

3.1.6 Comparison with the hydrogen bubble chamber

3.1.6-1 Missing-mass distribution of the π^0 in 1C fits. With a program, the fitted quantities (p,λ,φ) of each track were randomized according to the external errors of the equipment (bubble chamber or Omega). These external errors were those needed by the "GRIND" kinematic fitting program to give good χ^2 distributions for the fitted events. As a comparison, Figs. 3.1.8 a,b show the distribution of the missing π^0 mass in the reaction $\pi^+ p \to \pi^+ p \pi^+ \pi^- \pi^0$ for (a) the 2 metre hydrogen bubble chamber, and (b) the Omega. For the Omega, the distribution is a factor of two narrower than for the bubble chamber (essentially because of less multiple scattering).

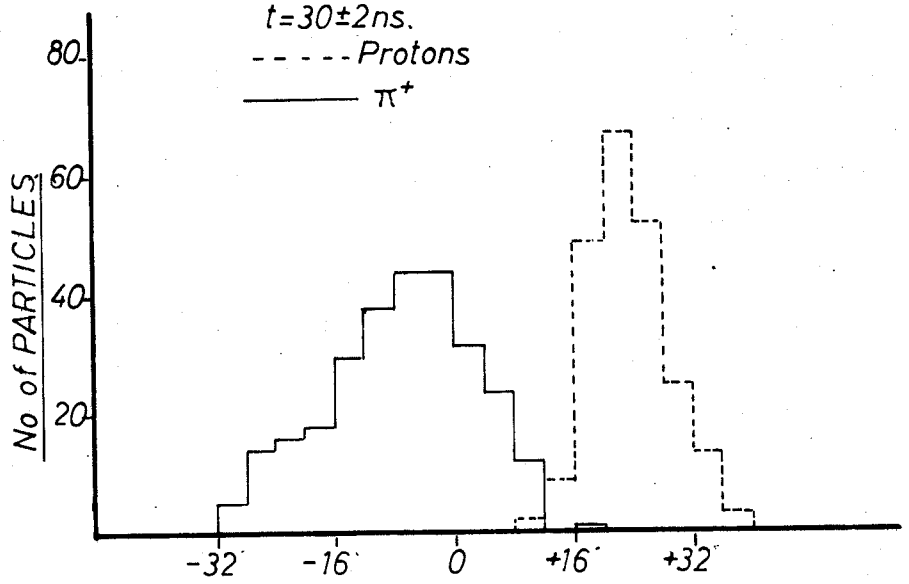

FIG 3.1.6. ø DISTRIBUTION, FOR PROTONS AND π^+ WITH FLIGHT TIME 30±2ns.

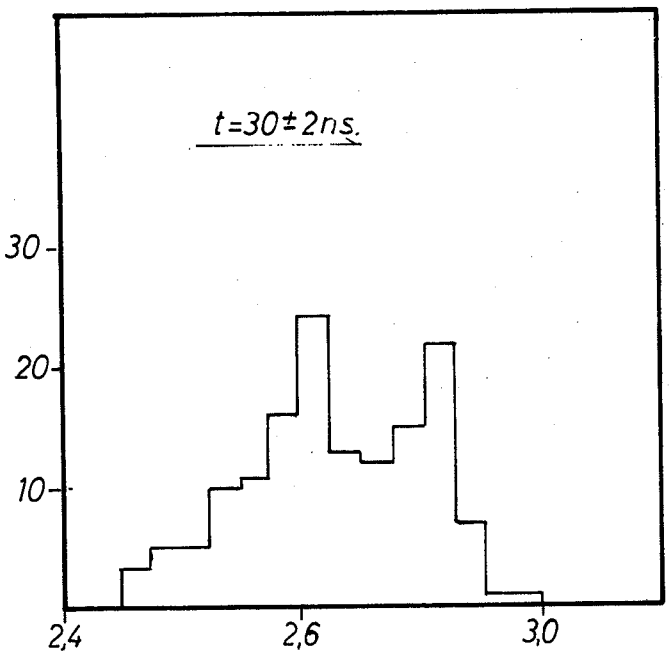

FIG. 3.1.7. MASS SELECTION BY FLIGHT TIME TRIGGER

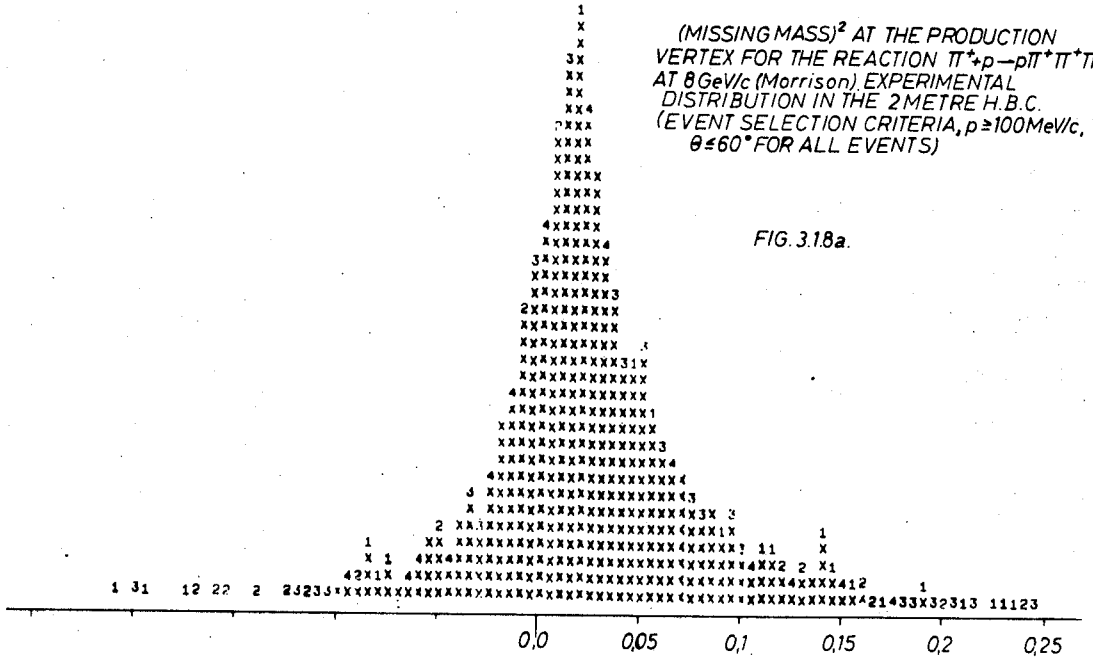

(MISSING MASS)² AT THE PRODUCTION VERTEX FOR THE REACTION $\pi^+ p \to p\pi^+\pi^+\pi^-\pi^0$ AT 8 GeV/c (Morrison) EXPERIMENTAL DISTRIBUTION IN THE 2 METRE H.B.C. (EVENT SELECTION CRITERIA, $p \geq 100$ MeV/c, $\theta \leq 60°$ FOR ALL EVENTS)

FIG. 3.1.8a.

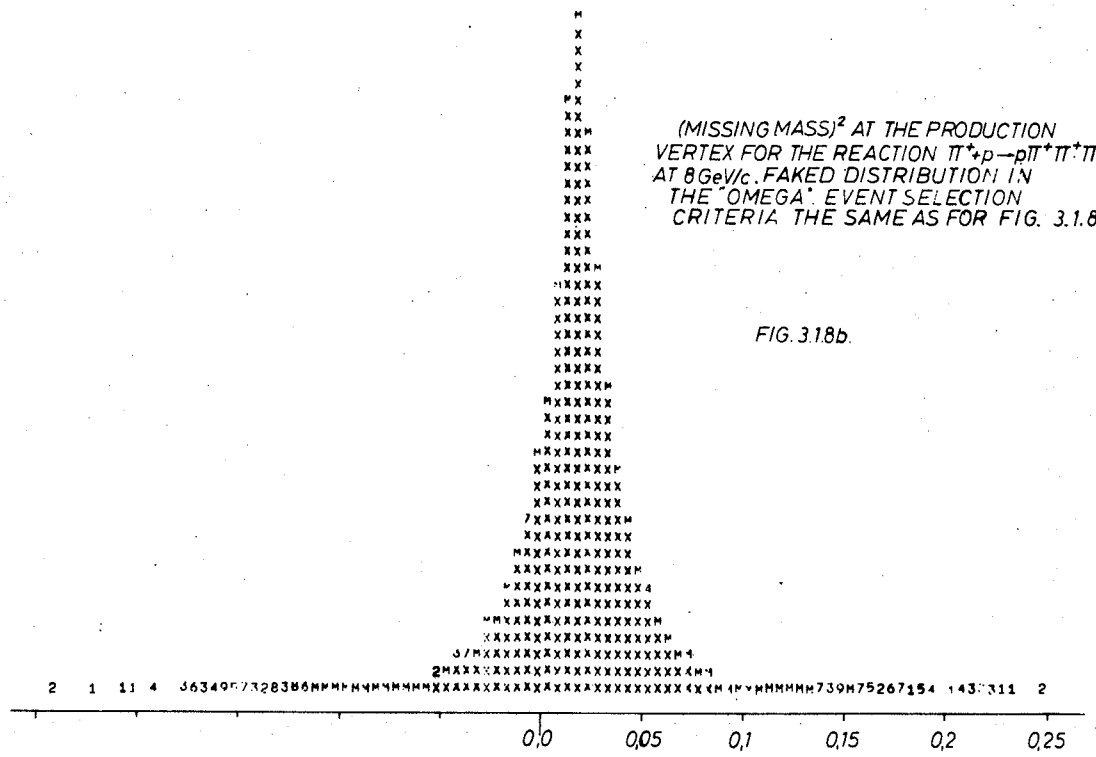

(MISSING MASS)² AT THE PRODUCTION VERTEX FOR THE REACTION $\pi^+ p \to p\pi^+\pi^+\pi^-\pi^0$ AT 8 GeV/c. FAKED DISTRIBUTION IN THE "OMEGA". EVENT SELECTION CRITERIA THE SAME AS FOR FIG. 3.1.8a.

FIG. 3.1.8b.

3.2 Study of baryon exchange processes

The class of reactions generally described as baryon exchange processes are ideally suited for study with the Omega system. They have a characteristic signature, namely a forward nucleon at close to the beam momentum; and their kinematics require the 4π geometry of the Omega for good efficiency.

3.2.1 Baryon exchange reactions. It is proposed to study processes in which an incident pion or kaon yields a high-energy proton in a small forward cone, such as:

$\pi + p \rightarrow p + \pi$ or $K + p \rightarrow p + K$,	backward elastic scattering	(1)
$\pi + p \rightarrow N^* + \pi$,	forward baryon resonance production	(2)
$\pi + p \rightarrow p + X$,	backward meson resonance production	(3)

plus similar reactions with incident K mesons and backward associated production. Some data is available on elastic scattering, but in the other processes the unique relation of the final-state particles is lost and it is essentially impossible to study them without a 4π geometry. In this sense this report describes how the Omega system could substantially improve an experiment now in progress at CERN.

Figure 3.2.1 gives some kinematics for backward pion scattering and shows the large angular range over which the scattered pion must be measured for a reasonable centre-of-mass range. The equivalent relations for Kp scattering are similar.

In reactions of type (2) in which a proton results from the N^* decay, the opening angle for the proton is small and can be detected with good efficiency; for example, it is 2.1° for the $N^*(1236)$ at 8 GeV/c. Class (3) reactions require the full 4π geometry because of the low velocity of the system X and hence the large opening angle of its decay.

3.2.2 The layout. Figure 3.2.2 shows the configuration for studying backward reactions at the Omega magnet. Upstream from the magnet are the Čerenkov counters and hodoscopes necessary to define the mass, momentum, and direction of the incident particle.

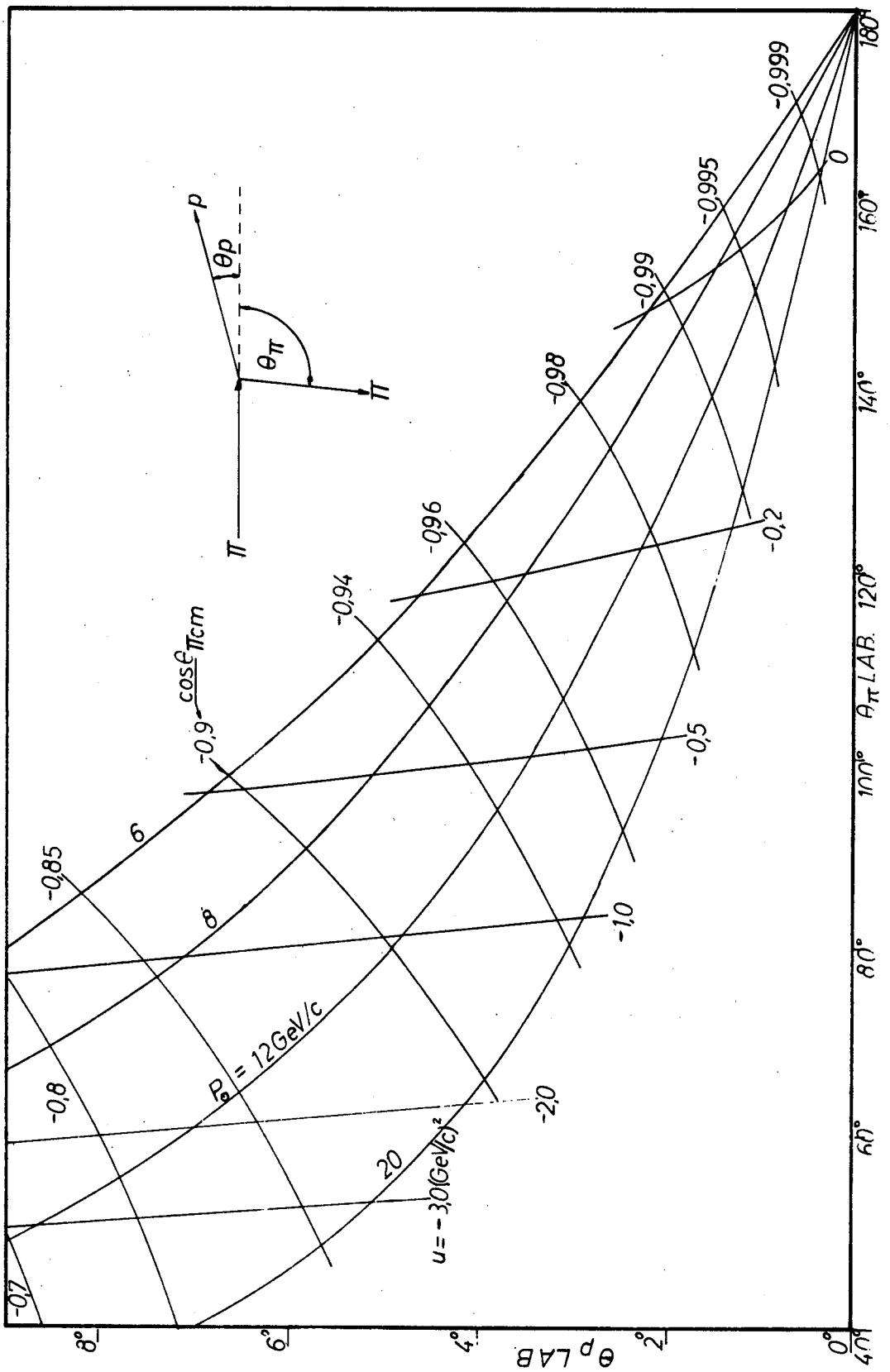

FIG 3.2.1. π-p BACKWARD ELASTIC SCATTERING

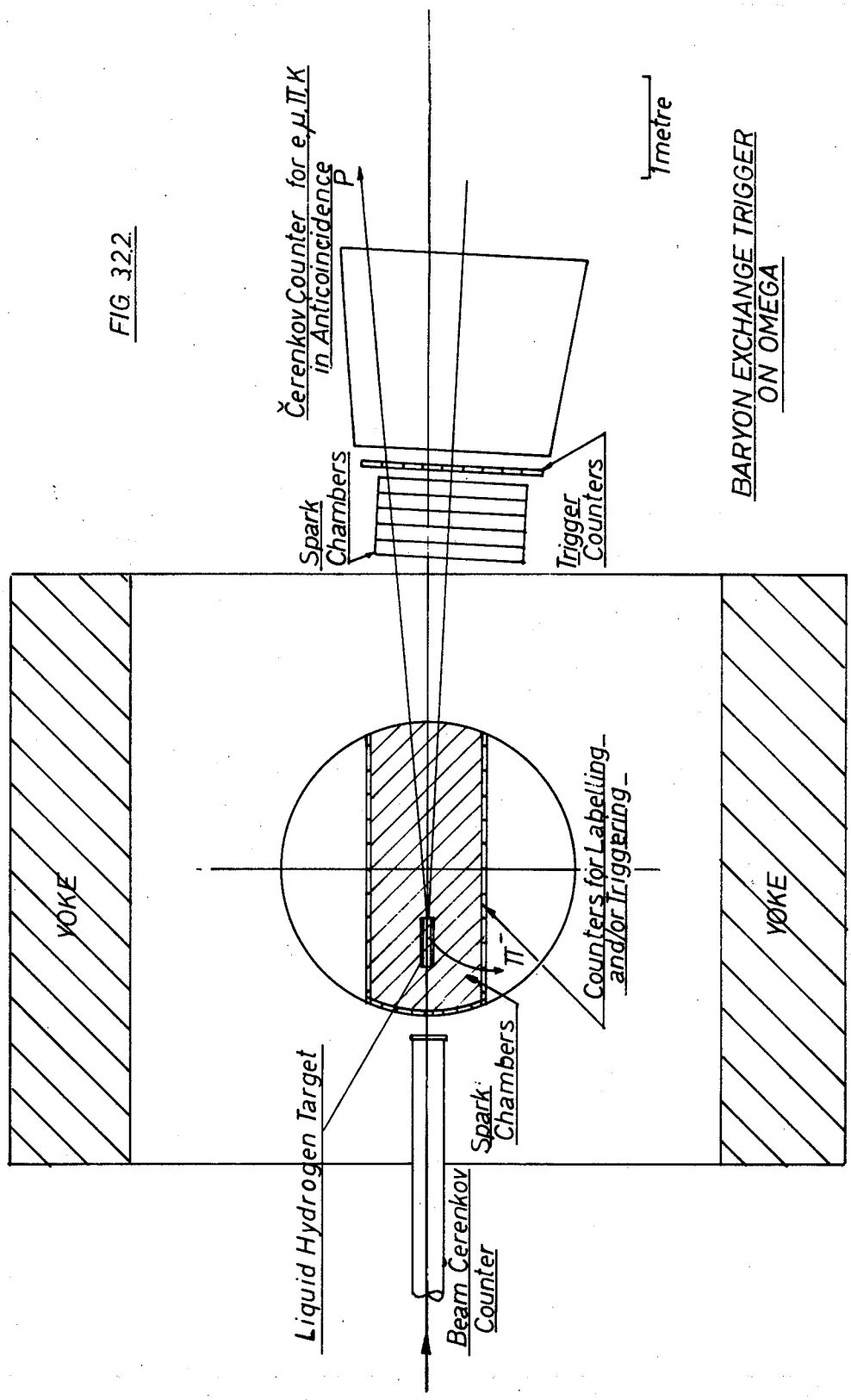
FIG 32.2
BARYON EXCHANGE TRIGGER ON OMEGA
1 metre
Čerenkov Counter for e,μ,π,K in Anticoincidence
P
Spark Chambers
Trigger Counters
YOKE
YOKE
Counters for Labelling and/or Triggering
π⁻
Liquid Hydrogen Target
Spark Chambers
Beam Čerenkov Counter

The baryon exchange trigger is downstream from the magnet and consists of a large-element hodoscope as a coincidence requirement and a large-aperture threshold Čerenkov counter to anticoincidence out all but the forward going protons. Elements of the hodoscope would be chosen as a triggering requirement to give the desired maximum proton angle about the zero degree line.

Spark chambers between the pole tips of the magnet fill a path one metre wide and two metres high along the beam line. Additional spark chambers downstream outside the magnet improve the momentum measurement of the proton, which is to a few tenths of a per cent. The liquid hydrogen target is mounted far enough into the field region to permit analysis of 180° scattering.

Particles emitted into the backward hemisphere (lab. system) have a momentum of less than 1 GeV/c in general, and a path length of 50 cm gives the momentum resolution that is permitted by the multiple scattering (a few per cent). A fence of trigger counters around the sides and back of the spark chambers could be used to reduce the triggering rate or could be used at high beam intensities to label the track of interest so as to distinguish it from accidental tracks in the chambers.

If optical chambers were used they could be mounted at 45° to the beam line thus permitting all scattering angles. If wire chambers were used, a more specialized chamber geometry would be possible with better angular coverage.

3.2.3 Trigger and event rates. Recent results on backward elastic scattering and on some backward inelastic processes permit reasonable estimates of rates. For example, at 8 GeV/c the Brookhaven-Carnegie Group*) have measured the total cross-section for backward elastic $\pi^- p$ scattering to be 1.5 μb, for the process $\pi^- p \to p\rho$ to be 1.8 μb, and for all processes in their geometry giving a high-energy forward proton about 100 μb. These results are consistent with other data which show that for reactions permitted by baryon exchange, and usually showing a backward peak, the ratios of the backward to forward cross-sections range from a few hundred to a few thousand. For other processes, the backward cross-sections are even smaller, as for example in $K^- p$ elastic scattering. These generalizations are only approximate, but they permit some estimates of rates with a baryon exchange trigger.

*) R.M. Edelstein, private communication.

With the configuration proposed here and a beam of $10^5 \pi^-$/burst striking a 50 cm liquid hydrogen target, a total interaction rate per burst of about 6000 is expected. The above data indicate that of these, at 8 GeV/c, approximately 20 could give rise to a forward proton, and of these 0.3 would be an elastic scattering and 0.4 a backward ρ production. The use of the appropriate fence counters in the Omega magnet could reduce some unwanted triggers. Beams of 10^5 pions per burst should be obtainable at the PS up to about 22 GeV/c.

The baryon exchange trigger alone is quite general and is better suited to wire chambers in which a number of processes could be studied simultaneously. For optical chambers, additional triggering conditions should probably be imposed.

A comparison of this proposal with an experiment now under way at CERN to measure the backward elastic scattering of pions and K mesons shows an increase in solid angle of a factor of 10 plus the momentum measurement of the scattered particle with the Omega. It also becomes feasible to study the inelastic channels.

A further refinement of the baryon exchange trigger would be the detection of a forward neutron instead of the proton. One could then do backward charge exchange scattering and studies with a deuterium target.

3.3 Experiments on leptonic hyperon decays

3.3.1 Introduction

The present*) experimental situation of leptonic hyperon decays needs considerable experimental clarification. A large number of experiments carried out so far has given only rather approximate information on the interaction rate. Only in a few cases have we indications on the form of the interaction by measurements of decay correlations.

On the other hand, current theoretical ideas based on Cabibbo's application of SU(3) to weak interactions appear to be quite capable of standing up to accurate tests. Ideally, one would like to accumulate in this field an amount of information comparable with the present information; for instance, on neutron beta decay

$$n \to p + e + \nu$$

for which about 10,000 events have been observed from a polarized ($\geq$ 90%) neutron beam.

More precisely, the Cabibbo theory is able to give exact predictions in the SU(3) limit for the absolute strength and the relative phase between the axial vector and vector interactions in terms of the phenomenological parameters F and D. A theorem due to Ademollo and Gatto ensures that, to the first order, the vector part is unaffected by the symmetry-breaking interactions. Quite accurate tests of the theory are therefore possible on the vector part of the weak coupling.

We list in Table 1 the main leptonic hyperon decay processes and the presently measured branching ratios [Brene, Veje, Roos and Cronström, Phys. Rev. 149, 1288 (1966)].

---

*) Of course, it is not known how many of the present questions on hyperon decay would still be open at the time of operation of the Omega project.

Table 1

Leptonic hyperon decays

Process	Branching ratio
$\Lambda \rightarrow pe^-\nu$	$(0.88 \pm 0.08) \times 10^{-3}$
$\Lambda \rightarrow p\mu^-\nu$	$(1.35 \pm 0.6\ ) \times 10^{-4}$
$\Sigma^- \rightarrow ne^-\nu$	$(1.28 \pm 0.16) \times 10^{-3}$
$\Sigma^- \rightarrow n\mu^-\nu$	$(0.62 \pm 0.12) \times 10^{-3}$
$\Sigma^+ \rightarrow ne^+\nu$	Forbidden by $\Delta Q = \Delta S$ rule
$\Sigma^+ \rightarrow n\mu^+\nu$	Two possible candidates detected (Columbia and Heidelberg)
$\Sigma^- \rightarrow \Lambda e\nu$	$(0.75 \pm 0.28) \times 10^{-4}$
$\Sigma^+ \rightarrow \Lambda e\nu$	$(0.13 \pm 0.13) \times 10^{-4}$
$\Xi^- \rightarrow \Lambda e^-\nu$	Only two events observed (questionable?)
$\Xi^- \rightarrow \Lambda\mu^-\nu$	Not observed
$\Xi^\circ \rightarrow \Sigma^+e^-\nu$	Not observed
$\Xi^\circ \rightarrow \Sigma^+\mu^-\nu$	Not observed

A particularly interesting decay is the strangeness conserving $\Sigma^\pm \rightarrow \Lambda^\circ e^\pm\nu$, which is predicted by Conserved Vector Current Theory to be only of the axial vector type.

From the point of view of the determination of the form of the interaction, it is required to measure for each decay the polarization of at least one of the hadrons in order to be sensitive to terms of the form $g_A \cdot g_V$, the correlations between momenta being sensitive only to terms of the form g_A^2 and g_V^2 (Weinberg). Therefore polarization measurements are very essential.

3.3.2 Experimental techniques

Until now the bulk of the information, apart from a few experiments, has been obtained from bubble chamber work.

There are two possible ways of searching for leptonic decays in a bubble chamber:

a) In an H_2 bubble chamber, by measuring all decays and identifying leptonic decays by lack of fit to the more likely (two-body) non-leptonic decay mode. About 10^3 - 10^4 events need reconstruction to yield one good leptonic count.

b) In a heavy-liquid bubble chamber, by recognizing electrons from the characteristic radiative losses. No information is available from production vertex (complex nucleus!) and multiple solutions are encountered in the fit. Furthermore, the polarization of the hyperon is unknown.

The Omega project, being a somewhat intermediate instrument between the bubble chamber and a counter arrangement, appears as an interesting detector in this field because of the possibility of triggering and the much higher incident flux of particles accepted. More precisely:

a) The leptonic (muons and electrons) decays can be readily identified by a threshold gas Čerenkov counter or by penetration of a thick shield. Recently, several experimental groups in CERN and elsewhere have operated threshold gas Čerenkov counters of atmospheric pressure capable of angular acceptances up to some 50 degrees in a variety of shapes and dimensions. The electron detector efficiency is essentially complete, while the rejection against particles below threshold can be as good as a few parts in 10^{-5} *). This clear identification of electrons is possible with the required rejection of non-leptonic decays.

---

*) We are grateful to Dr. V. Soergel for the illuminating discussions on this point.

b) The high incident flux accepted and electronic beam particle identification are such as to permit setting up the Omega spectrometer in an hyperon beam produced outside the detector. As we shall see, this would provide an intense source of hyperons of well-known direction and momentum. Alternatively, hyperons could be produced by a high-flux K^- beam incident on a hydrogen target located inside the dector.

c) The common characteristic of all decays listed in Table 1 is that hadrons at high energies are kinematically constrained to carry away the largest fraction (~ 90% on average) of the kinetic energy of the incident particle, and they are emitted in a narrow cone in the direction of the incident hyperon. For instance, in the decay $\Sigma^- \to \Lambda^0 e^- \nu$ for $p_{\Sigma^-} = 18$ GeV/c, the maximum emission angle for the Λ^0 is about 0.24° and the momenta lay in the interval 15.8 GeV/c < p_Λ < 18.0 GeV/c.

It is possible to construct reasonably small and efficient detectors to determine the direction of neutrons emitted in decays such as $\Sigma^- \to n e \nu$, $\Sigma^- \to n \mu \nu$. Protons emitted in decays such as $\Lambda \to \pi p$ can be recognized by threshold Čerenkov counters.

The above-mentioned points make of the Omega spectrometer a much more effective instrument than a bubble chamber in searching for hyperon β-decays. On the other hand, the accuracy in momentum and angle measurement being here quite comparable to the ones of a hydrogen bubble chamber, a very precise and complete event reconstruction is expected in general. However, the fact that the spark chambers give a signal every two centimetres of track length in the beam direction, requires that the decay path of the particles involved be larger than several centimetres. Thus high-energy beams are in general preferable.

3.3.3 Negative hyperon beam

We shall try to estimate hyperon fluxes for proton collisions at 24 GeV/c on a thick target. We shall assume a 3 metre beam path embedded in heavy shielding to prevent background from the proton beam. The return yoke of

the Omega magnet would probably constitute the major part of this shield. Suitable magnetic analysis selects a negative beam of about 18 GeV/c. The experimental information on hyperon production in p-p collision is limited to the case of Σ^-, and it comes from a BNL bubble chamber experiment*).

In an exposure of 180 km of proton tracks at 28.5 GeV/c, 15 Σ^- events were observed. Assuming forward-backward symmetry in the production from proton-proton collision and a transverse momentum, p_T distribution of the form $e^{-p_T/p_\perp}$ with $p_\perp = 0.25$ GeV/c, these authors estimate that on hydrogen:

$$\frac{dN_{\Sigma^-}}{d\Omega dp}\ (0^\circ,\ p_{\Sigma^-} = 19.0\ \text{GeV/c}) = 0.054\ \Sigma^-,\ \text{sr}^{-1}\ \text{GeV/c}^{-1}\ \text{int.p}^{-1}$$

with an estimated error of about a factor of 2. This flux is about a factor of 5 smaller than the negative pion flux at the same energies.

Completely arbitrarily we shall apply the "thumb rule" of reducing the yield by a factor of 10^2 at each additional strangeness unit of the emitted hyperon. This gives the following guesses:

$$\frac{dN_{\Xi^-}}{d\Omega dp}\ (0^\circ\ p_{\Xi^-} = 19.0\ \text{GeV/c}) = 5\times10^{-4}\ \Xi^-\ \text{sr}^{-1}\ \text{GeV/c}^{-1}\ \text{int.p}^{-1}$$

$$\frac{dN_{\Omega^-}}{d\Omega dp}\ (0^\circ\ p_{\Omega^-} = 19.0\ \text{GeV/c}) = 5\times10^{-6}\ \Omega^-\ \text{sr}^{-1}\ \text{GeV/c}^{-1}\ \text{int.p}^{-1}$$

A considerable loss is expected because of decays in flight. After a 3 metre path, for a momentum of 19.0 GeV/c the expected yields are as follows:

Particle	Yield at target	Yield at 3 m
	$\text{GeV}^{-1}\ \text{sr}^{-1}\ \text{int}^{-1}$	$\text{GeV}^{-1}\ \text{sr}^{-1}\ \text{int}$
Σ^-	5×10^{-2}	9×10^{-4}
Ξ^-	5×10^{-4}	8.2×10^{-6}
Ω^-	5×10^{-6}	1.75×10^{-8}

*) A. Thorndike et al. BNL. We are grateful to Dr. J. Sandweiss for providing us with this piece of information, and for many discussions on the subject.

Assuming Δp = 1 GeV/c, $N_p = 5\times10^{10}$, $\Omega = 10^{-4}$ sr, we get at 3 metres from target

Σ^-	Ξ^-	Ω^-	π^-
4500/pulse	40/pulse	0.08/pulse	1.2×10^6/pulse

These fluxes are quite adequate for several interesting experiments.

Particle identification in the incoming beam could be obtained with a differential Čerenkov counter DISC*). However a rather complicated beam transport with superconducting lens-elements is required to match the acceptance of the DISC with the emittance of the beam. More conservatively, a threshold gas Čerenkov veto-counter could be used to reject the bulk of fast particles (π^-, K^-), and hyperons could be further identified by the decay configuration and kinematics.

3.3.4 The decays of Ω^- particle

Fourteen Ω^--hyperon decays are known so far. The possible decay modes calculated as well as possible on the basis of SU(3) by Glashow [Physics Letters 10, 144 (1964)] are listed in Table 2 below:

Table 2

Decay mode	Decay rate ($\times 10^7$ sec^{-1})	Branching ratio (%)
$\Xi^0\pi^-$	178	39.5
$\Xi^-\pi^0$	86	19.1
ΛK	94	20.9
$\Sigma^0 K^-$	2.4	0.6
$\Sigma^0 \bar{K}_0$	0.8	0.2
$\Xi^{0*}\pi^-$	38	8.4
$\Xi^{-*}\pi^0$	22	4.9
$(\Xi\pi\pi)$ not res.	1	0.2
$\Xi^0 e^-\nu$	18	4.0
$\Xi^0\mu^-\nu$	12	2.7
$\Xi^{0*}e^-\nu$	2	0.4
$\Xi^{0*}\mu^-\nu$	0.1	0.02

*) R. Meunier has designed one of such counters for the present type of investigation. We are grateful to Dr. Meunier for stimulating and interesting remarks on the subject.

There is a considerable interest in detecting the two-body decay $\Lambda^0 K^-$, which could permit a convenient spin determination. Furthermore, it must be remarked that the leptonic decay rates are now predicted to be ~ 4% of all decays, and therefore it is probable that these decay channels would be accessible as well.

3.3.5 Experimental arrangements with negative hyperon beams

Every potential experiment would require its specific triggering logic. However, a number of remarks can be made:

i) The triggering could make use of the following points:

   a) the incident particle is slow, or has a given velocity if DISC is provided;

   b) there are a number of decay products coming from a region with little or no material;

   c) in case of leptonic, electron, or muon decays, the nature of lepton is identified;

   d) the last stable baryon is emitted with forward cone and identified by a neutron or proton detector.

ii) The polarization of the incoming hyperon would most likely be zero. Therefore non-leptonic decay processes are the main polarization analysers. In particular, the decays

$$\Lambda^0 \rightarrow \pi^- p$$
$$\Xi^- \rightarrow \pi^- \Lambda^0$$
$$\Xi^0 \rightarrow \pi^0 \Lambda^c$$

have large and well-known spin correlation coefficients.

4. FURTHER DEVELOPMENTS

4.1 Wire chambers

Wire chambers which could work and be read out inside the Omega magnet would offer the following advantages;

i) on-line control of the experiment;

ii) higher speed of data taking; the read-out time would be of the order of 5 msec for 3×10^5 wires;

iii) no need for a hole in the magnet pole. This means a 10% higher field strength.

The requirements on a wire chamber system are

i) momentum resolution comparable to that of optical chambers.

ii) realiability of the chamber and the read-out system operating in the magnetic field comparable to that of optical chambers.

4.1.1 Momentum resolution of wire chambers

As for optical chambers, one has to consider the errors in the momentum determination due to multiple scattering and due to the limited accuracy of position measurement. For a comparison with optical chambers it will be assumed that the number of chamber gaps is equal in both cases.

The radiation length of a wire chamber system -- made of 67 planes per metre consisting of 10 copper wires per cm, 100 μ diameter -- is 23 metres*), compared with 44 metres for the conventional 25 μ aluminium-plate chambers.

Either thinner copper wires or aluminium wires can be used to increase the radiation length. The corresponding values are:

for 100 μ aluminium wires : L_o = 100 m
for 60 μ copper wires : L_o = 55 m .

Thus the radiation lengths of low density wire chambers are comparable with those of 10 μ aluminium plate chambers (L_o = 86 m). In both cases the lifetime of the wires and the reliability of operation have to be investigated (60 μ copper-wire chambers are already in use).

*) Chamber gas and seven 0.1 mm mylar foils per meter are included.

The track position determination in wire chambers is not as accurate as in optical chambers. The best resolutions obtained so far in large wire chambers (1 mm wire spacing) are ±0.3 mm for core read-out as well as for magnetostrictive read-out. This has to be compared with ±0.2 mm for optical chambers. For high momentum particles, the reduced resolution could probably be compensated by measuring the tracks over larger lengths, that is to say further down to the fringing-field region of the magnet, which is not possible with optical chambers.

4.1.2 Read-out of wire chambers in a magnetic field

The commonly used core and magnetostrictive read-out techniques are not very well suited to operate in a strong magnetic field; they need special provisions in that case. Different non-magnetic read-out techniques are being discussed and have been partly tested. For these, one should require the same resolution as that obtained by conventional wire chambers outside a magnetic field. To get from each spark a two-dimensional position information (as one can with optical chambers), one has to read both the grounded and the pulsed plane. Otherwise the momentum resolution is reduced.

Up to now, measurements of wire chamber resolution have been performed only outside a magnetic field and for tracks nearly perpendicular to the wire planes. For a general spark chamber arrangement inside a magnetic field, larger angles between some tracks and the normal to the planes cannot be avoided. Thus, for any wire chamber system, the dependence of the measurement accuracy on the track angle should be investigated. This dependence has been measured for optical chambers but it may be different for wire chamber systems.

To avoid ambiguities of the spark positions in wire chamber systems planes of wires stretched in three different directions should be used.

4.1.3 Core read-out

Read-out by means of ferrite cores is most commonly used for chambers that are outside a magnet. In magnetic fields of more than some 50 or 100 gauss cores fail to operate. Thus for chambers inside a magnet, the core boxes would have to be placed outside the field region

and 300,000 connecting pairs of wires for 200 wire planes of 1.5 m width would be necessary. In spite of the fact that these connections could be made quite economically by means of multiwire strips and miniaturized plugs, many problems would have to be solved such as avoidance of cross-talk and induction of core-flipping currents by the high-voltage pulse. In particular, the read-out of the pulsed planes, which is already difficult for normal core read-out chambers, becomes a serious problem in a system having long connections between chamber wires and cores.

4.1.4 Magnetostrictive read-out

The magnetostrictive read-out technique is being used increasingly for wire chambers outside a magnet. At one end of each plane, the chamber wires are crossed by a read-out wire made of ferromagnetic material. The spark current flowing in the chamber wire produces a magnetic field pulse in the direction of the read-out wire. The magneto-strictive effect generates a longitudinal sound-wave, which runs along the wire and can be detected as a voltage pulse in a coil surrounding the read-out wire at its end. A permanent axial magnetic field has to be applied to the wire at the position of the detection coil.

The generation of the sound waves still works in high external magnetic fields (up to 20 kG) as long as the direction of the field is everywhere very nearly perpendicular to the wire. This cannot be realized in rather inhomogeneous fields. In that case the field has to be screened down to the order of one kilogauss, and the wire has to be tilted in such a manner that the field component along the magneto-strictive wire does not change sign. Otherwise insensitive transition regions would occur.

The detection coil can easily be screened against the external field. The detected signals have to be digitized by means of a set of scalers and a clock measuring the delay of the signals with respect to the HV pulse applied to the chambers. Since the signal propagation time in a 1.5 m long wire is about 0.3 msec, it is possible to connect about 20 read-out wires in series using one set of scalers*).

*) G. Brautti, CERN 66-30.

4.1.5 Non-magnetic read-out techniques

It is obvious that read-out systems avoiding magnetic materials are preferable for chambers working in a strong magnetic field. The most important techniques being developed are the "sparkostrictive chamber" and the capacitive storage.

a) "Sparkostrictive chamber"

It is known that a spark hitting a wire produces in it a longitudinal shock-wave. This signal can be detected by means of a piezoelectric crystal attached to the wire*). In test systems the amplified voltage signal had a width of about 0.5 μsec. The idea is to produce secondary sparks from the sparking chamber wires to a crossing read-out wire. A fine-meshed fibre-glass cloth keeps the distance between read-out wire and chamber wire constant. This method can perhaps be improved so as to increase the resolution. The detector is very sensitive, so that the spark current can be reduced to about 3 μ Coulombs per spark. With these currents, the lifetime of the wires is limited to some 10^5 sparks per chamber wire. The other properties of this system are similar to those of magnetostrictive chambers.

b) Capacitive storage and electronic read-out

In this case part of the spark charge is stored in a capacitor connected to the sparking wire. For each chamber wire one needs a storing capacitor and an electronic read-out circuit which gives the information to the output when a read pulse is fed in. These read-out circuits could be manufactured in the form of integrated units, each containing a couple of these circuits. First tests are being run using lumped circuits directly coupled to the chamber wires and hence reading only the grounded planes. To read also the pulsed plane, inductive coupling to the wires would have to be used. The advantage of this system is that it gives directly digitized information on the spark positions, as in the case of core read-out.

---

*) R. Grove, L. Kaufman and V. Perez-Mendez, UCRL-18003.

4.1.6 Conclusions

While optical spark chambers could be built directly for the use of Omega experiments, wire chamber systems still need development work. Very likely the associated problems will be solved during the construction time of the Omega magnet. Therefore all provisions for wire chamber operation at the Omega should be taken. Wire chamber systems allow extremely high data-taking speed and are therefore especially suited for experiments with high trigger rates.

4.2 Possible use of a polarized proton target in the Omega magnet

The main characteristics of a dynamic polarized proton target are:

- the sample X,
- its hydrogen density d_H,
- its contamination by bound protons $n(p \neq H)/n(H)$,
- the magnetic field H,
- its inhomogeneity $\Delta H/H$,
- the operating temperature T,
- the microwave frequency F,
- the target length L,
- and the maximum proton polarization P_n.

The table summarizes these values for (i) the present CERN targets, and (ii) the best results so far achieved in organic compounds.

X	d_H (g/cm^3)	$\frac{n(p \neq H)}{n_H}$	H (kG)	$\frac{\Delta H}{H}$	T (°K)	F (GHz)	L (mm)	P_n (%)	$P_n d_H^{1/2}$
(i) LMN	0.07	15	18.5	10^{-4}	1	70	45	70	1
(ii) Ethanol	0.14	3.3	25	5×10^{-4}	1	70	(45)*)	35	0.7

*) Measurements have been limited to L = 15 mm, but 45 mm should be feasible.

For experiments with a full kinematic separation between scattering events occurring on free protons and on bound protons it is possible that the statistical accuracy is proportional to $P_n d_H^{1/2}$, this quantity is given in arbitrary units in the table. Although in this respect organic targets are not yet as good as LMN targets, we feel confident that by the time the Omega project is achieved this situation will have changed. We thus suggest that the parameters defined for ethanol should be used with a possible stronger requirement on the field homogeneity.

As it is unlikely that the field of the Omega magnet in the position where the target will be located will have the required value and homogeneity, a special set of coils will have to be designed to correct the field shape and to increase locally the field strength. In this way it will also be possible to adjust independently the polarized target field and the field in the main volume of the Omega magnet.

4.3 Separated beams

Beams for electronics experiments - that need a high duty cycle - have so far been separated electrostatically. The efficiency of an electrostatic separator, however, decreases rapidly above ~ 5 GeV/c. RF separators can achieve separation at higher momenta, but room-temperature cavities would need excessive amounts of RF power for the duty cycle used in counter beams. Moreover, the flux of minority particles could not have been substantially enhanced by placing an RF separator into a normal secondary beam from an internal target. A large gain in the intensity of the wanted minority particles would require a beam intensity much higher than that now available from an internal target.

This situation may have changed by 1971 for the following reasons:

- higher internal proton intensity in the improved PS,
- higher flux in a secondary beam from an external target,
- possibility of a high duty cycle by superconducting RF separator cavities.

Because of radiation problems, the PS intensity seems to be limited around 3×10^{12} protons/sec; we assume 5×10^{12} protons/burst for a PS cycle of 1.7 sec. The superconductive separator is supposed to have adequate acceptance and separation power up to the highest energies considered here.

The numerical values for the gain in useful particles are derived from assumptions that are listed below:

PS intensity at 23.1 GeV/c	5×10^{12} p/burst	N
Target sharing	50%	N
Target efficiency	30%	N
Beam solid angle	10^{-4} sr	N
Momentum bite $\Delta p/p$	$\pm$ 1%	N
Note: The separator is assumed to be matched to this beam		
Beam length without separator	L_1 = 80 m	-
Additional beam length introduced by separator	L_2 = 50 m	E
Acceptable flux at Omega	2×10^5 p/burst	D

The beam intensities and the gain in useful particles by a separator are shown in Table 4.3.1.

Since here we assume conditions where the detector is always saturated by the unsepared beam, and since we are considering $K^{\pm}$ and $\bar{p}$ that are a small minority, the changes in gain can be simply related to the factors by which the assumptions are changed:

$$\text{factor multiplying gain} = \frac{\text{factors N}}{\text{factor D}} \cdot E,$$

where N and D refer to the last column in the list of assumptions, and

$$E = \exp\left(\frac{50 - L_2}{7.5 \times p}\right) \text{ for } K^{\pm}, \quad E = 1 \text{ for } \bar{p},$$

L_2 being the assumed additional length of the separated beam in metres and p the beam momentum in GeV/c. The data for the fluxes are taken from a report by B. Jordan*), with some extrapolations. A beryllium target is used.

Table 4.3.1

Comparison of negative separated and unseparated beams

Beam momentum GeV/c		6	8	10	12	14
Particles/burst emitted into beam	π^-	85	83	62	43	28×10^5
	K^-	4.7	3.2	1.9	0.99	0.46×10^5
	$\bar{p}$	0.61	0.40	0.20	0.058	0.0084×10^5
Corrected for decay in 80 m beam length	K^-	0.79	0.83	0.66	0.41	0.21×10^5
Particles/burst unseparated beam	π^-	2×10^5	2×10^5	2×10^5	2×10^5	2×10^5
	K^-	1850	2000	2100	1800	1500
	$\bar{p}$	1400	960	640	300	90
Particles/burst separated beam	K^-	8700	12000	11000	7750	4450
	$\bar{p}$	20000	13000	6000	1900	280
GAIN	K^-	4.7	6	5.3	4.3	3
	$\bar{p}$	14	13	9.4	6.3	3.1

*) B. Jordan, CERN 65-14 (1965).

Table 4.3.2

Comparison of positive separated and unseparated beams

Beam momentum GeV/c		6	8	10	12	14
Particles/burst emitted into beam 0 degrees	π^+	17	19	17	12	6.5×10^6
	K^+	1.54	1.8	1.5	0.90	0.38×10^6
	p	9.9	23	34	76	145×10^6
Particles/burst emitted into beam 5.7 degrees	π^+	2.8	1.3	0.47	0.11	0.022×10^6
	K^+	0.42	0.21	0.069	0.017	0.0033×10^6
	p	3.6	3.2	2.1	1.0	0.32×10^6
Unseparated beam, 5.7 degrees	π^+	86	57	36	19	13×10^3
	K^+	2.2	2.4	1.9	1.2	0.95×10^3
	p	112	141	162	180	186×10^3
Separated beam 0 degrees	K^+	26	62	81	64	33×10^3
GAIN	K^+	12	26	43	53	35